UCRL-11033
SPRING 1963

SEMIANNUAL REPORT
BIOLOGY and MEDICINE

DONNER LABORATORY
and DONNER PAVILION

LAWRENCE RADIATION LABORATORY · UNIVERSITY OF CALIFORNIA · BERKELEY

DISCLAIMER

LEGAL NOTICE

Printed in USA. Price $2.75
Available from the Office of
Technical Services, Department of Commerce,
Washington 25, D. C.

UCRL-11033
UC-48 Biology and Medicine
TID-4500 (19th Ed.)

DONNER LABORATORY AND DONNER PAVILION

LAWRENCE RADIATION LABORATORY — UNIVERSITY OF CALIFORNIA

BERKELEY, CALIFORNIA

SEMIANNUAL REPORT — BIOLOGY AND MEDICINE

SPRING 1963

John H. Lawrence, M.D., D.Sc., Editor

Tove Neville, Associate Editor

AEC Contract No. W-7405-eng-48

TABLE OF CONTENTS

Mt. Everest as seen from the southwest, showing the Khumbu icefall and the South Col in upper right corner. Base Camp is circled.

Preliminary Report on Studies of Erythropoiesis and Adrenal-Cortical Function on Mt. Everest

William E. Siri

Men engaged in climbing the highest Himalayan peaks are unique subjects for research on physiological adaptation, particularly the body's regulatory mechanisms. Driven by extraordinary motivation, climbers voluntarily subject themselves for extended intervals to submarginal environmental conditions that could not long be tolerated by subjects in a laboratory research setting. The state of stress induced by prolonged exposure to severe hypoxia and further aggravated by fatigue, cold, anorexia, insomnia, and psychogenic factors often leads to maximal adaptation followed by progressive deterioration when the homeostatic balance can no longer be maintained. Certain features of regulatory systems may become more evident under these conditions than in the more regulated circumstances of a laboratory experiment. This was the premise for the studies conducted on members of the American Mt. Everest Expedition in the Spring of 1963.

Among the more familiar responses to high altitude is the increased rate of red-blood-cell production. With continued exposure, this leads ultimately to a stabilized polycythemia that is related in an ill-defined way to severity of hypoxia. The processes, and more specifically the hormone erythropoietin, that accelerate erythropoiesis under hypoxic stimulus are presumed by most investigators also to be responsible for regulation of red-blood-cell volume under normal conditions.

Numerous studies of hematopoietic activity have been made at altitudes up to 15,000 ft, notably those of Hurtado and Delgado (1), Merino (2), Lawrence et al. (3,4) and Reynafarje et al. (5). More recent observations by the author at 17,000 ft in Bolivia suggest the possibility of an anomolous increase in hemoglobin synthesis relative to that anticipated by projection of observations made at lower elevations. The first object of the work on the Everest Expedition was to extend these observations to high altitudes corresponding to levels of hypoxia well below that for which human adaptation seems possible. The intended studies included observations on plasma-iron turnover to determine rate of hemoglobin synthesis, assay of erythropoietin in 24-hr urine collections, and changes in blood elements and chemistry as a function of altitude and duration of exposure.

The second object of the physiological studies was to examine indirectly the responses of the adrenal cortex to demands for maximal adaptation by the body to conditions that exceed physiological limits for chronic exposure. The vital roles played by the adrenal cortex as a regulatory organ and in adaptive processes are firmly established. Secretion of cortical hormones, mediated in part by ACTH, exercises a strong and often a controlling influence over metabolism, the cardiovascular and respiratory systems, and the body's chemistry.

The assessment of adrenal-cortical activity during the varied stresses imposed by the Expedition was based primarily upon urinary excretion of cortical steroids and their catabolites. Twenty-four-hour urine collections were obtained under conditions and at times when the climber was severely stressed, and particularly when he exhibited signs of deterioration. In each instance a second 24-hr urine collection was obtained following administration of ACTH. The differences in urinary ketosteroids before and after ACTH should provide a rough measure of adrenal cortical reserve. Whether or not the relative as well as total excretion rates of the several major adrenal corticoids is altered by stress may become evident on fractionation of the urinary ketosteroids.

Collateral tests of adrenal-cortical function were necessarily limited to simple procedures that could be performed at intervals under the restrictive conditions of the Expedition and environment. For the most part these included white-blood-cell differential, cardiovascular response to exercise, urine chemistry, and other tests described in the next section.

Base-line values of all the physiological parameters measured in the field were obtained from each climber at Donner Laboratory prior to departure of the Expedition.

Conditions conducive to severe hypoxia and prolonged stress were encountered in the course of climbing Mt. Everest, but it is difficult to assess the actual level of tissue hypoxia. The length of exposure was sufficient to acquire a high degree of acclimatization to hypoxia and to develop signs of general deterioration. Most climbers remained at 21,500 ft or higher for several weeks and one remained at this altitude for six weeks. The most telling effects of hypoxic exposure and exhaustion were evident in the five climbers and one Sherpa who reached the summit of Mt. Everest (29,028 ft), all of whom spent intervals ranging from three and a half to 8 hr above 28,000 ft without oxygen. Normally, however, supplemental oxygen was used above 23,000 ft at rates from 2 to 4 liters per minute for climbing and one half to 1 liter per minute for sleeping.

The description presented here of the studies on Mt. Everest is intended as no more than a preliminary report. Neither findings nor conclusions can be

offered until data and samples collected in the course of the Expedition are fully analyzed.

PRELIMINARY RESULTS

Erythropoietin, the hormone that stimulates red-blood-cell production, can neither be detected in the healthy person at sea level nor in persons chronically exposed to moderate altitudes where, presumably, the erythropoietin concentration is increased in response to hypoxia. Even at 17,000 ft, the author in collaboration with Dr. Donald Van Dyke was unable to detect erythropoietin in Bolivian natives who lived at this altitude (data to be published). The sensitivity of the bioassay for the hormone is inadequate for the low concentrations normally present. On the other hand, Van Dyke and Garcia, in this Laboratory, and others (6-10) found a transient high concentration in rats and mice during the first few days exposure to severe hypoxia. A clear indication of a similar response in man was reported from this Laboratory, describing results obtained when a human subject was acutely decompressed to a pressure equivalent to 16,400 ft and exposed for four days (11).

In pursuing this line of investigation on the Mt. Everest Expedition, 24-hr urine collections for erythropoietin assay were obtained from climbers two or three days after they had for the first time made an ascent from 17,800 ft to 23,000 ft or higher within the space of two days. Although this is a difference of only 5,000 ft the possibility existed that it would produce a tissue hypoxia comparable to that resulting from decompression from sea level to 16,400 ft and hence induce a detectable, if transient, concentration in erythropoietin.

Additional 24-hr urine collections were obtained from climbers who had spent more than a week at 21,500 ft and at 23,000 ft to determine if detectable steady state concentrations exist at these levels of hypoxia.

Urine collections were passed through collodion membranes for erythropoietin extraction. The membranes were dried, sealed under nitrogen, and sent to Donner Laboratory for assay by Dr. Van Dyke and his associates. None of the samples assayed thus far contained detectable amounts of erythropoietin. From this it must be concluded that: a) the level of tissue hypoxia in an acclimatized man at these altitudes is less severe than anticipated, or b) the erythropoietin was inactivated in the collection procedures, or c) erythropoietin makes an appearance only in response to acute exposure in unacclimatized subjects.

The rate of hemoglobin synthesis can be roughly determined from the turnover rate of iron in the plasma. These rates were measured in the climbers at Berkeley (sea level) prior to the Expedition's departure to establish normal values, using Fe^{59}-labelled plasma. The measurements were repeated at 17,500 ft and at 21,500 ft to determine the relative increases in hemoglobin synthesis for

these levels of hypoxia. In general, the rate of plasma-iron disappearance observed in the climbers at 17,500 ft, and therefore presumably the erythropoietic activity, was about double that for sea level. This is in agreement with earlier observations made in Bolivia on subjects at 17,000 ft, including residents at this altitude and also persons brought up from lower altitudes. The plasma-iron disappearance rate found at 21,500 ft was less clear. In one subject, it was nearly three times that for sea level; in another it was twice the rate.

Blood smears for reticulocyte counts were taken at intervals during the course of the Expedition. A preliminary examination of the slides suggest that these immature red cells may be elevated at 2 to 3.5% about the time the climbers reached Base Camp (17,500 ft) as compared to 0.5 to 2.0% for the pre-expedition values. Later when the climbers had been to much higher altitudes and returned to Base Camp they appeared to be devoid of reticulocytes. Slides for white-cell differential count were also taken but have not been counted.

Hemoglobin concentration increased rapidly on arrival at 17,500 ft to about 18 g percent. With continued exposure to this and higher altitudes, the concentration increased slowly to the range 20 to 23 g percent, but showed little tendency to rise significantly higher, although several climbers spent a month or more above 21,500 ft. Hematocrit and red-blood-cell count paralleled more or less the changes in hemoglobin concentration. There was no significant change in the platelet count.

A more striking change, because of its rapidity, was the reduction in hemoglobin concentration to the normal range on returning to low elevations. Within two weeks after leaving Base Camp, hemoglobin concentrations that were 22 g percent had dropped to 16 g percent. Rehydration does not appear implicated in this rapid reduction in hemoglobin concentration. It remains to be determined if complete cessation of red-cell production would account for the apparent rapid reduction.

Twenty-four-hour urine collections for adrenal-cortical-steroid analyses and urine chemistry were obtained under a variety of conditions, all of them involving stressful circumstances. At the end of the first collection, 80 I.U. of a long-acting ACTH preparation were given to the subjects, intramuscularly, before starting the second 24-hr urine collection. Such collections were obtained from all the climbers who reached the summit and from the support teams that went to the highest camps. The collections were started while the climbers were still high on the mountain and completed about the time they reached Base Camp. In one instance, a collection was started before a climber reached the summit and extended through the night in which he was forced to bivouac in the open at 28,000 ft without oxygen. Other climbers provided collections after prolonged stays at 21,500 ft and 23,000 ft during which they showed signs of

Medical officer Gilbert Roberts and William Siri, scientific coordinator of the American Mt. Everest Expedition, measure cardiac output with radioactive iron 59 in psychologist James Lester at Base Camp, using a portable scintillation probe.

progressive deterioration. The cortical steroids were concentrated from the urine collections by ether-ethanol extractions whose volume was then reduced by evaporation, and the concentrate was sealed under dry nitrogen. Results of cortical steroid assays and electrolyte analyses will be presented in a later report.

A variety of simple tests was made at intervals on members of the Expedition to detect gross responses to hypoxia and possibly to changes in adrenal cortical function. Among these were tests of heart rate and blood pressures at rest and following exercise, of breath-holding times, muscular strength, body weight, total body water, electrolyte excretion, and the common hematological measurements.

Basal heart rate and resting blood pressure increased almost immediately as the Expedition moved to higher altitudes. They remained elevated for several weeks after arrival at Base Camp but as acclimatization progressed, heart rate and blood pressure slowly returned toward pre-expedition values at sea level. After two months at altitude, the readjustment seemed complete, and for several climbers heart rate and/or systolic pressure were significantly lower than their normal values at sea level although diastolic pressure remained consistently elevated.

Cardiovascular response to moderate exercise was tested by observing the elevation and the recovery patterns of both heart rate and blood pressure following a three-minute exercise on a 15-inch-high step at the rate of 22 complete steps per minute. Measurements were made continually for five minutes after the exercise ended. In general, the rate of recovery to pre-exercise resting values did not appear to change significantly throughout the course of the Expedition, although there were notable exceptions. On the other hand, the elevation in

heart rate and pulse pressure produced by the exercise changed progressively with acclimatization. In the first week at altitude when symptoms of hypoxia were most evident, the exercise pulse pressure and heart rate were slightly higher than at sea level. During the two months that followed, these responses to the exercise decreased steadily until at the end of the period the elevation in pulse pressure was uniformly smaller, and for some climbers it was less than half that seen in the test at sea level. A similar trend was also observed for the heart-rate response to the test although in four climbers heart rate was hardly stimulated by the exercise. Among the half dozen Sherpas who were tested at 21,500 ft, heart-rate response and recovery were comparable to those for the American climbers, but four of the six Sherpas exhibited almost no elevation in pulse pressure. One of the remaining two showed responses comparable to those of the climbers, but the other was clearly hypertensive.

Breath-holding times were obtained after a normal expiration and after a maximal inspiration. Holding times under both conditions decreased markedly with altitude up to a point but did not appear to be greatly affected by length of stay at altitude. At low altitude(6,400 ft)breath-holding times were about 30 and 90 sec, respectively, for normal expiration and maximal inspiration. These times were reduced to 10 and 25 sec at 17,800 ft and were not substantially shorter at 21,500 ft. Degree of motivation did not seem to affect the holding time by more than a few seconds at altitude but may have had greater influence at low altitude where the end effects were less disagreeable and their onset slower.

Muscular strength was measured with a hand dynamometer by observing the maximum force exerted and the duration that one half the maximum force could be held. Some improvement occurred initially, probably the result of "training" in the use of the device, but no significant impairment of strength, as measured in this manner, developed later in the course of the Expedition as had been anticipated. In contrast to this it was uniformly the subjective feeling among the climbers that their capacity for heavy work diminished steadily during their stay on the mountain and that it was significantly impaired at the end of the Expedition.

Weight loss during the Expedition and particularly when climbers were higher than Base Camp was continuous and in a few instances severe. For all but two men losses ranged from one-eighth to one-fourth of body weights recorded in Berkeley prior to departure. This was also approximately the range in proportion of depot fat at the outset as determined from body density and total body water. While the bulk of the weight loss was unquestionably depot fat there were also strong indications of lean tissue wasting. This is supported by the significant reductions in total body water observed toward the end of the Expedition. Diminished appetites, which also grew more selective at high altitude,

and the relative deficiency of acceptable foods high in proteins may have resulted in negative nitrogen balances as well as insufficient caloric intake for most of the climbers. The exceptions to this were two climbers who maintained their weights by deliberately forcing themselves to eat adequately. It is perhaps significant that these were the two men who climbed Mt. Everest via the difficult West Ridge.

The absence of obvious signs of cerebral damage among the six men exposed for hours to altitudes as high as 29,000 ft without oxygen is perhaps remarkable. In the history of Himalayan mountaineering there is suggestive evidence of brain damage, in some instances perhaps irreversible, in climbers exposed to somewhat lesser altitudes. The effects are said to be expressed as impaired memory and personality changes, particularly chronic depression. These and other signs were not evident in the American Everest climbers, but it must be emphasized that a careful search for evidence of brain damage was not conducted.

EXPEDITION OPERATIONS

APPROACH MARCH. The 18 climbers who left Kathmandu on February 20, 1963, on the 180-mile march to Mt. Everest had been carefully selected for experience, skill, and character. Many of them had climbed to altitudes greater than 20,000 ft and were therefore familiar with hypoxia and known to tolerate it well. Sherpa climbers, 34 in number at the outset and later increased to 47, accompanied the Expedition as a service group. Their principal function was to carry equipment and supplies to camps on the mountain.

Members of the Expedition could not carry all the necessary supplies because of the quantity of materiel needed at the nine high-altitude camps and also due to the climbers' inability to carry heavy loads to high altitudes without supplemental oxygen. About twenty-five tons of Expedition supplies and equipment were first transported from Kathmandu to Base Camp on the backs of 909 porters. Later five tons of this materiel were carried to high camps by the Sherpas.

Acclimatization stops at intermediate altitudes during the approach march were essential. To proceed directly to Base Camp at 17,800 ft from the relatively low level of the approach march would have incapacitated the Expedition from mountain sickness, the symptoms of which include headache, nausea, vomiting, muscular weakness, loss of sleep and appetite, and a variety of mild mental abberations. From Namche Bazar, the Sherpa village at 12,000 ft, the Expedition therefore proceeded by easy stages to Base Camp. Although greatly reduced, mild symptoms of hypoxia asserted themselves in varying degrees among the climbers after they passed 14,000 ft.

The physiological studies were begun toward the latter part of the approach march when the effects of the steadily increasing altitude began to take

effect. However, the scope of the work was limited because of the daily movements of the Expedition, the temporary nature of camps, and persistent respiratory and gastrointestinal infections. Blood smears for reticulocyte and white-blood-cell differential counts were started at 12,000 ft. Pulse rate and blood pressure recovery after a standardized exercise were also measured, and such routine measurements as basal heart rate were recorded daily. Weights were checked every few days.

Base Camp was established on March 22 at the foot of the Khumbu Glacier ice fall, the only practicable route of ascent on Mt. Everest from the south. Along with other base facilities a laboratory tent, 10 by 10 ft, was erected and equipped for the physiological studies. Within a few days the first reconnaissance team had explored the lower half of the ice fall but did not establish a camp because of the hazards presented by the constant movement in the 2,000 ft of shattered ice, crevasses, and hanging ice walls.

A second reconnaissance ended at the midpoint in the ice fall when a huge ice wall collapsed without warning on the roped team of men. Climber John Breitenbach was killed instantly, and his body never recovered from beneath the hundreds of tons of ice. Other members of the six-man team were injured and buried but were able to effect their own rescue. During the months that followed, hundreds of man-days were spent without further accident in traversing the ice fall that, however, now was a mental as well as a physical challenge.

Within a short time Camp I (20,000 ft) was established at the top of the ice fall. Camp II (21,500 ft) and Camp III (23,000 ft) followed in quick succession. Using oxygen above 23,000 ft, the climbers firmly anchored Camp IV in the ice of the steep Lhotse face at 25,000 ft, and on April 16, Jerstad and Pownall climbed to the South Col, the 26,200-ft-high saddle between Mt. Everest and Lhotse where they placed Camp V. This was the route pioneered by the Swiss in 1952 and followed to the summit for the first time, by the British Expedition in 1953.

All climbing by Expedition members beyond Camp III was now brought to a halt partly by persistent storms but more by the need to supply the string of camps with provisions and equipment for the ascent. During this time a climber at Camp II developed thrombophlebitis in the lower right leg. Under the care of Dr. Roberts, the senior physician, no further complications developed and the man was removed permanently to Base Camp.

FIRST SUMMIT ASCENT. In late April all camps up to the South Col had been fully stocked by relay teams of Sherpas, and on the last day of the month James Whittaker and Nawang Gombu, with Norman Dyhrenfurth, leader of the Expedition, and Ang Dawa in support, were in position at Camp VI (27,300 ft) for a

summit attempt. Despite unusually high winds on May 1st, which drove clouds of fine, dry snow over the faces and ridges, Whittaker elected to make the summit attempt, realizing there would be no other opportunity. He and Gombu reached the summit in the early afternoon after 7 hr of climbing, using oxygen at 4 liters/min. However, the oxygen supply was exhausted at the summit and nearly 4 hr were spent without oxygen descending 500 ft to the point where spare tanks were cached.

Dyhrenfurth and Ang Dawa reached an elevation of 28,200 ft before they were compelled to turn back by a rapidly diminishing oxygen supply. Their feat was outstanding by any standards but in view of Dyhrenfurth's age of 45 years it was especially notable.

A few days preceding the first summit climb, a new, potentially serious medical problem arose when a climber in the support team was striken with primary pulmonary edema at 25,000 ft. Only in recent years has this acute form of pulmonary edema been described and generally recognized as a distinct disease entity. Its etiology is unknown, and specifically, it does not appear due to infection nor to primary cardiac failure, although it is thought by some authorities that ischemic heart disease and viral infection of the respiratory tract may predispose. The onset of the disease is rapid and if left untreated proceeds usually to fatal termination in 12 to 24 hr. Oxygen administration is essential and rapidly effective treatment; the value of digitalis in addition to oxygen is still conjectural.

In this instance the climber was given both oxygen and digitalis and moved permanently to Base Camp (17,800 ft) where he recovered without further treatment, although a tendency to fatigue continued for several weeks.

SECOND SUMMIT ASCENT. The original plans for the Expedition called for an attempt on Lhotse, Mt. Everest's 27,923-ft neighbor, following the ascent of Mt. Everest. Early in the Expedition, however, a great enthusiasm developed for pioneering a new route on Mt. Everest. Consequently, by common agreement, reconnaissance of the unexplored West Ridge of Mt. Everest took precedence over Lhotse as the secondary objective. The final plan called for a "summit meeting," in which a second ascent via the South Col would be made simultaneously with an ascent via the West Ridge. Work on the West Ridge, which began soon after the ice fall was penetrated, continued through April and May in the face of the severest difficulties.

During the weeks following the first ascent, climbers for the second assault rested at Base Camp while other climbers extended the West Ridge route and restocked the high camps leading to the South Col. The West-Ridge team had already suffered setbacks. An avalanche had wiped out a camp, attrition of

climbers and especially Sherpas severely cut support, and supplies were dwindling rapidly. On May 17, five days before the scheduled summit date, an intense storm struck at night, blowing two tents at the 25,000-ft camp on the West Ridge several hundred feet down the north face of Everest where its occupants were precariously held by climbing ropes. In the morning the remaining tent and equipment were blown into Tibet.

Two days later when the storm had spent itself, the group ascended the West Ridge again to 25,000 ft to rebuild the camp. The following day five climbers and the few remaining Sherpas fit for work carried loads to 27,200 ft, where Dr. Thomas Hornbein and Dr. William Unsoeld were left to carry on what was believed could now be only a high reconnaissance.

On the south side of the mountain, the summit team of Luther Jerstad and Barry Bishop, with Dr. David Dingman and two Sherpas one camp behind in support, ascended the South Col route, reaching the highest camp on May 21st.

May 22nd, the last possible day for the ascent, was windy and cold but tolerable. At six in the morning, Bishop struck a match to light the butane stove and from the violent explosion that followed he and Jerstad were left with smoldering remnants of beards, Jerstad with slightly injured eyes, but otherwise not seriously burned. Because of a late start as a result of the accident and the debilitating effects of weeks at high altitude, they reached the summit at the dangerously late hour of 3:30 PM, exhausting the last of their oxygen supply. At 10:00 PM that night they were still well above 28,000 ft attempting to descend in total darkness.

The same morning Hornbein and Unsoeld left their 27,000-ft camp on the West Ridge and continued to climb throughout the day, using only 2 liters per min oxygen and none at all when one stopped to belay the other. The climbing here was far more difficult, calling for a high order of skill on the smooth rock walls and down sloping slabs covered with fresh snow. By 1:30 PM they had expended all their climbing hardware, and to climb beyond this point meant they would have no alternative but to continue to the summit and then down the technically easier South Col route. After a careful appraisal of their situation they elected to go on, and at 6:30 PM they stood on the summit in rapidly dwindling daylight and with little remaining oxygen.

Late in the evening, descending the unfamiliar South Col route they encountered Jerstad and Bishop who had been halted by the obvious hazards of climbing at 28,000 ft at night without oxygen. Under the circumstances there was no choice but to bivouac until daylight. Bishop's toes and several fingers had already frozen, and by morning Unsoeld's toes were frozen, and Jerstad sustained frostbite in the toes and fingers but less severe than in the other men.

For reasons not altogether clear, Hornbein was relatively unaffected. In the light of early morning as the four men continued the difficult descent they were met by Dingman and a Sherpa bearing oxygen cylinders and fluids, and the descent to Base Camp continued without further serious incident. The damage from frostbite, however, required subsequent amputation of most of Unsoeld's and all of Bishop's toes.

ACKNOWLEDGEMENTS

The author gratefully acknowledges the cooperation given this project by Dr. John H. Lawrence, Dr. Hardin B. Jones and Mr. Norman G. Dyhrenfurth, Leader of the American Mt. Everest Expedition, and for assistance given by Drs. Gilbert Roberts, David Dingman, James Lester and Donald Van Dyke. Special thanks are due Mrs. P. Blanche and Mrs. F. Hughes.

The project was supported by the U. S. Atomic Energy Commission and by grants from the National Science Foundation, the U. S. Air Force Office of Scientific Research, and the National Aeronautics and Space Administration.

REFERENCES

1. Hurtado, A.; Merino, C., and Delgado, E.; J. Am. Med. Assoc. 75:5, 1945.
2. Merino, C. F.; Blood 5:1, 1950.
3. Lawrence, J. H.; Huff, R. L.; Siri, W. E.; Wasserman, L. R., and Hennessy, T. G.; Acta Med. Scand. 142:2, 1952.
4. Huff, R. L.; Lawrence, J. H.; Siri, W. E.; Wasserman, L. R., and Hennessy, T. G.; Medicine 30:3, 1951.
5. Reynafarje, C.; Lozano, R., and Valdivieso, J.; Blood 14:4, 1959.
6. Mirand, E. A., and Prentice, T. C.; Proc. Soc. Exptl. Biol. Med. 96:49, 1957.
7. Stohlman, F., Jr., and Brecher, G.; Proc. Soc. Exptl. Biol. Med. 100:40, 1959.
8. Prentice, T. C., and Mirand, E. A.; Proc. Soc. Exptl. Biol. Med. 106:501, 1961.
9. Scaro, J. L.; Rev. Soc. Arg. Biol. 31:1, 1960.
10. Stohlman, F., Jr., and Brecher, G.; J. Lab. Clin. Med. 49:890, 1957.
11. Siri, W. E.; Van Dyke, D.; Winchell, H. S.; Pollycove, M., and Parker, H. G.; Semiannual Report--Biology and Medicine, Lawrence Radiation Laboratory, UCRL-10683, Fall 1962.

AMERICAN MT. EVEREST EXPEDITION MEMBERS

Norman G. Dyhrenfurth, Leader		William E. Siri, Deputy Leader
Allen Auten	Richard M. Emerson	Barry W. Prather
Barry C. Bishop	Thomas F. Hornbein, M.D.	Gilbert Roberts, M.D.
John E. Breitenbach	Luther G. Jerstad	Lt. Col. James O. M. Roberts
James Barry Corbet	James T. Lester	James Ramsey Ullman
David L. Dingman, M.D.	Maynard M. Miller	William F. Unsoeld
Daniel E. Doody	Richard Pownall	James W. Whittaker

Studies on the Mammalian Radiation Syndrome with High-Energy Particulate Radiation. I.

Difference in Injury Mode and its Dose Rate Dependence for 100 kVp X rays and 730 MeV Protons

James K. Ashikawa, Charles A. Sondhaus, Cornelius A. Tobias, Glyde Greenfield, and Jerry Howard

The mammalian radiation syndrome has earlier been studied extensively in a number of species exposed to X, neutron and gamma radiation (1,2). The imminent advent of space travel has drawn increasing attention to the effects of proton exposure because a number of practical protection questions have already arisen in regard to this terrestrially rare but cosmically abundant radiation (3,4). A basic question is the following: Does the injury produced by high-energy protons differ basically from that resulting from other radiations? At what type of damage should protective or therapeutic measures best be directed?

Previous work has delineated two main patterns of acute injury in the irradiated animal: First, the damage to the rapidly proliferating intestinal epithelium which follows closely after the time of exposure (5), and second, the more gradual onset of damage to the blood-forming tissue of bone marrow and spleen (6). These somatic injury modes, the so-called gastrointestinal and hematopoietic syndromes, occur at moderate dose levels, lower than the supra-lethal doses required to produce central-nervous-system damage (7) but higher than the small doses which may ultimately result in malignant transformation or genetic mutation (8). In X- and gamma-ray exposures, the degree of damage has also been found to vary with dose rate (9) (as distinct from dose fractionation-recovery effects).

According to the relative predominance of gut or bone-marrow damage, the irradiated animal may respond to different protective measures or post-irradiation therapy. Thus, antibiotic or electrolyte therapy is useful in ameliorating gut damage (10) while spleen or marrow homogenate and lipid therapy is of specific benefit in treating damage to the blood-forming system (11,12). A knowledge of the behavior of high-energy protons in regard to injury mode is therefore of obvious practical importance in planning for the protection of human beings in space exploration.

MATERIALS AND METHODS

Randomly bred Swiss Webster white male mice from Simonsen Laboratory were used. All of the animals were innoculated against mouse pox one week before shipment. Immediately upon arrival the animals were dipped in 1% malathion (o,o-dimethyl dithio phosphate of diethyl mercaptosuccinate) and individually caged in pint-sized Mason glass jars, according to the procedure previously found necessary to assure reproducibility of mortality data (12). The mice were fed Simonsen Laboratory white diet and water ad libitum. The jars and water bottles were cleaned and sterilized at weekly intervals. During the two-week period of pre-experimental acclimatization and isolation in the glass jars, the animals were carefully examined and weighed. Mice showing any sign of illness, abnormal growth, or loss of weight during the last 3 days of pre-irradiation isolation were discarded. Only animals which weighed 28 ± 3 g were selected for experimentation. These animals were distributed equally among the experimental groups. All animals were kept in air-conditioned rooms that were continuously lit artificially.

In a series of four experiments, the time course of radiation mortality was followed in more than 700 total-body irradiated animals after exposure to the proton beam of the 184-inch cyclotron. An equal number of randomized litter-mate animals were exposed to 100 kVp X radiation. The radiation sources were a Phillips 250 kVp X-ray machine and the 184-inch cyclotron. X irradiation was effected at 100 kVp with 1.0 mm Al added filter with a half value layer of 2.0 mm Al. The animals were irradiated in individual plastic holders on the irradiation positioning wheels, dorso-ventrally in the X-ray beam and antero-posteriorly in the proton beam (13). The X-ray midline air-dose rates were 20 and 100 rads per minute. Exposures to the 730-MeV protons were made at 100 and 1,000 rads per minute. The mouse midline air dose varied from 500 to 1,100 rads per exposure. After irradiation, the animals were returned to their respective cages for the duration of the experiment.

RESULTS

Figure 1 shows the time course of mortality after various doses of proton radiation at 1,000 and 100 rad/min. In the proton-irradiated mice, peak mortality occurred at 4 to 6 days post-irradiation in the 30-day lethal range. Previous work at this and other laboratories has repeatedly demonstrated that death during this period in the mouse is due predominantly to gastrointestinal injury (14). Since this injury syndrome is well separated in time from the bone-marrow syndrome in the mouse, it was considered to be a reasonable assumption in this experiment that all mortality up to 8 or 9 days could be taken as gut death.

In Fig. 2, cumulative mortality is plotted in probit units vs. time after 730-MeV proton irradiation. For each dose rate, total mortality data are

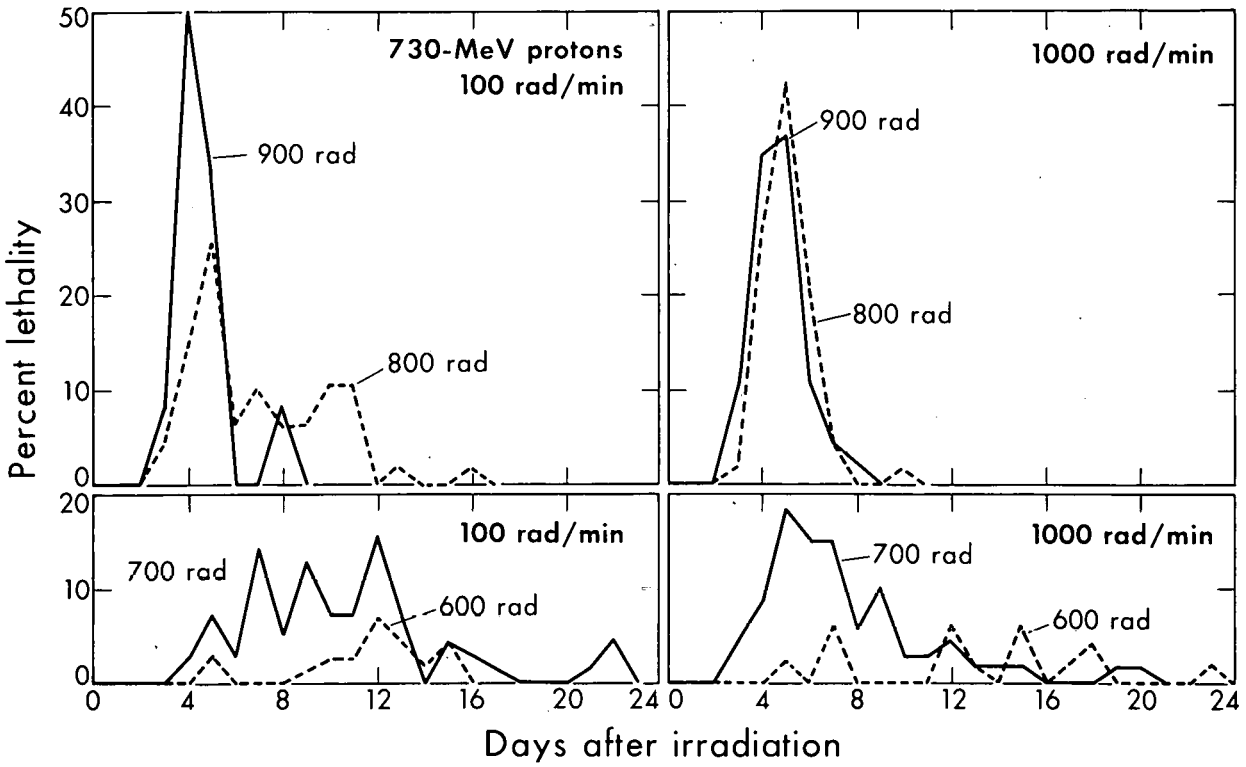

Figure 1. Mortality vs. time in mice irradiated with 730-MeV protons at 1,000 and 100 rad/min. MU-31910

combined for 700-,800-,and 900-rad air dose. The cumulative mortality data plotted on a probability scale linear in standard deviation units clearly illustrate the marked increase in incidence and abruptness of 4- to 6-day gut deaths in animals receiving a proton dose at 1,000 rad/min, compared to those irradiated at 100 rad/min. Thus at 5 days, 30% mortality was observed in the 100 rad/min animals, while 60% mortality had already been reached in the 1,000 rad/min groups, although the 30-day mortality was the same in both groups for a given total dose.

In mice irradiated with 30-day lethal doses of 100 kVp X rays, peak mortality occurred at 12 to 14 days post irradiation. Fig. 3 shows the time course of mortality after various doses of X radiation at 100 and 20 rad/min. Death during this period in the mouse has been shown to be due mainly to loss of hematopoietic function (14), and it was assumed in these experiments that all mortality after about 10 or 11 days post-irradiation could be considered as bone-marrow death.

In Fig. 4, cumulative mortality for 850, 1,000 and 1,150 rads is plotted on the probability scale vs. time after 100 kVp X irradiation. In animals irradiated with 30-day lethal doses, a fivefold increase in dose rate from 20 to

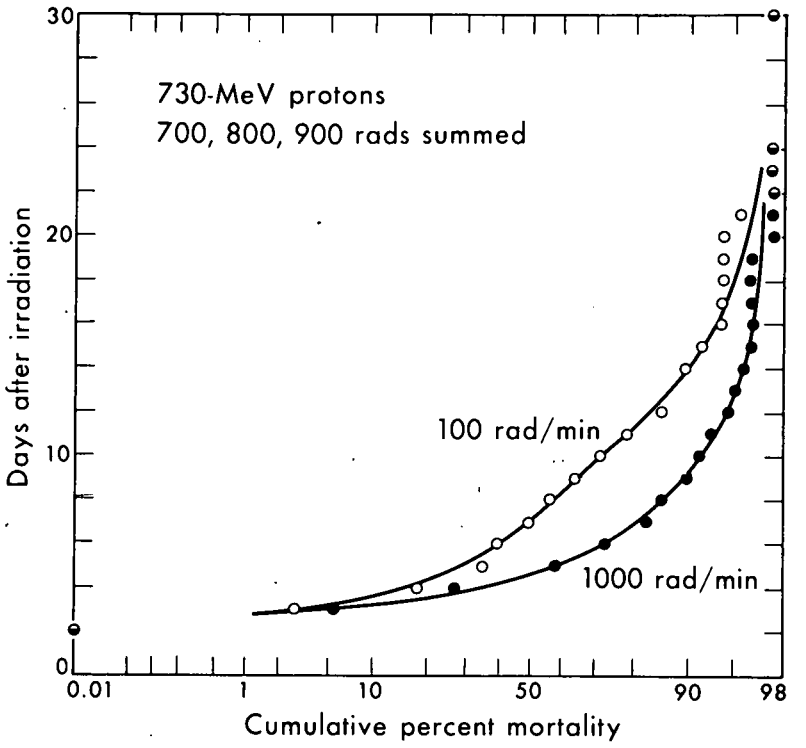

Figure 2. Cumulative mortality vs. time after proton irradiation (probit units). MU-31908

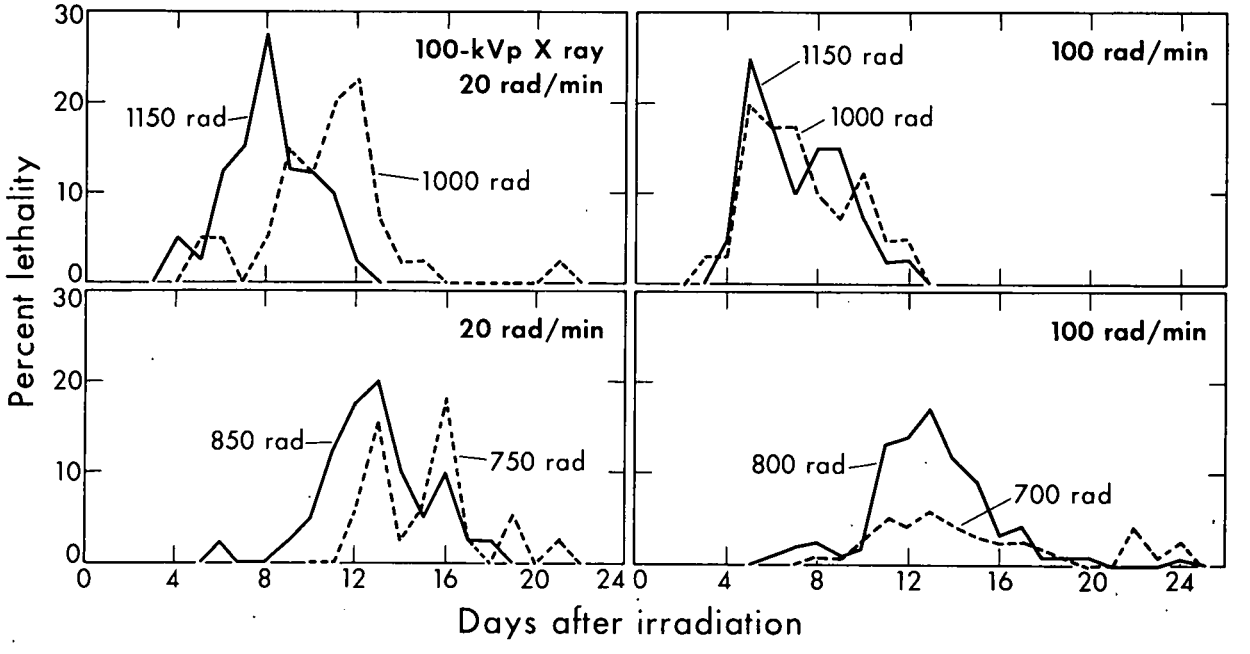

Figure 3. Mortality vs. time in mice irradiated with 100-kVp X rays at 100 and 20 rad/min. MU-31911

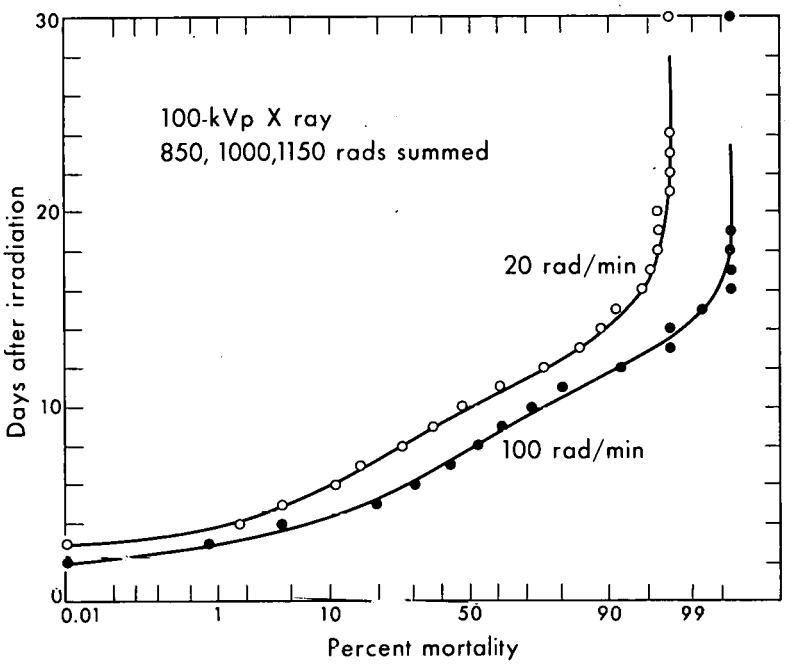

Figure 4. Cumulative mortality vs. time after X irradiation (probit units).
MU-31909

100 rad/min produced few deaths from the gut syndrome, but the higher dose rate did effect an enhancement of the marrow syndrome similar to that observed for the gut syndrome with protons. However, when a total X-ray dose high enough to produce 100% lethality in 12 days was given, gut death and the dose rate effect on it was again observed. When the data are combined for higher doses as shown in the figure, the latter effect is evident. Thus, 10% 6-day deaths were observed at 20 rad/min, while 30% 6-day deaths were seen at 100 rad/min. Since a dose rate higher than 100 rad/min was unobtainable with 100-kVp X rays, the effect of 1,000 rad/min could not be investigated.

DISCUSSION

Since the LET spectrum for 100-kVp X rays does not differ greatly from that of 730 MeV protons (15), the marked difference observed in mode of death in these experiments appears to be due to the difference in tissue-dose distribution in gut and bone marrow between the two radiations, rather than to a change in sensitivity of the mouse intestine with change in LET (16). In proton exposure, dose is uniform and thus comparable in both organs, with a constant relation to air dose. In exposure to soft X rays, calculation has shown that local dose in the marrow cavities may reach several times the average air dose (17), while the decrease in tissue dose with depth lowers the gut dose relative to air dose.

It thus becomes difficult to observe a bone-marrow death with high-energy protons, because the rapidly occurring gut syndrome will supervene first if a uniform dose high enough to produce either mode of death is given. With soft

X rays, on the other hand, either the high bone marrow/gut dose ratio or a greater radiosensitivity of the marrow causes the marrow death to appear first.

Each syndrome in turn is subject to the dose-rate effect characteristic of low-LET radiation (9); this has been found to appear in the gut syndrome with protons, and can be made to appear in either syndrome with X rays. If the total air dose is not high enough to produce gut death, either a high local marrow dose or a high marrow radiosensitivity produces marrow death, which also exhibits dose rate dependency.

By protecting the proton-irradiated animal against gut death, it should be possible to produce the marrow syndrome and to demonstrate its dose rate dependence with protons. It should then also be possible to determine what proton dose to the bone marrow is required to produce the syndrome, and thus to investigate the relative radiosensitivity of the bone marrow.

ACKNOWLEDGEMENTS

We wish to express our thanks to Dr. John H. Lawrence for his interest and support, to Mr. David Love for operation and dose measurement in the proton irradiations on the 184-inch cyclotron, and to Miss Vally Paschkes for her technical assistance. This work was supported by the National Aeronautics and Space Administration.

REFERENCES AND NOTES

1. Patt, H. M.; Ann. Rev. Physiol. 16:51, 1954.
2. Cronkite, E. P., and Bond, V. P.; Ann. Rev. Physiol. 18:483, 1956.
3. Winckler, J. R.; Radiation Res. 14:521, 1961.
4. Proceedings of the Symposium on the Protection Against Radiation Hazards in Space, Gatlinburg, Tenn., 1962, Book 1 and 2.
5. Quastler, H.; Lanzl, E. F.; Keller, M. E., and Osborne, J. E.; Am. J. Physiol. 164:46, 1951.
6. Jacobson, L. O.: The Hematologic Effects of Ionizing Radiation;in Radiation Biology, Vol. 1, edited by A. Hollaender, New York, McGraw-Hill Book Co., Inc., 1954, p. 1029.
7. Langham, W. H.; Rothermel, S. M.; Woodward, K. T.; Lushbaugh, C. C.; Storer, J. B., and Harris, P. S.; Los Alamos Scientific Laboratory Report LA-1643, 1953.
8. Furth, J., and Lorenz, E.:Carcinogenesis by Ionizing Radiations; in Radiation Biology, Vol. 1, edited by A. Hollaender, New York, McGraw-Hill Book Co., Inc., 1954, p. 1145.
9. Bateman, J. L.; Bond, V. P., and Robertson, J. S.; Radiology 79:1008, 1962.

10. Conard, R. A.; Cronkite, E. P.; Brecher, G., and Strome, C. P. A.; J. Appl. Physiol. 9:227, 1956.
11. Lorenz, E.; Congdon, C. C., and Uphoff, D.; Radiology 58:863, 1952.
12. Ashikawa, J. K.; Lawrence Radiation Laboratory Report, UCRL-9592, 1961.
13. Wang, C. C.; Lyman, J., and Tobias, C. A.; J. Nucl. Med., 1963, in press.
14. Quastler, H., and Zucker, M.; Radiation Res. 10:402, 1959.
15. Schaefer, H. J.; in Proceedings of the Symposium on the Protection Against Radiation Hazards in Space, Gatlinburg, Tenn., 1962, Book 1, p. 393.
16. Bond, V. P., and Easterday, O. D.; Radiation Res. 10:20, 1959.
17. Charlton, D. E., and Cormack, D. V.; Radiation Research 17:34, 1962.

James Ashikawa is a consultant to the University of California, Lawrence Radiation Laboratory, from Loma Linda University School of Medicine, Los Angeles County General Hospital, Los Angeles 33, Calif.

Depth Dose in Large Phantoms Irradiated Omnidirectionally with High-Energy Protons

Charles A. Sondhaus, Palmer G. Steward and Roger W. Wallace

In evaluating the effect of total body exposure of a large animal to a radiation flux, it is of considerable importance to know the distribution of tissue dose and of linear energy transfer (LET) at various depths in the animal (1,2). Although both quantities appear to be essentially constant at all points in even a large animal exposed to protons, if the proton energy is sufficiently high then two factors may produce deviations from uniformity. The first is the attenuation of the primary beam resulting in the production of secondary particles by the interaction of primary protons with nuclei of atoms in the tissue. The second is the scatter and energy degradation of the primary-proton flux by multiple coulomb interactions in passage through the material. The relative importance of each process varies with the energy of the incident proton flux as well as with the size of the animal.

A number of calculations have been made by different investigators in attempting to predict the behavior of dose and LET with depth for the case in which the proton flux is distributed in energy and is isotropically incident (3, 4,5) because present information indicates that these are the conditions under which an exposure to a solar-flare proton flux might occur during the course of a space flight. The numerical values of dose and the shapes of the depth-dose profiles resulting from such estimates differ somewhat according to the varying assumptions made in each investigation; the problem is a complex one, and detailed information on nuclear interactions and secondary-particle production is scarce. Furthermore, the energy spectrum of the solar-flare proton flux appears to vary greatly among different events and at different times during a given event (6), making the predicted values arbitrary to a certain extent.

In an effort to study this problem experimentally, Lucite phantoms will be exposed to the proton beam of the 184-inch cyclotron after it has passed through a scattering target that produces energy degradation and angular divergence in the emergent broad beam. Dose will be measured at a series of radial depths inward from the surface of a test sphere and in tissue-equivalent animal phantoms by means of fluorescence readings in silver-activated phosphate-glass dosimeters as well as with lithium fluoride thermoluminescent dosimeters.

As a preliminary phase of these experiments, a series of calculations have been programmed for the 7090 computer at UCLRL to predict approximately the dose, particle energy and LET distribution in an omnidirectionally irradiated spherical phantom as a function of incident primary-particle energy and of sphere diameter. The program was designed to allow the input of any chosen value for each of the parameters involved so that improvement resulting from further experimental determinations may easily be incorporated into the computations.

MATERIALS AND METHODS

The program of computation was divided into two parts. The first was the calculation of dose at given depth due to the primary-proton flux alone. Geometric differences in path length with angle of entry through a sphere lead to a distribution of energy in the primary-proton flux arriving at each dose point. The percent of total dose contributed by protons in each of several energy intervals has therefore been tabulated, and the sum of the partial doses then forms the total dose due to the primaries. A value of dE/dx and thus of average LET can be assigned to each energy, resulting in an average LET distribution at each point.

The second part of the computation is a recalculation of dose at each point to include the contribution of three classes of secondary particle-producing interactions: the nuclear cascades, the evaporation events and the elastic interactions with hydrogen. By assuming rough energy distributions for each and by carrying the cascade and elastically scattered proton secondaries through successive depths, a total additional dose due to each type of interaction at each depth point chosen can also be roughly broken down into energy intervals and added to the primary dose distribution. These calculations are in progress. Meson and neutron doses are not considered in the present program.

The first part of the calculation (the contribution from only the primary-proton flux) has been developed into an operating computer code, which may be described briefly as follows.

The number of protons per second, dn, reaching a test mass of volume dA·dr (see Fig. 1) from an incremental area $d\sigma$ on the surface of a sphere is given by

$$dn = \frac{\Phi}{4\pi} \, d\omega \cos\alpha \, d\sigma, \qquad 1)$$

where Φ = isotropic flux at $d\sigma$,

$d\omega = \dfrac{dA}{R_1(\theta)^2}$ = solid angle subtended by dA at distance $R_1(\theta)$ from $d\sigma$,

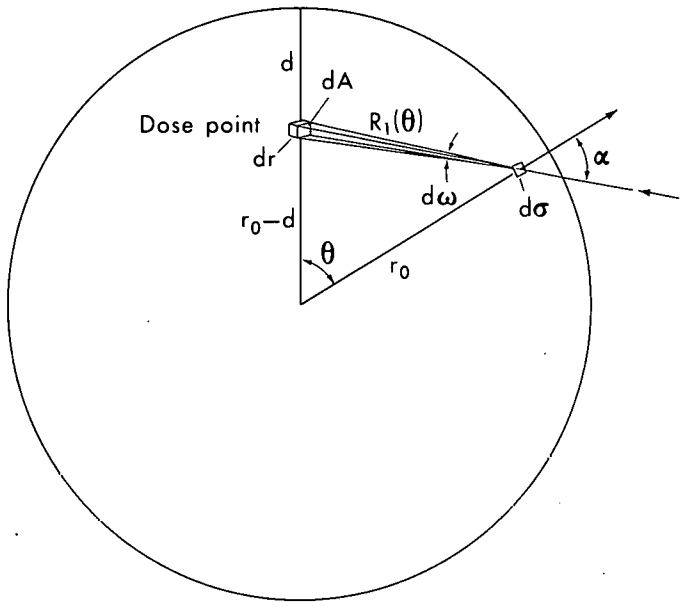

Figure 1. Geometrical representation of a proton-beam element entering the sphere of the radius r_o through dσ, spreading into the solid angle dω about $R_1(\theta)$, and striking the test volume dr·dA at depth d in the sphere.

MU-31936

$d\sigma = 2\pi\ r_o^2 \sin\theta\ d\theta$ = elemental surface area on sphere,

$$\cos\alpha = \frac{r_o^2 + R_1^2(\theta) - (r_o - d)^2}{2\ r_o\ R_1(\theta)} \quad \text{(law of cosines)}$$

r_o = sphere radius, and

d = depth of test mass in sphere.

To allow approximately for the contribution of secondaries, the attenuation due to interaction between the sphere material and the incident protons is neglected.

The dose rate, dD, produced in this same test mass due to the protons per second reaching the dose point from the surface area dσ is:

$$dD = \left(\frac{dE}{dr}\right)_E \frac{dr}{dm}\ dn \qquad 2)$$

$$= \left(\frac{dE}{dr}\right)_E \cdot \left(\frac{dr}{\rho dA dr}\right) dn$$

Where: $\left(\frac{dE}{dr}\right)_E$ = the stopping power for a proton of energy E in tissue,

dm = mass of test volume, and

ρ = density of test mass (1.0 for tissue).

Combining the above expressions and letting $\mu = \cos\theta$:

$$R^2(\theta) = r_o^2 + (r_o-d)^2 - 2r_o(r_o-d)\mu$$

and thus

$$dD = \frac{\Phi}{2}\ \frac{r_o^2}{\rho}\left(\frac{dE}{dr}\right)_E \cdot \frac{(r_o-(r_o-d)\mu)d\mu}{[r_o^2+(r_o-d)^2-2r_o(r_o-d)\mu]^{3/2}} \quad . \qquad 3)$$

To obtain an analytical expression for $\frac{dE}{dr}$, we break the range-energy curve for protons in tissue into five straight line segments on log-log graph paper, for each of which $R = p\ E^q$, where

R = residual range of the proton in tissue

E = proton energy

and p and q represent the intercept and slope respectively on log-log graph paper.

Note that if we let the variable E equal the proton energy at the dose point, and the constant E_o equal the incident proton energy, then

$$R_1(\theta) = p\ E_o^q - pE^q \ .$$

Choosing the variable E in preference to μ,

$$dD = \frac{\Phi}{4\rho}\ \frac{1}{(r_o-d)}\left[\frac{r_o^2 - (r_o-d)^2}{(pE_o^q - pE^q)^2} + 1\right]dE$$

so that

$$D = \frac{\Phi}{4\rho}\ \frac{1}{(r_o-d)}\int_{E_{min}}^{E_{max}}\left[\frac{r_o^2 - (r_o-d)^2}{(pE_o^q - pE^q)^2} + 1\right]dE \quad . \qquad 4)$$

Here,

$$E_{max} = \left(\frac{pE_o^q - d}{p}\right)^{1/q} \quad \text{for } pE_o^q - d > 0$$

$$E_{min} = \left(\frac{pE_o^q - r_o - (r_o-d)}{p}\right)^{1/q} \quad \text{for } pE_o^q - r_o - (r_o-d) > 0,$$

where E_{min} = minimum energy of protons reaching test mass

E_{max} = maximum energy of protons reaching test mass

r_o = radius of the sphere

d = depth in the sphere at which data are desired.

The computer code performs a numerical integration of equation 4) by the application of Simpson's rule. This expression of the total dose rate results in an extremely rapid calculation, each dose point requiring about 0.5 sec for a given

incident proton energy. For calculation of dose at 10 depths in each of six sphere diameters for protons of six to 10 different incident energies, the total computer time required was less than 3 min.

The following assumptions are implicit in the code:

A. The range-energy curve is broken into five segments, each represented by a function of the form

$$R = p_i E^{q_i} \quad 1 \leq i \leq 5$$

B. The only interaction considered between the protons and the sphere is ionization energy loss.

C. The effects of straggling are neglected; i.e., all protons of a given initial energy are assumed to reach peak ionization density at exactly the same path length.

For the second part of the calculation, a code is being developed which attempts to include removal of primary protons by nuclear collision and the contribution of secondary particles to the dose. Three types of secondaries, of first generation only, are considered:

1. Cascade protons resulting from inelastic collisions between primary protons and nuclei in the sphere.
2. Evaporation protons resulting from inelastic interaction between primary protons and nuclei in the sphere.
3. Recoiling hydrogen atoms and scattered primary protons resulting from elastic scattering of the primary protons on hydrogen atoms in the sphere.

The energy spectrum of the cascade-proton secondaries is represented by a power function, and it is assumed that they are all emitted in the forward direction (i.e., the secondary continues on in the direction of the incident primary).

The evaporation protons are assumed to have a Maxwellian energy distribution. Due to their low energy, it is assumed that all their energy is deposited at the point of formation.

The energy spectrum of recoiling hydrogen nuclei and scattered primary protons is calculated from the application of conservation of energy and momentum to the p-p differential elastic-scattering cross section. It is assumed that both the recoil hydrogen nuclei and the scattered incident protons are emitted in the forward direction with the energy calculated by the method indicated above.

RESULTS AND DISCUSSION

The output of the initial computer program is in the form of depth-dose

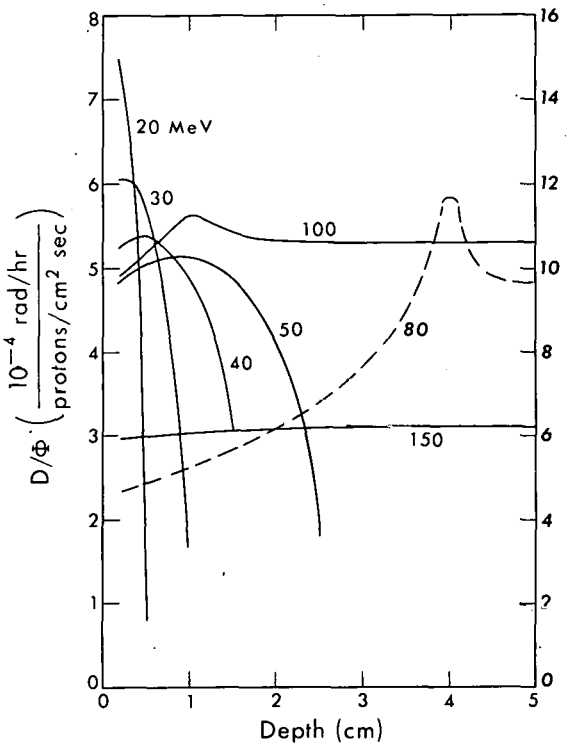

Figure 2. Dose rate produced by an isotropic proton flux upon a 10-cm-diameter sphere of tissue (primary-proton contribution only). Right-hand scale refers to dashed curve. Note pronounced peak.

MU-31937

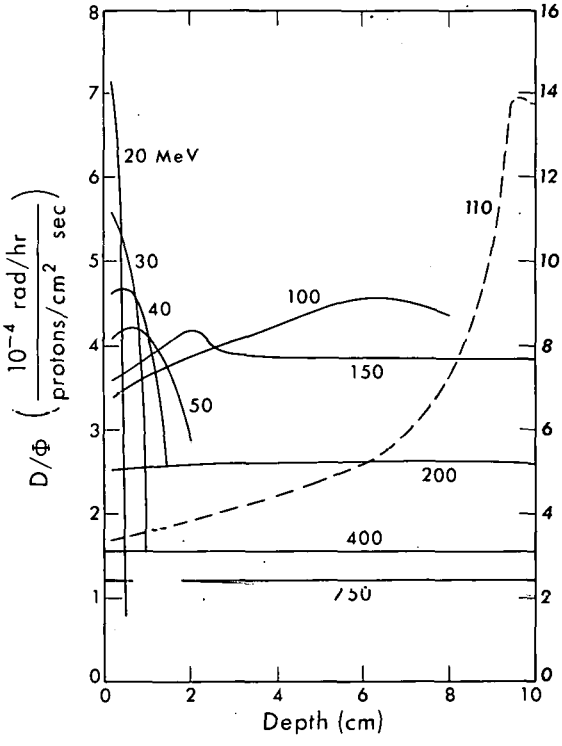

Figure 3. Dose rate produced by an isotropic proton flux upon a 20-cm-diameter sphere of tissue (primary-proton contribution only). Right-hand scale refers to dashed curve. Note pronounced peak.

MU-31938

data and fraction of dose due to protons in each of several energy intervals at each dose point in the sphere; average LET distribution is calculable from the latter at each depth. These data have been calculated for tissue-equivalent spheres of diameter 5 to 100 cm, exposed omnidirectionally to monoenergetic proton fluxes of energy between 20 and 730 MeV. The curves of depth dose for the 30-cm-diameter sphere are essentially flat down to about 200 MeV, indicating that uniform whole-body exposure of large animals is possible at this energy or higher. Below this energy region, the ratio of surface to midline dose increases rapidly with decreasing energy and increasing sphere diameter, the midline dose from primaries alone becoming zero at the lowest energies considered.

Some results available from the first code (primary-proton flux only) are presented in Figs. 2 through 5 and in Table I. In Fig. 2, depth-dose curves are shown for several proton energies incident on a sphere of tissue of 10-cm diameter. A pronounced peak dose occurs at 4-cm depth for 80-MeV protons. The unusual height of this peak is due to the fact that all incident 80-MeV protons approaching the center of the sphere reach the end of their range and therefore

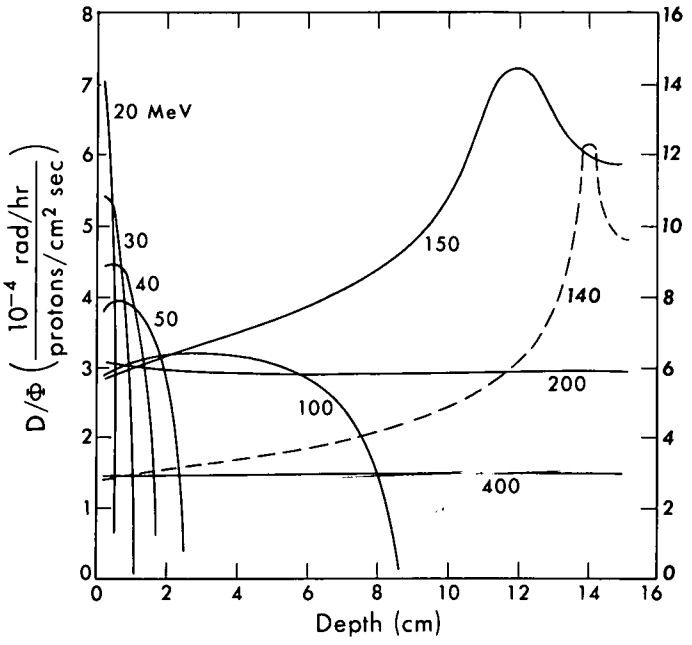

Figure 4. Dose rate produced by an isotropic proton flux upon a 30-cm diameter sphere of tissue (primary-proton contribution only). Right-hand scale refers to dashed curve. Note pronounced peak.

MU-31939

deposit their maximum energy density in a region of the sphere near its midpoint, resulting in a large $\frac{dE}{dx}$ contribution from all directions. The peak at 1-cm depth for 100-MeV protons is caused by the Bragg peak of protons that enter the sphere from directions such that a path length in the sphere of approximately 9 cm results. Protons with initial energy of 150 MeV or more produce an approximately flat depth-dose curve in the 10-cm sphere.

Figure 3 shows similar curves for a 20-cm diameter sphere, roughly equal in volume to a small primate. For this sphere, protons of energy 200 MeV and above produce an essentially flat depth-dose curve. Protons of about 110 MeV cause a pronounced peak near the center of the sphere as seen in the figure.

Protons of 140 MeV cause the corresponding peak in the 30-cm diameter sphere (Fig. 4). For 200-MeV protons, the beginning of a peak is seen near the surface of the sphere. Similar cases occur at certain proton energies for any sphere diameter.

A consequence of this depth-dose pattern is that in uniform exposure by rotation, approaching the omnidirectional case, a Bragg ionization peak at depth d cannot be produced by irradiating with monoenergetic protons of range d since the smearing out of ionization peaks by the rotation produces a continuously decreasing dose distribution with depth. Instead, protons with energy large enough to cross the sphere with range ($2\ r_o$-d) must be used, where r_o is the radius of the spherical tissue volume. The center of the sphere and all other points within it would thus always receive some dose but less than the point receiving the Bragg-peak dose.

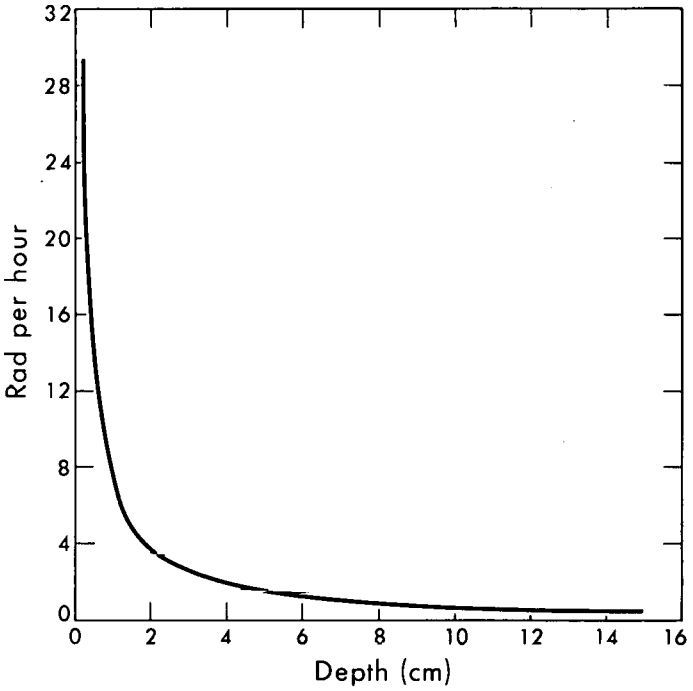

Figure 5. Depth-dose rate curves for a 30-cm-diameter sphere of tissue using Bailey's idealized energy spectrum of solar protons -- 16 hr after onset of the radiation surge.

MU-31940

Table 1 is an example of the information the code computes, which is intended to make possible the calculation of average LET versus depth for any incident proton energy. The specific data tabulated are for the case of a 30-cm-diameter sphere exposed omnidirectionally to a flux of 150-MeV protons. At 12-cm depth, the large contribution to the dose of the low-energy protons, shown in Fig. 4, is seen; about 75% of this dose is contributed by protons of energy between 20 and 80 MeV with a LET distribution of average value of about 1.5 to 2 keV/μ. About 5% of the 12-cm depth dose is contributed by protons of 5 MeV and less, with average LET about 20 keV/μ.

Table 2 gives an idealized solar-flare energy spectrum (6) that was used together with Fig. 4 to calculate a depth-dose curve for a 30-cm-diameter sphere of tissue. The result, shown in Fig. 5, is in general agreement with this particular case as treated elsewhere (2,3). A large surface dose is contributed by low-energy flare protons in an unshielded sphere. The effect of shielding may be estimated by recognizing that, for example, the curve remaining from 1- to 15-cm depth represents a depth-dose curve in a sphere of 28 cm diameter shielded by 1 cm of water. The depth-dose distribution for this solar-flare case would be fairly well duplicated by an exposure to 50-, 100-, and 400-MeV protons in the intensity ratio 5:2:1.

The dose distribution in a sphere exposed to any arbitrary solar-proton spectrum may be similarly obtained from this computer code by summing the contributions from each energy interval in an assumed spectral distribution. By

Table 1. Depth dose data for the case of 150-MeV protons incident upon the 30-cm-diameter sphere of tissue equivalent material

Depth (cm)	Total dose rate (rad/hr) 10^6 proton/cm^2-sec	Dose rate per energy interval 0-5 ~20	5-10 6.0	10-20 3.7	20-40 2.2	40-80 1.2	80-150 ~0.7	Energy interval, MeV LET, KeV/μ
0.2	285	4.95	4.95	9.89	19.8	40.0	205.	
0.5	290	5.19	5.19	10.4	20.9	42.6	206.	
1.0	299	5.59	5.59	11.2	22.6	47.1	207.	
1.5	307	6.05	6.05	12.1	24.5	51.8	207.	
2.0	315	6.50	6.50	13.0	26.5	56.7	206.	
3.0	331	7.50	7.50	15.1	30.7	67.2	203.	
6.0	387	11.5	11.5	23.4	48.1	100.	192.	
9.0	481	19.0	19.0	38.4	79.5	186.	138.	
12.0	724	32.0	40.0	81.1	168.	398.	4.72	
15.0	590	0	0	0	0	590	0	

Table 2. An idealized (omnidirectional flux) solar-flare proton-energy spectrum 16 hours after onset of the radiation surge (Data from reference 6)

Energy group (MeV)	Protons group (cm^2-sec)
15-25	2.52×10^4
25-35	1.01×10^4
35-45	5.03×10^3
45-70	7.16×10^3
70-125	3.17×10^3
125-175	7.41×10^2
175-225	1.76×10^2
225- ∞	6.29×10^1

reproducing experimentally the dose distribution predicted for a test sphere, the proper exposure times and proton energies at the 184-inch cyclotron can be chosen to simulate the solar-flare condition to a degree sufficient for animal irradiation. A large-animal rotator has been constructed for use in total-body omnidirectional exposures. Experimental dose determinations to confirm the predicted distributions can be made with the phantom or test sphere placed within the rotator.

ACKNOWLEDGEMENTS

We wish to express our appreciation to Dr. John H. Lawrence and Dr. Cornelius A. Tobias for their interest and support, and to Mrs. Barbara

Levine for her assistance in programming and performing the calculations on the 7090 computer.

This work was supported by National Aeronautics and Space Administration.

REFERENCES

1. Bond, V. P.; Carter, R. E.; Robertson, J. S.; Seymour, P. H., and Hechter, H. H.; Radiation Res. 4:139, 1956.
2. Bond, V. P.; Cronkite, E. P.; Sondhaus, C. A.; Imrie, G. W.; Robertson, J. S., and Borg, D. C.; Radiation Res. 6:554, 1957.
3. Proceedings of the Symposium on the Protection Against Radiation Hazards in Space Travel, Gatlinburg, Tenn., November, 1962, TID-7652.
4. Evans, R. D.; Technical Report to the National Aeronautics and Space Administration, A. D. Little Co. Report 63270-05-01, July 1961.
5. Schaefer, H. J.; Aerospace Med. 31:807, 1960.
6. Bailey, D. K.; J. Geophys. Res. 37:391, 1962.

The Alpha-Particle or Proton Beam in Radiosurgery of the Pituitary Gland for Cushing's Disease

John A. Linfoot, John H. Lawrence, James L. Born and Cornelius A. Tobias

In the early days of the modern nuclear era, one of the first studies for assessing the danger from nuclear radiations investigated the biologic effects of neutron rays. These neutral heavy particles, having the approximate weight of a proton, are nearly two thousand times as heavy as electrons. The early workers around the cyclotron were being bombarded constantly by these particles, in addition to gamma rays, and they were naturally concerned with the safe daily dose. For this reason it was extremely important to study the biologic effects of these heavy particles as a means of predicting damage to workers, and thereafter to set safety standards and thus avoid the history of radiation damage seen in the early workers with radium and X rays.

Our first studies in 1935 served to compare standard 200-kV X rays with neutron rays, using as test objects the whole bodies of mice and rats, and transplantable forms of cancer in mice (1,2). It was found early that neutrons had a biologic effect several times greater than equal doses of X rays, and appropriate safety standards were established. Also at that time, indications were that neutron rays might have a favorable differential effect over X rays on tumor tissue as compared to normal tissue--that is, a relatively greater effect on neoplastic tissues. These early experiments, therefore, suggested that neutrons might have value in the therapy of cancer. Consequently, a study was carried out on advanced cancer, but the results were disappointing largely owing to the fact that these neutron rays had poor penetration and great scatter (3,4).

Also in 1935, heavy, charged particles, with higher energies became available with the development of the increasingly larger accelerators. It seemed important to investigate heavy particles further because these high-energy particles had, in addition to the previously observed greater biologic effect at the Bragg peak, great penetration and little scatter (5,6,7). In the intervening years such studies have been carried out on both animals and man. When the so-called Bragg peak of these high-energy, heavy, charged particles is used in the delivery of radiation energy to various tissues, one can predict that, like in the early neutron studies, a greater biologic effect per unit of ionization will result (6,8,9). With the added properties of greater

penetration and little scatter, it is possible to produce localized lesions in the tissue and nervous system with little damage to surrounding structures (10).

In 1954 we set out upon a study in clinical medicine, in which these high-energy protons and alpha particles have been used in various forms of so-called "bloodless" surgery, or radiosurgery. This has led to their use in the direct treatment of tumors and the suppression or ablation of the function of the pituitary gland in such conditions as advanced breast cancer, diabetic retinopathy, malignant exophthalmos and acromegaly (11-17). They have also been used in the production of lesions in the thalamic nuclei in the treatment of kinetic disease (18,19). This report deals with our experience in treating Cushing's disease.

Pituitary basophilism or Cushing's disease, first described by Harvey Cushing (20) in 1932, can now be explained on the basis of excessive hormonal secretion by the adrenal cortex. Cushing's early interpretations of the symptomatology and physical, laboratory, and pathological findings led him to relate the condition to either hyperplasia or adenoma of the basophilic cells of the anterior lobe of the hypophysis. Typical of the early cases was that reported by one of us in 1935 during work with Dr. Cushing (21). We found a small basophilic pituitary adenoma associated with bilateral adrenocortical hyperplasia and adenomas and a parathyroid adenoma. In those early days, therapy initially was directed toward the pituitary gland. However, partial surgical procedures and ortho-voltage X-ray therapy were only irregularly associated with adequate and sustained remissions (22,23), and, furthermore, diffuse basophilic hyperplasia or adenomas of the pituitary were infrequently found.

During the ensuing years there has been a tendency to attribute the syndrome to pituitary-adrenocortical hyperplasia, and, with the advent of adrenocortical steroids, total or nearly total adrenalectomy became the treatment of choice (24,25). However, the recognition of pituitary tumors in patients after adrenalectomies for adrenal hyperplasia (26,27) and the development of more effective methods of studying adrenal hyperfunction (28) have indicated that the primary disturbance is frequently due to excessive ACTH secretion by the anterior pituitary gland, in line with Cushing's early thinking (29).

In spite of great progress in the knowledge of the chemistry and physiologic function of the pituitary hormones, no truly satisfactory pharmacological method of suppressing pituitary function has yet been developed. Treatment of pituitary hyperfunction and tumors has been limited to surgery, X rays or gamma rays. A review of the results in cases treated with pituitary irradiation shows that a higher incidence of permanent and satisfactory remissions has been associated with the administration of larger doses of irradiation (30,31).

Unfortunately the use of conventional X rays or gamma rays has been limited by the dose (2,000 to 3,000 r) that can safely be delivered to the sella turcica (32). Because of relatively great scatter and low biologic effectiveness, doses of adequate depth cannot be attained with these radiations without endangering the surrounding structures such as the cranial nerves, hypothalamus and temporal lobes. Heavy particles, however, with the advantageous properties mentioned above, offer a method of suppressing pituitary function and alleviating the symptoms and signs of Cushing's disease. This paper describes and discusses the use of 900-MeV alpha particles for this purpose.

CASE REPORTS

CASE 1. R.K. A 37-year-old white housewife was referred to the Donner Laboratory in April, 1959, because of bilateral adrenal hyperplasia. In the spring of 1957 she had begun to gain weight, and during the next 18 months her weight had increased from 116 to 149 lbs. By January, 1958, she complained of weakness, lethargy and was observed to have mild hypertension. During the next few months amenorrhea, hirsutism and backache developed. Since 1957 she had been quite emotionally unstable.

Physical examination showed an obese woman with rounding and plethora of the face and a prominent cervicodorsal fat pad. There was a fine hair growth over the face and trunk but no pigmented striae. The blood pressure was 140/100.

Preliminary laboratory studies revealed a slight lymphopenia and a diabetic glucose tolerance curve. The hemoglobin was 13.5 g/100 ml. The serum calcium, phosphorus, creatinine and electrolytes were normal. X-ray examination showed demineralization of the lumbar and dorsal spine; the sella turcica was not enlarged. The basal excretion of urinary 17-hydroxycorticosteroids was 16.5 mg/day, and this increased to 58.6 mg/day after an 8-hr infusion of ACTH (20 units). A three-fold increase in urinary 17-hydroxycorticosteroids was observed after the 4-hr infusion (30 mg/kg of body weight) of Metopirone (33). The urinary 17-ketosteroids were also elevated. Adrenal steroid excretion was not suppressed by the administration of dexamethasone, 2 mg/day for 3 days, but was suppressed when a dose of 8 mg/day was similarly administered. The adrenal glands appeared normal on a presacral air study.

Studies repeated in our laboratory confirmed these findings and in addition, the 24-hr thyroid I^{131} uptake was 16%, the PBI was 3.9 μg/100 ml and the urinary gonadotropins were negative at 1:12.5 mouse uterine units.

Eighty-five hundred rads of 900-MeV alpha particles were delivered to the pituitary gland over an 11-day interval, ending on May 16. One month after irradiation the patient began to menstruate, having been amenorrheic

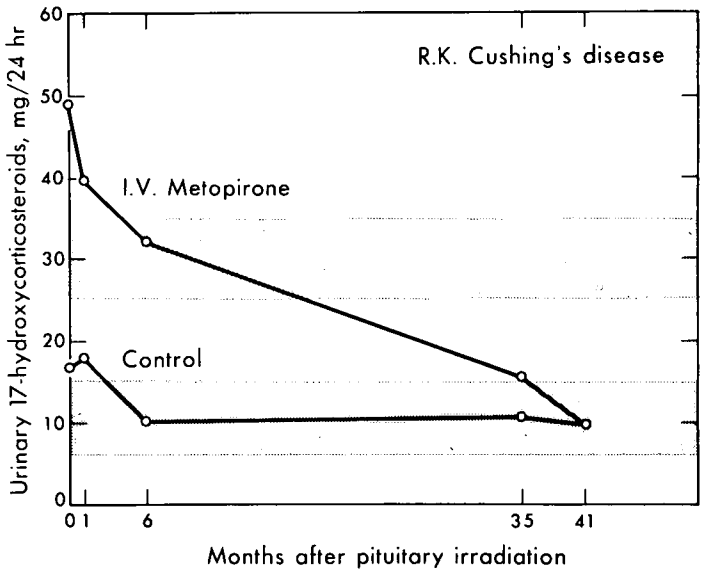

Figure 1. Serial changes in the response to intravenous Metopirone in patient R. K. The normal ranges are represented by the shaded areas.
MU-29271

for the preceding 15 months. There was little change in her other symptoms or appearance. The urinary 17-hydroxycorticosteroids remained elevated at 17.2 mg/day; however, the 17-ketosteroids had fallen from 13.5 to 7.0 mg/day (normal 5-10 mg). The urinary gonadotropins were now positive at 1:12.5 mouse uterine units.

To determine the histological adrenal status, the left adrenal gland was resected on August 14. Pathological examination showed nodular adrenal hyperplasia.

In November the patient was greatly improved. The menses were regular, and she was clinically euthyroid. She had lost 14 lbs in weight and there was significant regression of the cushinoid features. The blood pressure was 130/80. The urinary 17-hydroxycorticosteroids had fallen to 10.1 mg/day and the exaggerated responses to ACTH and Metopirone were no longer present (Fig. 1 and 2).

By January, 1960, her appearance was normal (Fig. 3) The next two and a half years she remained asymptomatic. The menstrual periods continued, and she was euthyroid. In October, 1962, the PBI was 3.5 μg/100 ml and the thyroid I^{131} uptake 23%. The urinary gonadotropins remained positive at 1:12.5 mouse uterine units. The 24-hr urinary 17-hydroxycorticosteroids were 9.5 mg; the 17-ketosteroids were 5.7 mg. Urinary adrenal steroids did not increase after a 4-hr intravenous infusion of Metopirone. The response to intravenously injected ACTH was normal.

CASE 2. J.R. A 32-year-old secretary was referred to Donner Laboratory

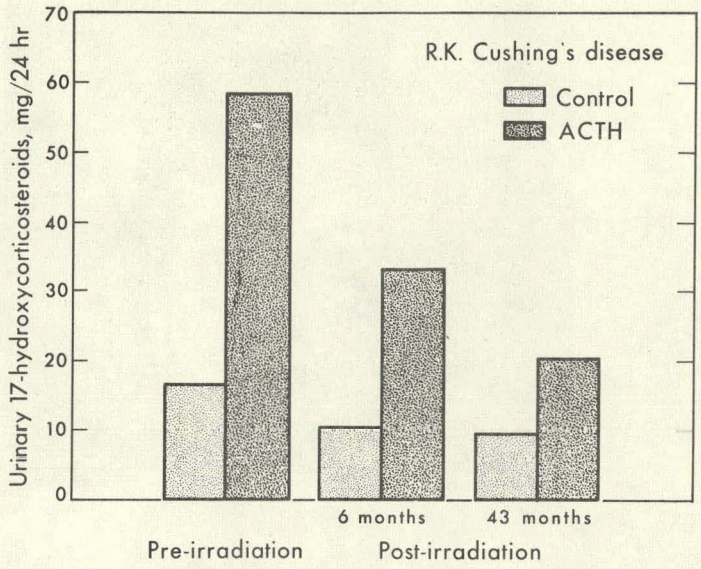

Figure 2. Intravenous ACTH tests, performed on patient R. K., show the characteristic response observed in Cushing's disease prior to treatment and compare the changes that occurred at 6 months and 43 months after treatment.

MU-29272

in 1961 because of a "ballooned" sella turcica and hyperpigmentation. Although she had been overweight for many years, she became progressively more obese since her 1st pregnancy in 1950. Subsequently, facial hairgrowth, acne, back pain and weakness developed and she felt confused at times. In January, 1954, she was seen by a private physician because of headache and amenorrhea.

In July she was admitted to another hospital. Physical examination revealed truncal obesity, acne, plethora, hirsutism and pigmented striae. The blood pressure was 142/114. Pelvic examination was normal. The white-cell count was 10,000 per cubic millimeter, predominantly neutrophils. The hemoglobin was 14 g/100 ml. The fasting blood sugar and serum electrolytes were normal. The urinary excretion of 17-ketosteroids was 36 mg, and that of 17-hydroxycorticosteroids 18 mg per 24 hr. A presacral air study suggested some enlargement of the left adrenal gland. Skull films were interpreted as showing a normal sella turcica. A diagnosis of Cushing's syndrome due to bilateral adrenal hyperplasia was made. The left adrenal gland was totally excised, and the right sub-totally. Microscopical examination of the adrenal glands revealed no prominent abnormality.

After operation, the menses returned, and the other symptoms gradually improved. The patient was maintained on small doses of cortisone. In September, 1955, the urinary 17-ketosteroids were 5.6 mg/24 hr. She had lost 50 lbs in weight and was normotensive. Subsequently, she was able to discontinue cortisone. In April, 1957, she had the florid features of hyperadrenocorticism again. In addition there was some pigmentation of the hands. The urinary 17-hydroxycorticosteroids were 20 mg, and the 17-ketosteroids 14 mg, per 24 hr. The sella turcica was somewhat deeper than seen in earlier X-ray studies on the

Figure 3. Photographs showing patient R. K. before pituitary irradiation (left), and 8 months after treatment (right). JHL 2514; JHL 2612.

skull, but considered normal. Her condition remained unchanged and in November, 1957, the right adrenal remnant was removed. The pathological diagnosis was "regenerative nodular hyperplasia." She had a stormy postoperative course owing to multiple episodes of adrenal insufficiency, but was finally discharged on 37.5 mg of cortisone and 0.125 μg of 9-alphafluorohydrocortisone per day.

After operation, the symptoms of hyperadrenocorticism improved. She had numerous episodes of adrenal crisis usually associated with infection. She failed to return for follow-up study for several years and was not seen until August, 1961, when she was admitted to the hospital in adrenal crisis. She was diffusely pigmented. Although pigmentation of the hands had been noted in 1957, it was apparently first noticed by her in 1958. It did not become prominent until 1960 and had been gradually increasing. X-ray study of the skull showed further enlargement of the pituitary fossa with erosion of the dorsum sellae and the floor of the fossa.

In September, 1961, the patient was admitted to Donner Pavilion. She had no complaints except for a rare headache and some menstrual irregularities. Physical examination revealed a pleasant obese woman with generalized brownish pigmentation of the skin. The pigmentation was particularly prominent in the creases of the hands and over the elbows and knees. The blood pressure was 110/80. The remainder of the physical examination was unremarkable. The visual fields were normal. Laboratory studies revealed a normal hemogram. The fasting blood sugar was 73 mg, PBI 5.6 μg, and the serum cholesterol 228 mg per

100 ml; urinary gonadotropins were positive at 1:12.5 mouse uterine units. The basal excretion of urinary 17-ketosteroids was 1.9 mg, and that of 17-hydroxy-corticosteroids 5.6 mg, per 24 hr on replacement therapy. ACTH stimulation did not produce any increase in steroid excretion. The plasma ACTH assay was 30 milliunits/100 ml. This level was not altered by the administration of 2 mg of dexamethasone for three days or by 8 mg given for an additional 3 days. Serial review of previous skull films revealed that the area of the sella turcica measured 9 by 12 mm in 1954, 12 by 13 mm in 1957 and 15 by 16 mm in October, 1961.

Five thousand rads of alpha particles were delivered to the pituitary gland over an 11-day interval ending on November 10, 1961. The treatment period was uneventful.

The patient was next seen in April 1962. She continued to work as a secretary and was well except for several minor episodes of adrenal insufficiency associated with respiratory infections. The menses were normal. Physical examination was unchanged, except that there appeared to be a little lessening of the pigmentation. The PBI was 6.2 μg/100 ml and the I^{131} uptake 16% in 24 hr. Urinary gonadotropins were negative at 1:12.5 mouse uterine units.

In October, 1962 (10 months after irradiation) there had been some definite lessening of the skin pigmentation. The menstrual periods had been somewhat irregular. She appeared euthyroid. The PBI was 4.9 μg/100 ml and I^{131} uptake 13%. The pituitary fossa had not changed. The plasma-ACTH level was less than 30 and greater than 2 milliunits/100 ml.

DISCUSSION

These two cases illustrate most of the problems that are encountered in the management of patients with hyperadrenocorticism due to bilateral adrenal hyperplasia. Although complete adrenalectomy can produce a prompt remission of the symptoms of hyperadrenocorticism, the surgery is not without risk, and the management of totally adrenalectomized patients is often difficult in spite of available replacement steroids. The appearance of pituitary tumors in many patients adrenalectomized for Cushing's disease is an additional problem associated with this form of therapy. Recent studies of pituitary and adrenal function (28), as well as a more frequent recognition of pituitary tumors in patients with Cushing's disease, require that the pituitary gland be considered primarily in the treatment of many cases of bilateral adrenal hyperplasia. Recently, a number of cases have been successfully treated by surgical hypophysectomy (34) or by the implantation of radioactive sources such as Y^{90} or Au^{198} (35). The latter methods of radiation have been resorted to because previous experience with X rays or gamma rays has not been entirely satisfactory, since these types of therapy have been limited by the amount of radiation

that can be delivered safely without damage to neighboring central-nervous-system structures. Prolonged remissions after X-ray or gamma-ray therapy have been infrequently observed, and partial response and relapse occur in at least 70% of the patients so treated (28,36,37). The best results have often been achieved only after several courses of radiation, these being seen in patients receiving the largest amount of X rays or gamma rays (30,31,38,39). Surgical hypophysectomy and surgically implanted radiation have certain risks and side effects that it would be desirable to avoid. A method of adequately inhibiting anterior pituitary function by an externally-delivered energy source would be the most suitable form of treatment. This can now be accomplished by the use of heavy particles, such as protons and alpha particles, which are imparted extremely high energies in the large accelerator and delivered to the sella turcica in desired amounts.

Case 1 received a significantly larger dose (8,500 rads of alpha particles) than the second patient. Her remission has lasted for more than three years. One month after radiation the menses resumed. Other signs of pituitary irradiation effect are evident in the less exaggerated response to the intravenously administered Metopirone (Fig. 1) and the fall in the excretion of the 17-ketosteroids. These changes occurred before adrenalectomy. Furthermore, the fact that there were progressive changes in the response to the administration of ACTH (Fig. 2) and Metopirone (Fig. 1) after adrenalectomy suggests that the exaggerated responsiveness of the residual adrenal gland was changing and that removal of the left adrenal gland was probably not of major importance. Serial observations of the changes in the response to Metopirone appear to be helpful in determining the adequacy of pituitary suppression. It was of interest that in the study of the effects of intravenously administered Metopirone and ACTH in one of our diabetic patients, who had had a unilateral adrenalectomy before being referred for pituitary irradiation for diabetic retinopathy, the responses were normal and uninfluenced by the absence of one adrenal gland. Remissions after unilateral adrenalectomy have been reported by Soffer et al. (30), who observed better results when they combined unilateral adrenalectomy with X rays given to the pituitary gland and believe that, although administration of the radiation promptly after removing the adrenal was desirable, the clinical response was directly related to the amount of radiation.

It should be emphasized that although Case 1 received a relatively large amount of alpha-particle radiation, the only manifestations of altered pituitary function are the remission of the disease and the reduced "ACTH reserve"; basal steroid excretion is normal, the menses are regular, and she is clinically euthyroid.

Case 2 demonstrates several difficulties that one may encounter in the

surgical treatment of bilateral adrenal hyperplasia. The small adrenal remnant hypertrophied under constant ACTH stimulation and approximately twenty months after the original operation, the symptoms of hyperadrenocorticism gradually returned, requiring the removal of the residual adrenal tissue. At this time the presence of the pituitary adenoma was suggested by an enlarging sella and the pigmentation of the hands. Further growth of the pituitary tumor followed the complete removal of adrenal tissue and the clinical picture of an ACTH-secreting adenoma developed (26).

This patient was treated in the same manner as Case 1 except that the pituitary received only 5,000 rads of alpha particles in 11 days. This treatment was selected because there was no urgent clinical need to suppress hormone production, and the dose was similar to that employed by us in the successful treatment of other pituitary tumors (15). The improvement has been less dramatic, but she began to show definite loss of skin pigmentation one year after treatment, and there has been no further enlargement of the pituitary fossa. The thyroid and gonadal functions are normal. The plasma ACTH remains elevated, but it is still within the range observed in patients subjected to total adrenalectomy for adrenal hyperplasia (40). Although this may represent some radiation resistance by this particular tumor, further improvement may be anticipated because our previous studies have shown that the rate of pituitary suppression is determined by the dose of radiation--that is, a more rapid response might have been anticipated if the dose employed had been similar to that of Case 1. If further pituitary irradiation becomes necessary this may be given, for we have determined that much larger doses can be safely delivered to the pituitary fossa.

The successful treatment of these 2 patients* with Cushing's disease has several important therapeutic implications. First of all, it has been shown that by the use of heavy particles, such as alpha particles and protons, one can teletherapeutically deliver larger amounts of ionizing radiation than can be administered by X-ray or gamma-ray sources. Second, this radiation can be accurately localized to the pituitary gland and delivered with little scatter, thus reducing the danger to surrounding central-nervous-system structures. Third, a favorable skin-depth dose relationship and greater biologic effectiveness can be achieved with these particles than from X rays or gamma rays, owing to a unique property of these penetrating particles referred to as the Bragg peak effect, which provides a Linear Energy Transfer (LET) like that in our original studies with neutrons (1,2). Although the Bragg peak was not employed in the treatment of the cases reported, it has been used in pituitary irradiation in other conditions (14) and provides a means by which the dosage delivered

*A third patient, previously untreated, received heavy particles to the pituitary in May 1963, and is now showing signs of metabolic improvement.

to a desired depth not only is several times greater than the surface dose but also the effect per unit of dose is greater. Finally, it is suggested that these ideal teletherapeutic properties be used further in the treatment of Cushing's disease due to bilateral adrenal hyperplasia. Since cyclotrons and other accelerators capable of delivering heavy particles are available in many medical centers throughout the world (41), the preliminary studies reported here and in our previous papers can be applied widely in investigational and therapeutic studies.

SUMMARY

Recent studies of pituitary and adrenal function as well as a greater awareness of pituitary tumors in patients with bilateral adrenal hyperplasia require that the pituitary gland again be considered primarily in the treatment of Cushing's disease. Two patients, one without a demonstrable pituitary tumor and another with an ACTH-secreting pituitary adenoma, were successfully treated by pituitary irradiation with alpha particles, which were imparted extremely high energies in a large accelerator. These penetrating heavy particles provide a more satisfactory form of teletherapy than X-ray or gamma-ray sources because larger amounts of ionizing radiation can be delivered safely to the sella turcica.

ACKNOWLEDGEMENTS

We are indebted to Dr. Peter Forsham, Director of the Metabolic Unit, University of California Medical Center, and Dr. Laurance Kinsell, Director of the Institute for Metabolic Research, Highland Alameda County Hospital, who referred their patients to us and gave us valuable advice and cooperation in the subsequent study and care of these patients, and also to Dr. Don Nelson, of the University of Southern California School of Medicine, who performed the plasma-ACTH assays.

Supported by the Atomic Energy Commission through the Lawrence Radiation Laboratory.

REFERENCES

1. Lawrence, J. H., and Lawrence, E. O.; Proc. Nat. Acad. Sci. U. S. 22:124, 1936.
2. Axelrod, D.; Aebersold, P. C., and Lawrence, J. H.; Proc. Soc. Expertl. Biol. & Med. 48:251, 1941.
3. Stone, R. S.; Lawrence, J. H., and Aebersold, P. C.; Radiology 35:322, 1940.
4. Stone, R. S.; Am. J. Roentgenol. Radium Therapy 59:771, 1948.
5. Rosahn, P. D.; Tobias, C. A., and Lawrence, J. H.; Am. J. Pathol. 28:37, 1952.
6. Tobias, C. A.; Anger, H. O., and Lawrence, J. H.; Am. J. Roentgenol. Radium Therapy Nucl. Med. 67:1, 1952.

7. Brustad, Tor; in Advances in Biological and Medical Physics, Vol. 8, New York, Academic Press, 1962, p. 161.
8. Sillesen, K.; Lawrence, J. H.; Lyman, J., and Wang, C. C.; this report, p. 139.
9. Storer, J. B.; Harris, P. S.; Furchner, J. E., and Langham, W. H.; Radiation Res. 6:188, 1957.
10. Van Dyke, D., and Janssen, P.; J. Neurosurg. 20:289, 1963.
11. Tobias, C. A.; Lawrence, J. H.; Born, J. L.; McCombs, R. K.; Roberts, J. E.; Anger, H. O.; Low-Beer, B. V. A., and Huggins, C.; Cancer Res. 18:121, 1958.
12. Lawrence, J. H.; Cancer 10:795, 1957.
13. Lawrence, J. H., and Tobias, C. A.; Cancer Res. 16:185, 1956.
14. Lawrence, J. H.; Tobias, C. A.; Born, J. L.; Wang, C. C., and Linfoot, J. A.; J. Neurosurg. 19:717, 1962.
15. Lawrence, J. H.; Tobias, C. A.; Born, J. L.; Sangalli, F.; Carlson, R. A., and Linfoot, J. A.; Acta Radiol. 58:337, 1962.
16. Lawrence, J. H.; Tobias, C. A.; Linfoot, J. A.; Born, J. L.; Gottschalk, A., and Kling, R. P.; Diabetes, the Journal of the American Diabetes Association, in press, 1963.
17. Falkmer, S.; Fors, B.; Larsson, B.; Lindell, A.; Naeslund, J., and Stenson, S.; Acta Radiol. 58:33, 1962.
18. Larsson, B.; Leksell, L., and Rexed, B.; Acta Chir. Scand. 125:1, 1963.
19. Kjellberg, R. N.; Lochler, A. M.; Preston, W. M., and Sweet, W. H.: Biological and clinical studies using the Bragg peak of the proton beam; paper presented at the Second International Congress of Radiation Research, Harrogate, Yorkshire, England, August 11, 1962.
20. Cushing, Harvey; Bull. Johns Hopkins Hosp. 50:137, 1932.
21. Lawrence, J. H., and Zimmerman, H. M.; Arch. Internal Med. 55:745, 1935.
22. Lisser, H.; J. Nervous Mental Disease 99:727, 1944.
23. Tompson, K. W., and Eisenhardt, L.; J. Clin. Endocrinol. 3:445, 1943.
24. Sprague, R. G.; Weeks, R. E.; Prisetly, J. T., and Salassa, R. M.; in Modern Trends in Endocrinology, edited by H. Gardiner-Hill, New York, Paul B. Hoeber, Inc., 1961, p. 84.
25. Glenn, F.; Karl, R. C., and Horwith, M.; Ann. Surg. 148:365, 1958.
26. Nelson, D. H.; Meakin, J. W.; Dealy, J. B., Jr.; Matson, D. D., and Thorn, G. W.; New Eng. J. Med. 259:161, 1958.
27. Salassa, R. M.; Kearns, T. P.; Kernohan, J. W.; Sprague, R. G., and Mac Carthy, C. S.; J. Clin. Endocrinol. 19:1523, 1959.
28. Liddle, G. W.; Island, D., and Meador, C. K.; Recent Prog. in Hormone Res. 18:125, 1962.
29. Montgomery, D. A. D.: Pituitary tumors in Cushing's syndrome; paper presented at the Twelfth Annual Meeting of Congress of Neurological Surgeons, Inc., Houston, Texas, November 1, 1962.
30. Soffer, L. J.; Iannaccone, A., and Gabilove, L.; Am. J. Med. 30:129, 1961.

31. Dohan, F. C.; Raventos, A.; Boucot, N., and Rose, E.; J. Clin. Endocrinol. 17:8, 1957.
32. Lawrence, J. H.; Nelson, W. O., and Wilson, H.; Radiology 29:446, 1937.
33. Gold, E. M.; DiRaimondo, V. C., and Forsham, P. H.; Metab. Clin. Exptl. 9:3, 1960.
34. Luft, R.; Olivecrona, H.; Ikkos, D., and Hernberg, C. A.; Acta Endocrinol. 24:1, 1957.
35. Joplin, G. F.; Fraser, R.; Steiner, R.; Laws, J., and Jones, E.; Lancet 2:1277, 1961.
36. Plotz, C. M.; Knowlton, A. E., and Regan, C.; Am. J. Med. 13:597, 1952.
37. Bishop, P. M. F.; deMowbray, R. R.; Glover, F. N., and Thorne, M. C.; Lancet 2:1137, 1954.
38. Ellis, Frank; Proc. Roy. Soc. Med. 42:853, 1949.
39. Johnsen, S. G.; Acta Med. Scand. 144:165, 1952.
40. Nelson, Don H.; personal communication.
41. Gordon, H. S., and Behman, G. A.; Section 8i, in American Institute of Physics Handbook, 2nd Ed., New York, McGraw-Hill Book Co., 1963, in press.

Preliminary Report on Histopathological Changes in Brain Following Heavy-Particle Irradiation

Larry W. McDonald, James L. Born, John H. Lawrence and John T. Lyman

The effect of ionizing radiation on tissues of the central nervous system has been of increasing interest because of biological investigations with high-energy particles (1). Today the interest in the subject is even greater with the availability in many centers of the world of particle accelerators for medical investigation and therapy (2). High-energy particles have been used for the irradiation of intracranial lesions, the pituitary gland and lesions outside the central nervous system (3). Accelerator-produced neutrons, alpha particles, protons, etc., make possible the delivery of higher radiation doses to intracranial sites, with even less dose exposure to intervening brain tissue than previously experienced with other radiation sources. This report determines the dose-level at which histological changes are produced in the intervening brain following pituitary gland irradiation with heavy particles and the variations in histological changes which occur with different doses at various times after exposure.

The 17 cases reported here were patients with metastatic carcinoma of the breast who received 900-MeV alpha-particle radiation to the pituitary as palliative therapy. The effectiveness of pituitary ablation in palliation of carcinoma of the breast is well established, although it is not yet clear which factors are most important in determining which patients will obtain the best result (4). The methods and techniques used in pituitary irradiation with high-energy particles in these patients have been previously described (5,6). In this method, rotational techniques or rotation plus the Bragg peak are used with the pituitary as the center of the axis of rotation. The maximum dose is therefore at the center of the pituitary, intervening tissues receiving progressively less (7). Attention in the present study is directed to histological changes occurring in those areas of the brain nearest the pituitary. Of particular interest is the uncus and the temporal pole, which are adjacent to the sella turcica and located in the radiation field. The uncus and temporal pole are generally located 1.5 cm lateral to the center of the pituitary. In this group of cases the dose at 1.5 cm lateral to the center of the pituitary ranged from 19 to 46% of the pituitary dose, the variation being due to the difference in size of the radiation beam-defining aperture. The dose values 1.5 cm and 2.1 cm from the center of the pituitary were computed for each individual case and are shown in

Table 1. The dosimetric methods which were employed were those of Birge et al. (8). Isodose curves were computed by simulating the treatment schedule on the IBM 7090 computer. An isodose curve for one representative case is shown in Fig. 1.

MATERIALS AND METHODS

Sections of the temporal lobe were taken from the formalin-fixed brains through the anterior portion of the amygdaloid nucleus and stained with hematoxylin and eosin. Nerve fibers and polysaccharide were stained with Luxol fast blue and PAS, mucopolysaccharide with Alcian blue, and glial fibers with Holzer stain.

In addition, most sections were stained for Nissel substance with cresyl echt violet, for free fat with Sudan black, for nerve-cell processes with an adaptation of a Cajal rapid silver method, for calcium with alizarin red S and for ferric iron with Perls stain. Sections from the same specimen were also taken outside of the radiation field from the hippocampus at the level of the frontal plane including the pineal body. In addition, comparable sections of the temporal lobe of seven patients who died of metastatic breast cancer and received no pituitary irradiation were made and used as a control series. All sections were examined for cysts, necrosis, vessel sclerosis or hyalinization, endothelial proliferation, eosinophilic coagulum, gitter cells, lipid accumulation, PAS positive bodies, eosinophils, large astrocytes, astrogliosis, neuronophagia, satellitosis, demyelination, distended perivascular spaces, blood vessel thrombosis and "vessel wall swelling."

RESULTS

Histological changes occur which appear to have some relationship to the area of the brain receiving the larger amounts of radiation. These are recorded in Table 1. For purposes of comparison the series is divided into five groups according to the amount of radiation received at the surface of the temporal lobe. The lowest dose group is group I which received less than 4 krads to the cortex. The other groups received correspondingly greater doses.

Many PAS positive spheres, most with a laminated structure typical of corpora amylacea, are present in the molecular layer (most superficial layer) of the cortex of controls as well as in the irradiated cases, although generally there seem to be a few more of these bodies in this location in the irradiated cases. Similar PAS-positive bodies are distinctly more numerous in irradiated areas near small blood vessels in the deeper layer of the cortex, the amygdaloid nucleus and especially in the white matter adjacent to the medial and inferior borders of the amygdaloid nucleus. As can be seen from the table this change is marked and correlates well with radiation doses to the temporal-lobe cortex above 5.5 krads, except when frank necrosis develops.

Table 1

Case No.	Age	Sex	Dose 1.5 cm lateral to center of pituitary krads/days	Dose 2.1 cm lateral to center of pituitary krads/days	Pituitary dose krads/days	Survival Post-rad (days)	Necrosis	Small vessel wall swelling	Lipid accumulation	Demyelination	Alcian blue PAS positive bodies	Astrogliosis	Other significant disease
Group I < 4 krads.													
1	48	F	2.5/5	1.2/5	14.0/5	30	0	0	-	1	1	2	Some NIII signs not due to radiation
2	44	F	2.7/5	1.3/5	14.0/5	30	0	0	-	1	2	1	Extensive metastases especially to bone
3	48	F	3.1/5	1.5/5	17.0/5	82	0	2	1	0	1	1	Extensive metastases
4	54	F	3.2/5	1.6/5	17.0/5	203	0	0	0	0	0	0	None significant
5	64	F	3.7/12	1.8/12	17.0/12	127	0	2	1	0	1	1	Extreme weakness
Group II 4-5 krads.													
6	31	F	4.2/11	2.1/5	17.0/11	222	0	0	1	2	0	2	Muscle weakness
7	50	F	4.6/11	2.3/11	17.0/11	108	0	0	1	1	0	2	Extensive lung, cerebral metastases
8	47	F	4.7/12	2.3/12	17.0/12	301	0	2	2	3	1	1	Small cerebellar metastases
Group III 5.0-5.5 krads.													
9	58	F	5.1/11	2.5/11	18.6/11	577	0	0	2	3	2	2	Extensive metastases to bone, Thrombosis of lt. middle cerebral artery.
Group IV 5.5-9.0 krads.													
10	53	F	5.6/12	2.8/12	17.0/12	136	0	1	2	1	3	2	Extensive metastases, one cerebral
11	52	F	6.1/21	3.0/21	27.0/21	1722	+	0	2	3	1	2	Transient NIII changes
12	62	M	6.4/10	3.2/10	18.6/10	428	0	1	2	1	3	1	Extensive metastases to bone
13	52	F	6.8/5	3.4/5	17.5/5	102	0	2	2	0	3	2	Extensive osseous and cutaneous metastases
14	60	F	7.5/12	3.7/12	30.6/12	1371	+	1	3	3	2	2	No cranial nerve weakness
15	47	F	7.8/12	3.9/12	17.0/12	324	0	1	2	3	3	1	Extensive metastases
Group V > 9.0 krads.													
16	52	F	9.3/11	4.6/11	22.8/11	781	0	1	2	2	3	1	None significant
17	76	F	14.2/11	7.1/11	34.7/11	1261	+		Inadequate fixation				Clinical evidence of NII, NIII, NIV, NVI damage
Controls													
1	49	F					0		1	0	1	0	
2	61	F					0		0	0	2	0	
3	58	F					0		1	0	0	0	
4	55	F					0		0	0	1	0	
5	76	F					0		1	1	1	0	
6	39	F					0		0	0	1	0	
7	37	F					0		1	0	1	0	

Code for Grading

Necrosis
- 0 - none
- + - present

Small vessel wall swelling
- 1 - equivocal
- 2 - definite
- 3 - marked

Lipid accumulation
- 1 - limited to gitter cells about blood vessels, occasional vessel with 1 to 6 cells.
- 2 - As (1) but with greater than 6 gitter cells about occasional vessels.
- 3 - All vessels with 1 or more gitter cells.
- 4 - Lipid in gitter cells away from vessels plus (2) above.

Demyelination
- 0 - none
- 1 - slight relative decrease in myelin stain, limited perivascular.
- 2 - distinct loss in myelin stain, limited perivascular.
- 3 - extending beyond perivascular areas.

PAS and Alcian blue positive bodies in white matter adjacent to inferior and medial border of amygdaloid nucleus.
- 0 - none
- 1 - 2 to 5 about occasional vessel.
- 2 - 5 or more about most vessels.
- 3 - as in (2) plus many between vessels.

Astrogliosis
- 0 - none
- 1 - slight relative
- 2 - definite absolute

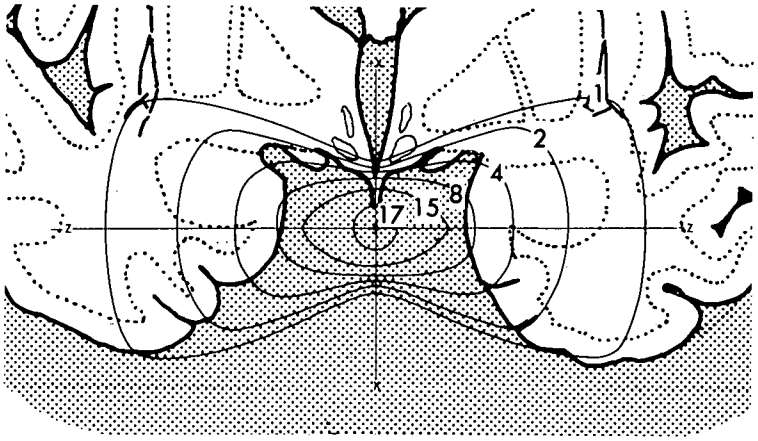

Figure 1. Isodose lines for case No. 13. The numbers on the lines refer to the krad dose along the line.
MU-32051

Demyelination occurs regularly in cases surviving more than 225 days following irradiation and receiving a dose of 4.7 krads (case 8) or more to the surface of the uncus.

No correlation can be made between vessel hyalinization or sclerosis and radiation in those cases where there is no necrosis (not tabulated in Table 1). In some instances, however, where death occurred less than a year after irradiation, there appears to be some swelling of the walls of small arterioles with more clear or lightly staining area between nuclei, but this is not consistently observed. Astrogliosis or better staining of astroglia in the group with survival between 100 and 225 days is noted but does not correlate well with radiation dose. These changes are shown in Fig. 2 and 3.

Three of the 17 cases showed frank necrosis. These were two cases of group IV and one of group V of Table 1; all received a pituitary dose of more than 25 krads, and more than 6.0 krads to the cortex. All are long survivals of between two and a half and four years following irradiation. There appears to be no selective necrosis of white matter. The necrosis is present in the areas of maximum dose involving the inferior portion of the uncal cortex, the cortex of the temporal pole, amygdaloid nucleus and the white matter immediately adjacent to the inferior and medial border of the amygdaloid nucleus (Fig. 4). The extent of the necrosis is least in case 11, a small cystic defect 0.5 cm in diameter being present on the right side and a small area of hemorrhage on the left. In case 14 there is a distinct cavity filled with a grossly tan translucent gelatinous material. Fig. 5 is a photograph of the gross specimen of case 14.

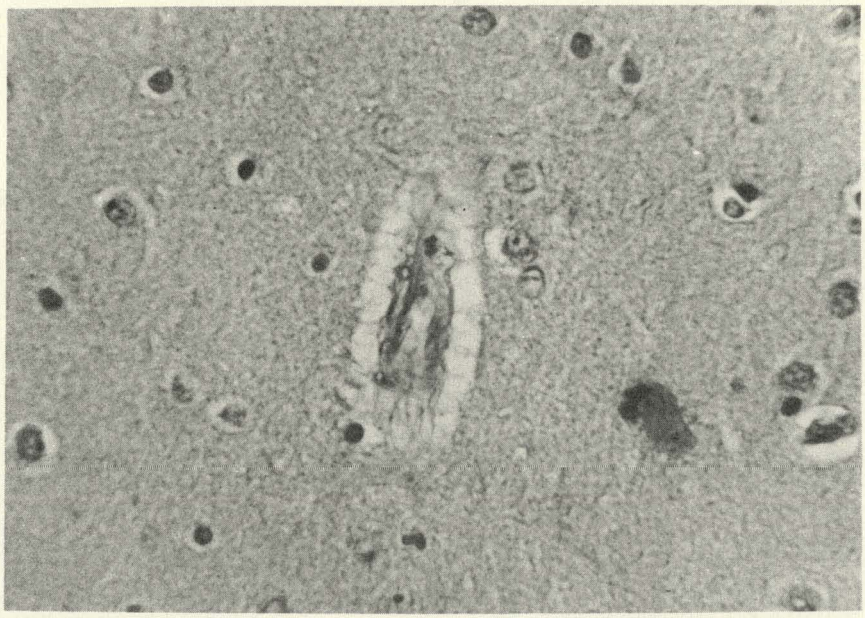

Figure 2. Small arteriole from uncal cortex showing swelling of vessel wall with increase in light staining areas between nuclei of muscular wall. X400 H&E stain. Case No. 13.

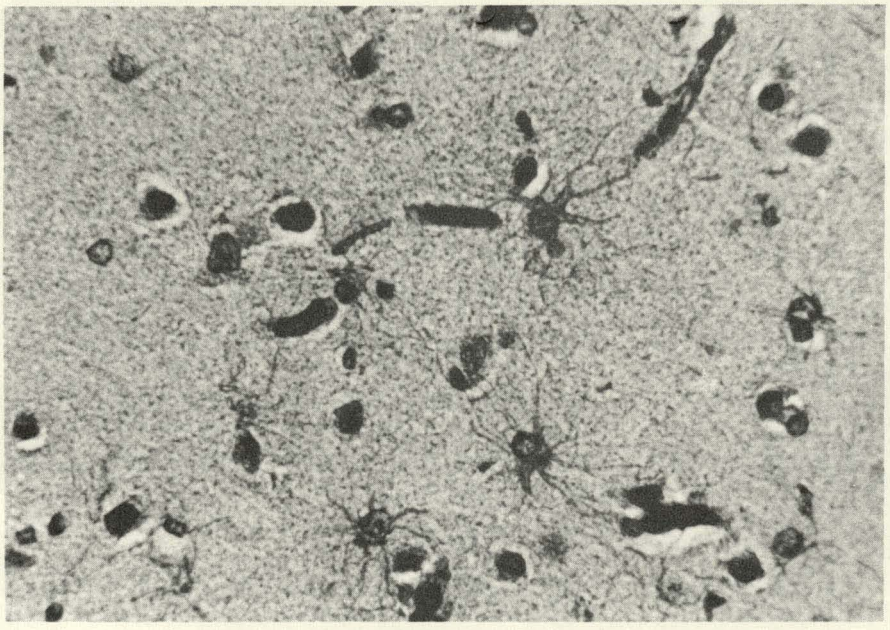

Figure 3. Area of amygdaloid nucleus showing increase in number of stainable fibrillary astrocytes. X400 Holzer stain. Case No. 10.

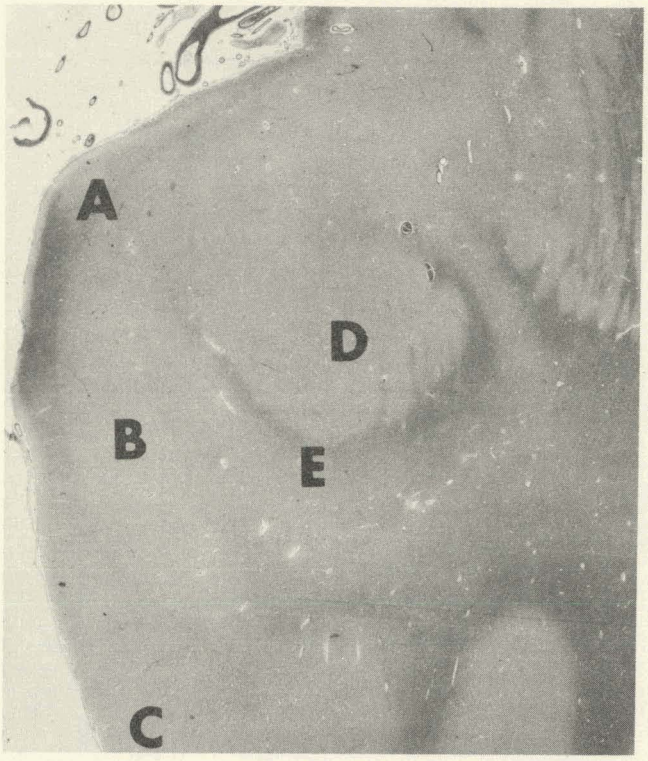

Figure 4. Section through anterior portion of amygdaloid nucleus showing more macroscopic features. "A" is the superior portion of the cortex of the temporal pole, "B" the middle portion, and "C" the inferior portion. "D" is the amygdaloid nucleus. "E" is the white matter along the inferior and medial border of the amygdaloid nucleus which showed markedly increased numbers of PAS positive bodies in cases No. 10, 12, 13, 15 and 16. In these five cases area "B" received 5.6 to 9.3 krads and area "E" about 5 krads. X4 H&E stain.

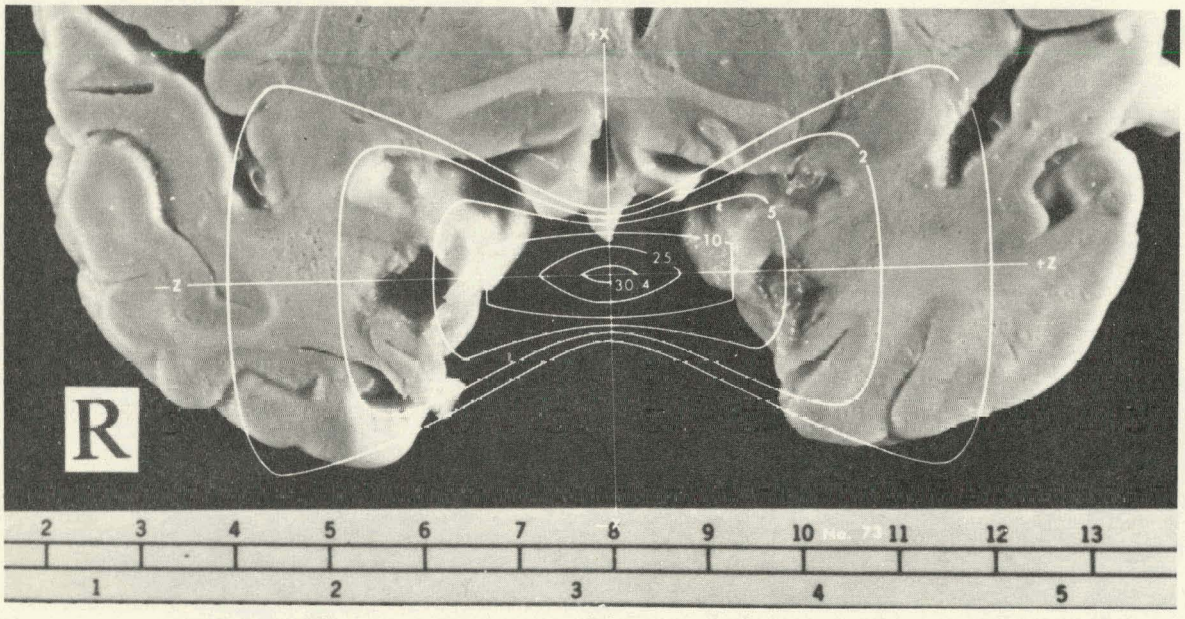

Figure 5. Photograph of gross specimen showing cystic area of necrosis involving the cortex of the temporal pole and adjacent underlying tissue. Bilateral depression of the temporal poles following necrosis has resulted in a shift of the center of the area of involvement from between 10- and 5-krad lines to between 5- and 2-krad lines. Case No. 14

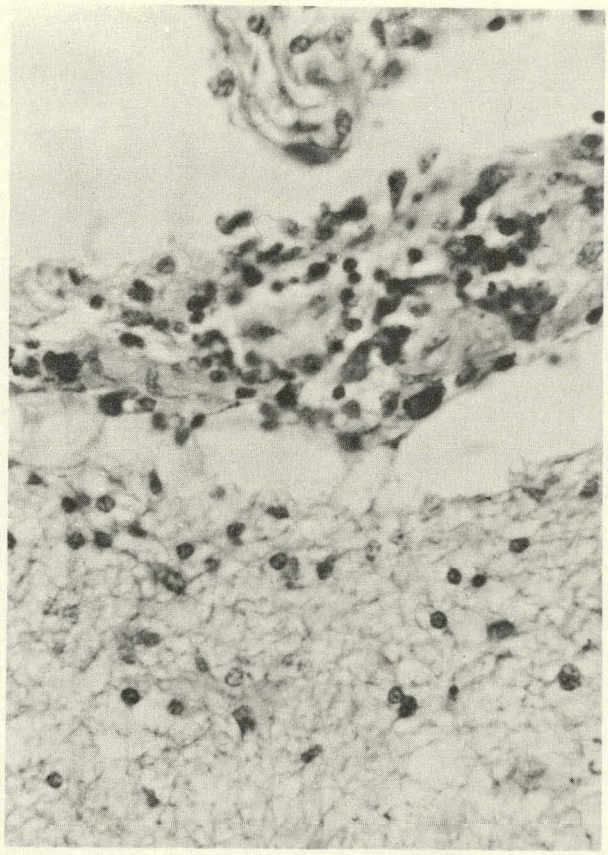

Figure 6. Photomicrograph of wall of cystic area of necrosis. The contents of the cystic area of necrosis have mostly been lost from the section at the top of the photograph, although a few round cells in the loose palely basophilic network of fibers can be seen (zone 1). The eosinophilic coagulum (zone 2) is not present in this field. The intermeshing fibers with round cells forming the wall of the cyst are seen across the central part of the photograph. At the bottom of the photograph the more compactly arranged fibers are seen (zone 3). X400 H&E stain. Case No. 14.

Microscopically the central cavity of the area of necrosis contains a few scattered round cells in a loose palely basophilic network of fibers. At several points along the edge of the cystic space there are lakes of eosinophilic coagulum with a glassy homogeneous appearance and a few vacuoles. This material is PAS positive and generally Alcian blue negative. Most walls of the cystic cavity consist of loosely arranged, poorly staining, intermeshing fibers in which small round cells, presumably lymphocytes, are focally abundant (Fig. 6). Next, peripheral to this, is a layer in which there are ghost outlines of blood vessels, often with thickened walls. In this area the fibers are more compactly arranged and sometimes continuous with the zone of intense astrogliosis which is located next peripherally. Here the walls of blood vessels, particularly small arterioles, show increase in poorly staining area between nuclei. Small round cells are often found in the perivascular space (Fig. 7), and abundant PAS positive bodies (Fig. 8). Astrocytes with numerous processes are seen in this zone and extend peripherally. Many of these astrocytes have large vesicular nuclei. The astrogliosis extends furthest peripherally in the white matter, but this appears related to secondary degeneration of axis cylinders. Four subdivisions of the areas of cystic necrosis may be recognized proceeding from the center peripherally as follows:

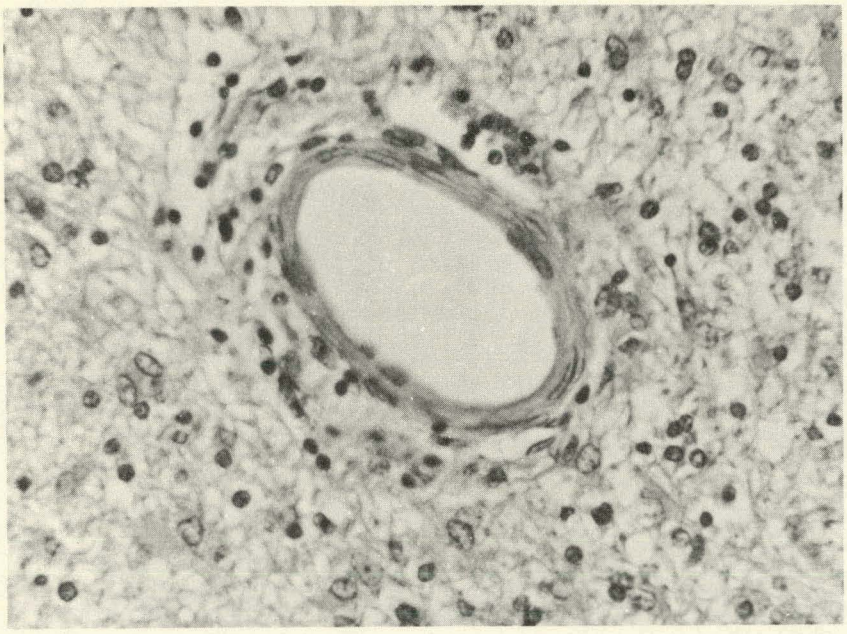

Figure 7. Small arteriole from tissue near necrosis (zone 4). Infiltration of adjacent areas by small round cells is moderate. X400 H&E stain. Case No. 14.

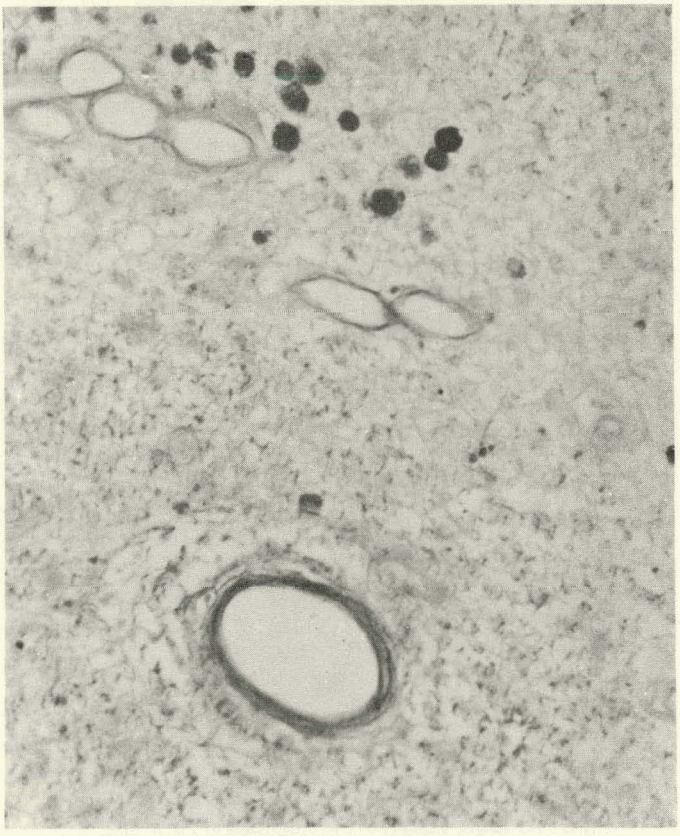

Figure 8. Photomicrograph of tissue near area of necrosis (zone 4). Bodies, which are morphologically corpora amylacea and PAS positive, are shown near small blood vessels, presumably veins, at the top of the photograph. X230 Luxol fast blue - PAS stain. Case No. 14.

1. Central cavity containing an occasional round cell in a very loose palely basophilic network of fibers (zone 1).
2. Focal lakes of eosinophilic coagulum along the edges of the central cavity (zone 2). This coagulum is Alcian blue negative.
3. Zone 3 consists of poorly staining fibers in which round cells may be focally collected. In addition there are occasionally groups of typical gitter cells here. More compactly arranged fibers, in which ghost outlines of blood vessels can be seen, make up the more peripheral part of this zone. A few astrocytes are recognizable here. This zone is 100 to 300 μ thick.
4. In zone 4, astrogliosis is intense centrally. Round-cell infiltration about arterioles is often present. PAS and Alcian blue positive bodies are present near some small veins. Zone 4 is 0.5 mm to 4 mm thick.

Case 11 has poor differentiation between zones 1 and 2, the area of necrosis being so small. In case 14 there are plasma cells in the layer of pia-arachnoid which folds into some areas of the cystic cavity.

The pia-arachnoid generally remains intact although infiltrated by round cells. It was located in an area of greater radiation exposure than the underlying cortex and white matter that have undergone necrosis. A small part of the molecular layer of the cortex often remains in continuity with the pia. PAS and Alcian blue positive bodies are abundant in this remaining superficial layer of the cortex.

In this series of cases, pituitary irradiation was fractionated over a period of time. In three of the four cases in group I the irradiation was given in three increments over a 5 day period. In all of the cases in the remaining groups the irradiation was given over an interval of 10 to 12 days with the exception of cases 11 and 13. From the broad groups of cases studied here no differences can be observed that appear related to the number of days over which the irradiation was given. This may be due to the short post-irradiation survival of some of these patients.

DISCUSSION

In 1943 when Warren (9) reviewed the early experimental work on irradiation of the brain it appeared that the nervous system was resistent to radiation doses below about 5,000 rads. During the 20 years since then, many experiments with improved dosimetry have shown that this resistance is relative and not absolute. In the more recent review by Zeman (10) it is stated that between 1,000 and 3,000 r are necessary to produce delayed necrosis of brain affecting interstitial elements. These latter doses were based on experiments in which large areas of animal brain were irradiated.

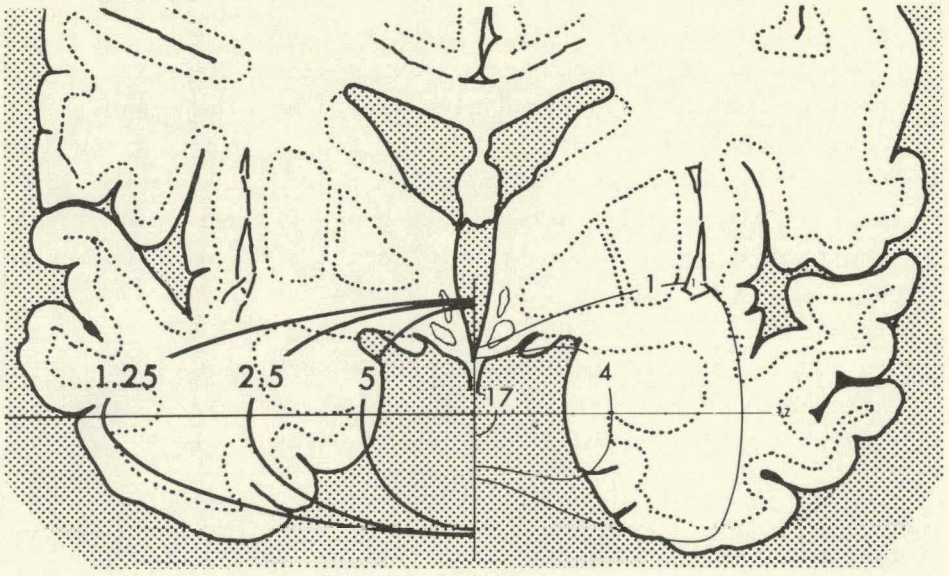

Figure 9. Isodose curves for alpha-particle irradiation (right) to the pituitary compared to supervoltage X ray (left, vertical rotation, circular field 5 cm in diameter, 2 MeV). MUB-2117

In the present study only small areas of brain received any significant radiation exposure. Using alpha-particle radiation and rotational techniques the isodose lines are spaced very closely so that the decrease in dose is very sharp. Thus the dose at the medial surface of the temporal pole falls to half at the distance of 0.6 cm further lateral (amygdaloid nucleus), (Fig. 4). Fig. 9 shows isodose curves for 2-MeV moving-field X-ray to the pituitary superimposed upon those for alpha-particle irradiation. The marked differences in dose distribution explain the more widespread diffuse necrosis observed by Crompton and Layton (11) in their study of delayed radionecrosis of the brain following pituitary irradiation for acromegaly. The six cases of group IV with doses to the cortex above 5.5 krads all have many PAS and Alcian blue positive bodies about small blood vessels unless there is frank necrosis. Similar bodies have been noted in increased numbers about blood vessels in irradiated rat brains (12) and monkey brains (13). Although not indicated in Table 1, there is some granular PAS positive material in some of the gitter cells of the remaining uncal cortex of the cases which have the frank necrosis. An occasional astrocyte in the cortex contains some similar material, but the neuroglial cells of the white matter contain none of this material. The material in gitter cells about blood vessels in the white matter is not stained by the PAS reaction, but does stain for free fat with Sudan black or oil red O.

The increase in the number of the PAS positive bodies and demyelination are the only changes, besides the delayed necrosis, that correlate well with radiation dose.

Some of these bodies have the typical glassy laminated appearance of corpora amylacea. Many others, however, are more homogeneous and translucent, often with more irregular globular borders. These latter bodies are often between 5 and 15 μ in diameter, much smaller than typical corpora amylacea, which are 15 to 30 μ in diameter. It is believed that corpora amylacea are formed by degeneration of astrocytes (14). In the material of this study there appear to be occasional transitional stages between astrocytes containing a great deal of PAS positive material and slightly laminated PAS positive spheres, which are typical corpora amylacea.

Among the 17 cases there was increase in the number of stainable astrocytes and their processes with a dose of more than 4.2 krads to the cortex and a survival less than 300 days. The gliosis of the amygdaloid nucleus was greater than or equal to that found in the grey matter in sections through the posterior part of the hippocampus of the same brain. This mild gliosis with doses above 4.2 krads has also been noted in some of the histological sections from earlier cases not included here. The same degree of gliosis, however, can be seen when cerebrovascular disease is severe.

The "vessel wall swelling" appeared limited to the area of radiation, but did not have any correlation with dose or survival following irradiation. Astrocytes with large swollen nuclei were observed in two cases (No. 9 and No. 10). Large astrocytes were numerous in the gliosis surrounding the areas of frank necrosis in the cases of Group IV and V.

Janssen et al. (15) found changes in both neurons and astrocytes at a Bragg-peak dose of about 9.0 krads of alpha particles in rats. At a Bragg-peak* dose of about 4.5 krads, these investigators believed a definite loss of some nerve cells and fading of others took place. Fig. 10 from case No. 14 shows apparently intact nerve cells only 500 μ away from the area of frank necrosis. Some decrease in the number of dendritic processes of the nerve cells appears to be present, but this is difficult to evaluate because of the great variation of the collections of neurons into small groups in this area of the cortex. Although it has been assumed in the preceding discussion that the dose delivered to the surface of the temporal lobe (molecular layer of cortex) is the dose effective in producing changes, this approximation is probably higher than the actual effective dose. The dose received by the internal pyramidal layer at a distance of about 3 mm from the surface is only about 75% of the surface dose. This would mean that case No. 15, which has an estimated dose of 7.8 krads at the surface of the cortex, would have 5.8 krads at the internal pyramidal layer. This brings the dose received for all cases except those of group V close to

*The Bragg-peak portion of the ionization produced in tissue has a greater relative biologic effect due to higher linear energy transfer (16, 17).

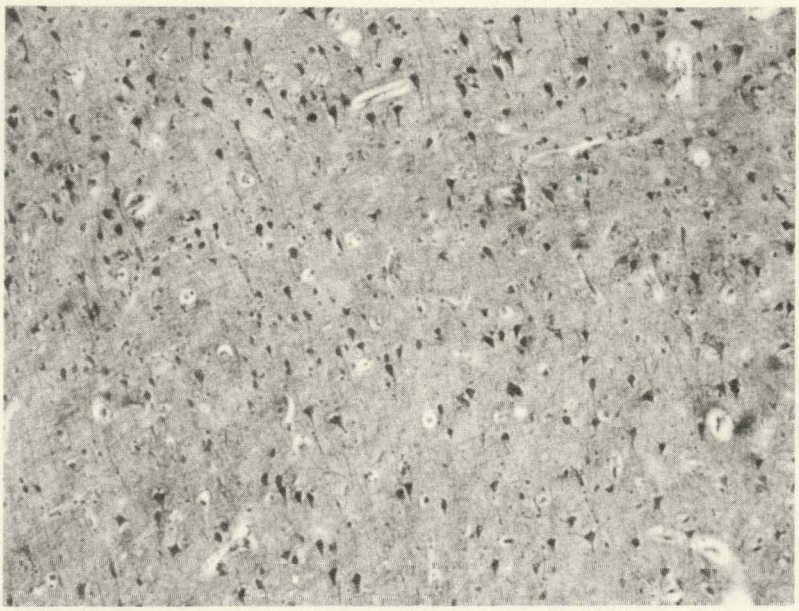

Figure 10. Photomicrograph of area located 500 μ from the frank necrosis (outer zone 4). The necrosis was to the left of this field. Axons appear intact although dendrites appear reduced in number. X100 Silver impregnation for nerve cell processes by a modified Cajal technique. Case No. 14.

that responsible for the earliest nerve cell changes, as seen in the rat by Janssen et al. (15).

The presence of increased numbers of PAS positive bodies or corpora amylacea, astrogliosis and the swelling of vessel walls all indicate the vascuo-astrocytic unit as the histological component of brain most vulnerable to radiation damage. Others have come to similar conclusions (18). Whether the effect is on the vessel wall with secondary effects on the astrocyte through their foot plates or primarily on the astrocyte is not determined.

Several of the cases in this group had shown clinical signs of cranial nerve damage. (As noted in reference (7) the doses now used no longer result in the cranial-nerve or temporal-lobe complications.) Case No. 1 had vague ocular symptoms more suggestive of a Horner's syndrome due to tumor metastases rather than due to radiation cranial nerve damage. Examination by our ophthalmologist failed to show any evidence of cranial nerve damage. Case No. 11 had some transient but well substantiated evidence of oculomotor nerve damage. This case had some frank necrosis in the temporal lobes. Case number 17 had very extensive and permanent clinical evidence of cranial nerve damage. Symptoms consisted of blurring of vision, double vision and then loss of vision in the left eye. On

examination there was ptosis of the left eyelid, loss of all extraocular movements except for lateral rectus function, and paralysis of the pupils; these changes were most marked and appeared earliest on the left, at two months following irradiation. There was necrosis in both temporal lobes of the autopsy specimen of case 17.

Symptoms attributable to lesions in the temporal lobe of the brain are difficult to evaluate and are usually vague. One patient (case No. 14) developed severe episodes of inattention suggestive of what is sometimes described as a Kluver-Bucy syndrome, but these episodes gradually abated. There was some frank necrosis in the temporal lobe of this case. The other two cases showing necrosis in the temporal lobe had no symptoms attributable to the lesion.

In none of these cases was clinical evidence of cranial nerve damage present without necrosis being found in the temporal lobes. Clinical signs and symptoms of oculomotor nerve damage have been transient, but necrosis has been found to involve a small area of the temporal pole in the autopsy specimen. However, when persisting signs of cranial nerve damage from radiation are present, necrosis is always found in the temporal pole in this preliminary series of 17 cases.

The presence of many lymphocytes about vessels and around the area of necrosis suggests a tissue-graft reaction. This could be accounted for on the basis of a breakdown of the blood brain barrier with exposure to normally isolated tissue components (especially lipoproteins) to the immunologically competent cells of the body. The histopathological findings of delayed radionecrosis of brain have suggested a similar mechanism to other observers (10).

SUMMARY

In studies of histopathological changes in brain after heavy-particle irradiation, the following observations were made:

1. The threshold for observable radiation change in the cerebrum was about 4.0 krads in 11 days of alpha-particle irradiation in a series of 17 cases. Better correlation was found with an exposure of more than 5.5 krads.

2. The changes at the dose levels of 4 to 9 krads in 11 days appear related to alterations in the vasculoastrocytic unit, with early swelling of cells of the vessel walls, particularly of the small arterioles. Astrogliosis was seen early but was not a prominent feature. Increase in the number of PAS positive bodies was noted with a 5.6- to 9-krad exposure.

3. No definite change could be noted in the nerve cells in the dose range of 4 to 9 krads.

A graft rejection type reaction is suggested to account for the delayed necrosis of brain which occurred at doses above 6.0 krads with a survival of over 1,000 days.

ACKNOWLEDGEMENTS

The authors wish to thank Mr. John Sabatini and Mrs. M. Winnogene Palmer for preparing the many sections of tissue for microscopic examination in this study.

REFERENCES

1. Tobias, C. A.; Anger, H. O., and Lawrence, J. H.; Am. J. Roentgenol. Radium Therapy Nucl. Med. 67:1, 1952.
2. Gordon, H. S., and Behman, G. A.; in Section 8i, American Institute of Physics Handbook, 2nd Ed., New York, McGraw-Hill Book Co., 1963, in press.
3. Lawrence, J. H.; Tobias, C. A.; Born, J. L.; Gottschalk, A.; Linfoot, J. A., and Kling, R. P.; J. Am. Med. Assoc., 1963, in press.
4. McCalister, A.; Welbourn, R. B.; Edelstyn, G. J. A.; Lyond, A. R.; Taylor, A. R.; Gleadhill, C. A.; Gordon, D. S., and Cole, J. O. Y.; Brit. Med. J. 1:613, 1961.
5. Lawrence, J. H., and Tobias, C. A.; Cancer Res. 16:185, 1956.
6. Tobias, C. A.; Lawrence, J. H.; Born, J. L.; McCombs, R. K.; Roberts, J. E.; Anger, H. O.; Low-Beer, B. V. A., and Huggins, C.; Cancer Res. 18:121, 1958.
7. Lawrence, J. H.; Tobias, C. A.; Born, J. L.; Wang, C. C., and Linfoot, J. A.; J. Neurosurg. 19:717, 1962.
8. Birge, A. C.; Anger, H. O., and Tobias, C. A.; in Radiation Dosimetry, edited by G. J. Hine and G. L. Brownell, New York, Academic Press, 1956.
9. Warren, S. ; AMA Arch. Pathol. 39:109, 1943.
10. Zeman, Wolfgang; in Fundamental Aspects of Radiosensitivity, Brookhaven Symposium in Biology, No. 14, 1961.
11. Crompton, M. R., and Layton, D. L.; Brain 84:85, Part I. March, 1961.
12. Brightman, M. W.; Exptl. Neurol. 1:97, 1959.
13. Pitcock, J. A.; J. Neuropathol. Exptl. Neurol. 22:120, Jan., 1963.
14. Hicks, S. P., and Warren, S.: Introduction to Neuropathology, New York, McGraw-Hill Book Company, Inc., 1950, p. 34.
15. Janssen, P.; Klatzo, I.; Miquel, J.; Brustad, T.; Behar, A.; Haymaker, W.; Lyman, J.; Henry, J., and Tobias, C.: Proceedings of an International Symposium held at Northwestern University Medical School, Sept. 7-9, 1960, edited by T. J. Haley and R. S. Snider, New York, Academic Press, 1962, p. 383.
16. Lawrence, J. H., and Lawrence, E. O.; Proc. Nat. Acad. Sci. 22:124, 1936.
17. Sillesen, K.; Lawrence, J. H., and Lyman, J.; this report, p.139.
18. Clemente, C. D., and Richardson, H. E., Jr.: Proceedings of an International Symposium held at Northwestern University Medical School, Sept. 7-9, 1960, edited by T. J. Haley and R. S. Snider, New York, Academic Press, 1962, p. 411.

Modification of Radiation Effects with Magnetic Fields

Nabil M. Amer

The results of many attempts to find effects of magnetic fields are controversial. In the current paper the author demonstrated the modifying effect of a constant magnetic field on the course of wing development of Tribolium confusum.

In 1961, Amer et al. (1,2,3,4) reported the finding of existing synergistic action between relatively elevated temperatures and X irradiation in the induction of wing abnormality in the course of development of Tribolium confusum. The spontaneous incidence of wing abnormality when the pupae are incubated at 30°C is 1.5% ± 0.5. Incubation at 38°C results in 4.5% ± 1.5 incidence of such deformities (5). However, in the present study it was found that pupae incubated at 38°C in a magnetic field of 3.6 kG exhibit only 2.7% ± 0.9 wing abnormality in the adult stage (Table 1). It was therefore of interest to study the behavior of synergism, i.e., X irradiation combined with elevated temperatures, when magnetic fields were superimposed on such a condition.

Pupae of Tribolium confusum were irradiated with 1,200 r of 250 kVp X rays (1,000 r/min). Seven minutes after irradiation, one group of the irradiated animals was placed in glass vials between the poles of a permanent magnet with a field intensity of 3.6 kG; the animals were in the uniform and constant portion of the field. The other group was placed between the poles of a dummy magnet of the same geometry and served as control. Both groups were incubated, in the same incubator, at 38°C ± 0.5. After seven days, the adults that emerged were removed from the magnetic field, and the number of wing abnormalities was counted. The results are given in Table 2. The experiment was repeated six times.

In order to study the effect of variations of the intensity of the magnetic field, pupae were irradiated with 1,200-r X rays of the specifications mentioned above and incubated at 38°C in a magnetic field of 2.2 kG. The results are shown in Table 3. The effect of a given magnetic intensity as a function of dose was studied when this experiment was repeated with a dose of 1,350 r. It was interesting to find that the increase in the dose administered resulted in a decrease in the degree of modification of this particular

Table 1. 3.6 kG + 38°C

Treatment	Normal	Abnormal	Molting failure	% Abnormal
B*	207	6	9	2.7% ± 0.9
Control	221	11	14	4.5% ± 1.5

*B is the magneto-treated group.

Table 2. 3.6 kG + 38°C + 1,200 r

Treatment	% Normal	% Abnormal	Number of animals
B	54.8 ± 8.7	45.2 ± 9.2	634
Control	18.9 ± 7.3	81.1 ± 10.5	551

Table 3. 2.2 kG + 38°C + 1,200 r

Treatment	% Normal	% Abnormal	Number of animals
B	44.3 ± 6.8	55.3 ± 8.3	332
Control	16.0 ± 9.4	83.1 ± 8.9	319

Table 4. 2.2 kG + 38°C + 1,350 r

Treatment	% Normal	% Abnormal	Number of animals
B	15.0 ± 4.8	85.0 ± 5.4	296
Control	0.9 ± 0.05	99.1 ± 0.6	278

Table 5. 9.7 kG + 30°C + 1,500 r*

Treatment	% Normal	% Abnormal	Number of animals
B	50.1	49.9	203
Control	38.7	61.3	225

*Results from one experiment only.

radiation effect when compared with the degree of modification at 1,200 r. (Table 4).

The next step was to find whether the modifying effect obtained with magnetic fields holds for incubation at optimal temperature (30°C), i.e., investigating the effect of magnetic fields outside the region of synergism. The above mentioned experiments were repeated with the same parameters, with the exception that incubation was at 30°C instead of 38°C. Neither of the experiments showed any statistically different behavior from that of the corresponding control.

However, pupae treated with 1,500 r of X rays were divided into two groups. One group was incubated at 30°C in a magnetic field of 9.7 kG; the other group was incubated at the same temperature between the poles of a dummy magnet of the same geometry as the 9.7-kG magnet. The results are given in Table 5. This experiment was performed only once, but the author intends to repeat it.

In all experiments, it was noticed that the wing abnormality in the group exposed to the magnetic field was of a lesser degree of intensity in comparison with the deformed wings of the control group. From the data obtained, the following conclusions could be made:

1. At a given temperature and X-ray dose, a higher magnetic field produced relatively greater protective effect.

2. Magnetic field has a significantly decreasing effect on spontaneously occurring wing abnormality at 38°C but not at 30°C, where very few abnormalities are found.

3. Post-irradiation protection by magnetic fields is much more marked at 38°C than at 30°C. At 38°C the effect was significant at 2.2 and 3.6 kG and at each X-ray level tested; whereas, at 30°C the 2.2-and 3.6-kG pupae exposed to radiation did not show any effect at all. However, there was a small protective effect at the field of 9.7 kG.

We conclude from this that post-irradiation magnetic field protection is most effective where synergism between X ray and temperature occurs. It is possible that the protection acts not on the primary X-ray lesions, but on its development by temperature. A detailed study involving metastable states, free radicals, and solid-state effects is planned in order to arrive at a possible explanation for these findings which are statistically significant.

ACKNOWLEDGEMENTS

The author wishes to acknowledge the stimulating discussions with Professors Cornelius A. Tobias and John V. Slater. He would also like to thank Drs. Howard G. Parker and Donald Van Dyke for providing the 3.6-kG magnet.

This work was supported jointly by the United States Atomic Energy Commission and the National Aeronautics and Space Administration.

REFERENCES

1. Amer, N. M., and Slater, J. V.; Lawrence Radiation Laboratory Report UCRL-9897 1961.
2. Amer, N. M., and Slater, J. V.; Nucl. Sci. Abstr. 16:1258, 1962.
3. Amer, N. M.; Slater, J. V., and Tobias, C. A.; Radiation Res. 16:574, 1962.
4. Amer, N. M., and Slater, J. V.; Science, in press.
5. Slater, J. V.; Rescigno, A.; Amer, N. M., and Tobias, C. A.; Science 140: 408, 1963.

Multicompartment Interpretation of Radiation-Damage Curves

Aldo Rescigno

If a population of cells is exposed to a dose r of radiation, a number of them shows a certain effect. By increasing the dose from r to r + dr and by observing only that particular effect, the fraction of cells affected by the radiation is increased by the quantity $x(r)dr$, where $x(r)$ is a function of r, defined and continuous in the interval $0 \leq r < +\infty$. The fraction of cells cumulatively affected by a dose r is $\int_o^r x(\rho)d\rho$; as

$$1) \qquad \lim_{r \to \infty} \int_o^r x(\rho)d\rho = 1,$$

the fraction of cells saved by the same dose r is $\int_r^\infty x(\rho)d\rho = 1 - \int_o^r x(\rho)d\rho$. If the number of cells affected by an infinitesimal increase dr of the dose is proportional not only to dr, but even to the number of nonaffected cells, we say that the cells are formed, in respect to the particular effect we are observing, by one compartment (1).

Therefore a compartment is a system such that the equation

$$2) \qquad x(r)dr = K \left[1 - \int_o^r x(\rho)d\rho\right] dr$$

holds.

Solving equation 2) with condition 1), one obtains

$$3) \qquad x(r) = K e^{-Kr}.$$

We can suppose a cell formed by two compartments 1 and 2, the partial damage in each of them being described by the equations

$$x_1(r)dr = K_1 \left[1 - \int_o^r x_1(\rho)d\rho\right] dr,$$

$$x_2(r)dr = K_2 \left[1 - \int_o^r x_2(\rho)d\rho\right] dr,$$

identical to equation 2) of the one-compartment cells; furthermore the damage to the whole cell may be the result of

a) both compartment 1 AND compartment 2 being affected;
b) either compartment 1 OR compartment 2 being affected.

The structure of the cell of the type a) can be represented by the symbol 1A2; the structure of the cell of the type b) can be represented by the symbol 1V2 (V stands for VEL = OR).

The damage to a cell with the structure 1A2 is described by the expression

$$4) \qquad x_{1A2}(r)dr = [\int_o^r x_1(r-\rho)x_2(\rho)d\rho]\ dr;$$

the damage to a cell with the structure 1V2 is described by the expression

$$5) \qquad x_{1V2}(r)dr = x_1(r)dr + x_2(r)dr - [\int_o^r x_1(r-\rho)x_2(\rho)d\rho]\ dr.$$

From the expressions 4) and 5) we can deduce that the structures 1A2 and 2A1 are equivalent, and so are the structures 1V2 and 2V1.

We can now suppose a cell formed by three compartments. These structures are possible:

(1A2)A3	(1A3)A2	(2A3)A1
(1A2)V3	(1A3)V2	(2A3)V1
(1V2)A3	(1V3)A2	(2V3)A1
(1V2)V3	(1V3)V2	(2V3)V1

But some of them are equivalent; so the only different structures with three compartments are:

1A2A3

(1A2)V3	(1A3)V2	(2A3)V1
(1V2)A3	(1V3)A2	(2V3)A1

1V2V3

By increasing the number of compartments, the number of structures increases very rapidly.

A convenient way to represent the structure of a cell is by means of an oriented graph (2). Each compartment is represented by an arrow; two compartments connected by the operation A are represented by connecting the terminal point of an arrow to the initial point of the other arrow, the order of the two arrows being irrelevant; two compartments connected by the operation V are represented by connecting the two initial points and, separately, the two terminal points. The groups of two arrows so obtained are treated as single arrows and are combined again, and so are the groups of three or more arrows, until a single group, with one initial point and one terminal point, is obtained.

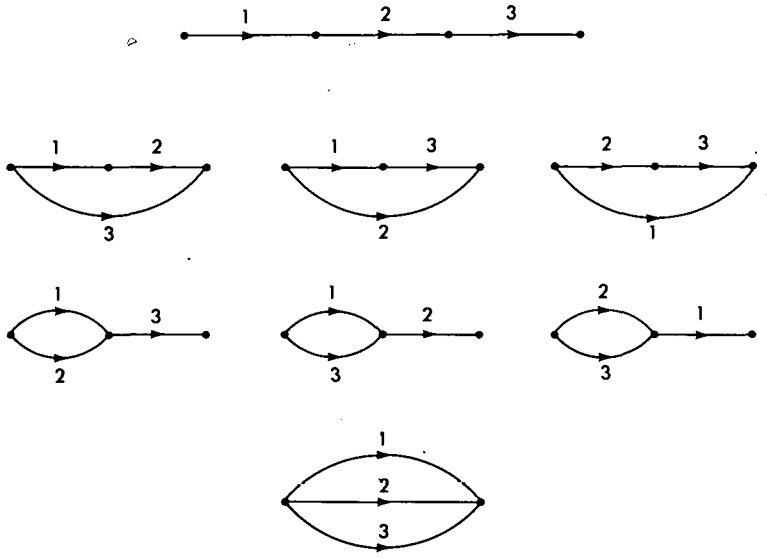

Figure 1. Graphs of all possible three-compartment systems. MU-31344

For example, the three-compartment structures listed before are represented by the graphs of Fig. 1.

In a graph, a path is defined as a succession of arrows, such that the initial point of the first arrow is the initial point of the graph, the initial point of each of the other arrows is the terminal point of the preceding arrow, and the terminal point of the last arrow is the terminal point of the graph.

For instance, the graph of Fig. 2, representing the seven-compartment system {[(aAb)V(dAeAf)]Ac}Vg, has three different paths: g, a-b-c, d-e-f-c.

From the definition of path, the rule follows:
A system is affected when at least all compartments corresponding to a path of its graph are affected.

In the last example, the effect in the system is observed when at least the compartment g, or the compartments a and b and c, or the compartments d and e and f and c are affected.

The calculation of the function x(r) for any system is easy by using the Mikusinski operational calculus (3).

For a compartment the function 3) is written:

6) $$\{x\} = K/(s + K)$$

and the expressions 4) and 5):

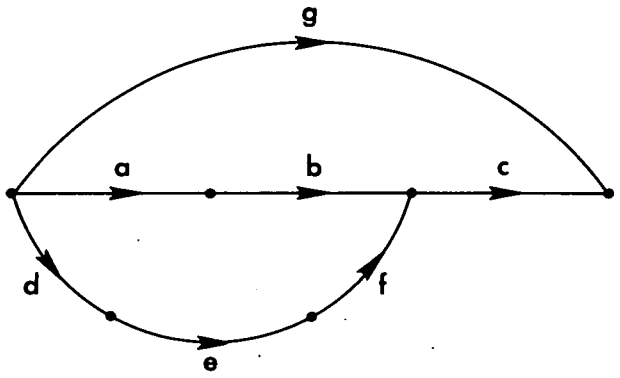

Figure 2. Graph of the system
{[(aAb)V(dAeAf)]Ac}Vg.
MU-31342

7) $$\{x_{1A2}\} = \{x_1\} \cdot \{x_2\} ,$$

8) $$\{x_{1V2}\} = \{x_1\} + \{x_2\} - \{x_1\} \cdot \{x_2\} .$$

As all the {x} are meromorphic functions in s, the difference between the degree of the denominator and the degree of the numerator in the function resulting from operation 7) is equal to the sum of the differences in the two component functions; and the difference between the degree of the denominator and the degree of the numerator in the function resulting from operation 8) is equal to the smallest difference in the two component functions. It follows that the difference between the degree of the denominator and the degree of the numerator of the function {x} of a multi-compartment system is equal to the number of arrows composing the shortest path of its graph.

For the same reason, the coefficient of the term with the highest degree in s in the numerator of the function {x} is equal to the product of the constants K of the compartments corresponding to the shortest path of the graph, or to the sum of such products, if there are two or more paths with the same minimum number of arrows.

As an example, suppose the function

$$S = 2\, e^{-2r} - e^{-r}$$

is found experimentally, where S is the fraction of cells surviving a dose r. As

$$S = 1 - \int_0^r x(\rho)d\rho,$$

$$x(r) = - dS/dr,$$

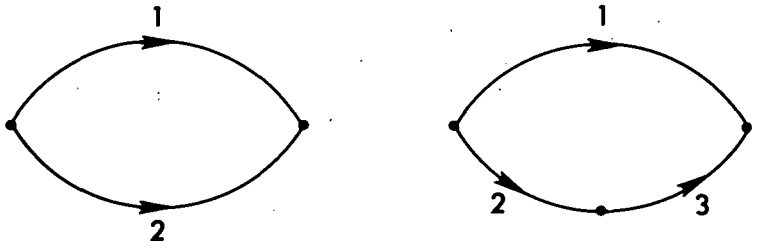

Figure 3. Two possible structures for the system whose function is $\{x\}=(3s+2)/(s+1)(s+2)$.

(a) 1V2
$\{x_1\}= 1/(s+1)$
$\{x_2\}= 2/(s+2)$

(b) 1V(2A3)
$\{x_1\}= 3/(s+3)$
$\{x_2\}= 1/(s+1)$
$\{x_3\}= 2/(s+2)$

MU-31343

therefore

$$x(r) = 4\ e^{-2r} - e^{-r},$$

$$\{x\} = (3s + 2)/(s + 1)(s + 2).$$

The difference of the degrees is 1, therefore the shortest path is formed by one arrow; if we suppose there are two paths of one arrow, then $3 = K_1 + K_2 = 1 + 2$,

$$\{x\} = 1/(s + 1) + 2/(s + 2) - 2/(s + 1)(s + 2),$$

and the corresponding graph is illustrated in Fig. 3a.

If we suppose there is only one path of one arrow, it corresponds to the compartment whose function is $\{x_1\} = 3/(s + 3)$; operating the inverse of the operation 8) on $\{x\}$ and $\{x_1\}$, we obtain the function

$$2/(s + 1)(s + 2) = 1/(s + 1) \cdot 2/(s + 2),$$

corresponding to two compartments; the resulting graph is illustrated in Fig. 3b.

ACKNOWLEDGEMENTS

This work was supported jointly by the United States Atomic Energy Commission and the National Aeronautics and Space Administration.

REFERENCES

1. Rescigno, A.; Ann. N.Y. Acad. Sci. 108:204, 1963.
2. Rescigno, A.; Biochim. Biophys. Acta 37:463, 1960.
3. Mikusinski, J.: Operational Calculus, London, Pergamon Press, 1959.

Operational Calculus in Two Variables

Aldo Rescigno

Many applications were found in biology for the convolution integral $\int_0^t a(t-\tau)b(\tau)d\tau$ (see for instance Branson (1), Rescigno and Segre (2), Stephenson (3), Zierler (4)). Using the two operations of addition and convolution, Mikusinski (5) developed an algebra, that can also be applied to biological problems, Rescigno (6,7).

If a and b are functions of two variables u and v, the integral

$$1) \qquad \int_0^v \int_0^u a(u-x,v-y)b(x,y)\,dx\,dy$$

will be found in many problems involving linear partial derivative equations with two variables. An algebra using the addition and the two-variable convolution as its fundamental operations, may be of great heuristic value in many biological problems, and may easily be extended to functions with any number of variables.

Let $a(u,v)$, $b(u,v)$, $c(u,v)$, ..., be continuous functions, defined for any nonnegative value of the variables u and v. The elements $\{a\}$, $\{b\}$, $\{c\}$, ..., and the operations

$$2) \qquad \{a\} \cdot \{b\} = \left\{ \int_0^v \int_0^u a(u-x,v-y)b(x,y)\,dx\,dy \right\}$$

$$3) \qquad \{a\} + \{b\} = \{a + b\}$$

form a commutative ring. To prove this, it is sufficient to verify that the integral 1) has the properties of commutativity, associativity and distributivity with respect to addition.

The equation $\{a\}\cdot\{b\}=\{0\}$ implies $a(u,v)\equiv 0$ or $b(u,v)\equiv 0$. The proof of this theorem will be published elsewhere. Because of this theorem, we can define a field whose elements are represented by two functions separated by a bar: $\{a\}/\{b\}$, $\{c\}/\{d\}$, ..., and whose two operations are defined by

4) $$\frac{\{a\}}{\{b\}} + \frac{\{c\}}{\{d\}} = \frac{\{a\}\cdot\{d\} + \{b\}\cdot\{c\}}{\{b\}\cdot\{d\}}$$

5) $$\frac{\{a\}}{\{b\}} \cdot \frac{\{c\}}{\{d\}} = \frac{\{a\}\cdot\{c\}}{\{b\}\cdot\{d\}} ,$$

with the condition that the function beneath the bar be nonidentically zero. As a consequence

6) $$\frac{\{a\}}{\{b\}} = \frac{\{c\}}{\{d\}} \quad \text{if and only if} \quad \{a\}\cdot\{d\} = \{b\}\cdot\{c\} .$$

In this field we can include any element for which the two operations 4) and 5) are sufficiently defined; this is the case, in particular, for the elements of the ring. The element $\{1\}$ is especially important, because

7) $$\left\{1\right\} \cdot \left\{a(u,v)\right\} = \left\{\int_0^v \int_0^u a(x,y)\, dx\, dy\right\} .$$

Two elements p and q can be defined, such that

8) $$p\cdot\left\{a(u,v)\right\} = \left\{\int_0^u a(x,v)dx\right\} ,$$

9) $$q\cdot\left\{a(u,v)\right\} = \left\{\int_0^v a(u,y)dy\right\} ;$$

as a consequence

10) $$p\cdot q = \left\{1\right\} .$$

If a(u) and b(u) are two functions of the variable u alone, then, for the 4):

$$\frac{\{a(u)\}}{q} + \frac{\{b(u)\}}{q} = \frac{q\cdot\{a(u)\} + q\cdot\{b(u)\}}{q\cdot q} = \frac{\{a(u) + b(u)\}}{q} ,$$

and for the 5):

$$\frac{\{a(u)\}}{q} \cdot \frac{\{b(u)\}}{q} = \frac{\{a(u)\}\cdot\{b(u)\}}{q\cdot q} = \frac{\{\int_0^u a(u-x)b(x)dx\}}{q} .$$

Therefore for an element such as $\{a(u)\}/q$, the rules of the one variable operational calculus apply; we can introduce the notation

$$\frac{\{a(u)\}}{q} = \left[a(u)\right] .$$

For the same reason we can put

$$\frac{\{a(v)\}}{p} = \left[a(v)\right]$$

for any function $a(v)$ of the variable v.

If α and β are constants, the 4) and the 5) are

$$\frac{\{\alpha\}}{\{1\}} + \frac{\{\beta\}}{\{1\}} = \frac{\{1\}\cdot\{\alpha\} + \{1\}\cdot\{\beta\}}{\{1\}\cdot\{1\}} = \frac{\{\alpha+\beta\}}{\{1\}},$$

$$\frac{\{\alpha\}}{\{1\}} \cdot \frac{\{\beta\}}{\{1\}} = \frac{\{\int_o^v \int_o^u \alpha\beta \, dx \, dy\}}{\{1\}\cdot\{1\}} = \frac{\{\alpha\beta\}}{\{1\}} ;$$

therefore for an element such as $\{\alpha\}/\{1\}$, the rules of the arithmetic apply; we can introduce the notation

$$\{\alpha\}/\{1\} = \alpha.$$

Because

$$\int_o^v \int_o^u \frac{\partial^2 a(x,y)}{\partial u \partial v'} \, dx \, dy = a(u,v) - a(u,0) - a(0,v) + a(0,0),$$

and because of 7), we can write

$$\left\{1\right\} \cdot \left\{\frac{\partial^2 a}{\partial u \partial v}\right\} = \left\{a(u,v)\right\} - \left\{a(u,0)\right\} - \left\{a(0,v)\right\} + \left\{a(0,0)\right\} .$$

Introducing the new elements r and s such that

$$p \cdot r = 1,$$

$$q \cdot s = 1,$$

the previous relation can be written

$$\left\{\frac{\partial^2 a}{\partial u \partial v}\right\} = r\cdot s\cdot \left\{a(u,v)\right\} - r\cdot s\cdot \left\{a(u,0)\right\} - r\cdot s\cdot \left\{a(0,v)\right\} + r\cdot s\cdot \left\{a(0,0)\right\} ,$$

$$\left\{\frac{\partial^2 a}{\partial u \partial v}\right\} = r\cdot s\cdot \left\{a(u,v)\right\} - r\cdot \left[a(u,0)\right] - s\cdot \left[a(0,v)\right] + a(0,0).$$

In the same way we can obtain

$$\left\{\frac{\partial a}{\partial u}\right\} = r\cdot \left\{a(u,v)\right\} - \left[a(0,v)\right] ,$$

$$\left\{\frac{\partial a}{\partial v}\right\} = s.\left\{a(u,v)\right\} - \left[a(u,0)\right] .$$

Many other elements and relations can be introduced, making this calculus a powerful tool for the solution of problems related to two-variable linear systems.

A similar calculus, but based on the Laplace-Carson transform, and therefore valid for a more limited class of functions, was developed by Ditkin and Prudnikov (8).

ACKNOWLEDGEMENTS

This work was supported jointly by the United States Atomic Energy Commission and the National Aeronautics and Space Administration.

REFERENCES

1. Branson, H.; Ann. N. Y. Acad. Sci. 108:4, 1963.
2. Rescigno, A. and Segre, G.: Drug and Tracer Kinetics, New York, Blaisdell, in press.
3. Stephenson, J. L.; Bull. Math. Biophysics 22:1 and 113, 1960.
4. Zierler, K. L.; Circulation Research 10:393, 1962.
5. Mikusinski, J.: Operational Calculus, London, Pergamon Press, 1959.
6. Rescigno, A.; Ann. N. Y. Acad. Sci. 108:204, 1963.
7. Rescigno, A.; Multicompartment Interpretation of Radiation-Damage Curves, this report, see p.59.
8. Ditkin, V. A., and Prudnikov, A. P.: Operational Calculus in Two Variables and Its Applications, London, Pergamon Press, 1962.

Sedimentation Properties of Nucleated and Nonnucleated Cells in Normal Rat Bone Marrow

Howard C. Mel

Blood-cell sedimentation has been observed for more than 2,500 years and studied quantitatively for more than 200 years (1). Yet many physical as well as biological aspects of this phenomenon remain poorly understood today. Partly, the complications are those in common with cell sedimentation in general (2), partly, they seem peculiar to these particular cells that can stick together, form rouleaux, and otherwise interact in ways still being elucidated currently (3,4). This phenomenon is of both analytical and preparative interest. The medical diagnostic value of the "blood sedimentation" test is indisputable. However, the dependence of the results on the details of the test procedure used is well known (1,5). Furthermore, the usual time-average sedimentation rates, measured on concentrated blood-cell suspensions, should not be considered characteristic of individual noninteracting cells.

Centrifugal techniques, in a great variety of forms often involving density gradients, are most common for separating blood and bone-marrow cells (6,7, 8). When cells are banded in known density gradients, this approach can also provide analytical information, i.e., cell density, but for cells and similar objects, "density" or "size" are far from unambiguous in meaning. The widely accepted viewpoint about differential cell sedimentation is that cell density rather than size is the determining factor. It has even been explicitly stated in the literature that individual cells do not sediment (float) and separate according to size (9). It has also been reported that cells cannot be separated in a density gradient by sedimentation under gravity alone, but only under higher centrifugal fields (8).

The purpose of this paper is to discuss the differential sedimentation leading to separation of the nonnucleated and nucleated cells in bone marrow. This sedimentation process, which takes place in a continuously flowing system under 1 g only, is believed to depend strongly on cell size. It results in apparently anomalous sedimentation behavior of the red and white cellular components as elaborated below.

MATERIALS AND METHODS

A suspension of single marrow cells is mechanically prepared as follows. Male, Long Evans rats of approximately 200-g body weight are exsanguinated by decapitation, and the six long bones--femur, tibia, and humerus--are removed. Both ends of each bone are punctured with a No. 18 hypodermic needle, and the marrow is forced out in chunks or in a plug with 3 to 4 cc of chilled isotonic saline. The liquid and marrow are poured into the barrel of a 10-cc plastic syringe fitted in the bottom with stainless wire mesh of No. 60 guage. The plunger is replaced in the barrel and the mixture gingerly expelled into a small beaker, keeping the syringe tip under the surface of the liquid. The suspension is sucked up and expelled three times, then filtered through a Nylon mesh bag (No. 9331 MBCO Disposable Filter, Macalaster Bicknell Co., Cambridge, Mass.). The remaining clumps of cells are broken up by expelling the suspension through a No. 25 needle at the rate of about 10 cc per 18 sec. The cells are centrifuged for 5 min at an average of 125 times gravity at 3°C, are gently resuspended, then counted in a hemocytometer, and finally diluted to 2.6×10^7 cells/cc (the starting sample concentration). A single animal handled in this manner yields about 7×10^8 cells, which by standard eosin Y staining (10) generally test over 90% viable.

The sedimentation study is carried out by the stable-flow free-boundary (STAFLO) method, using 1 g only as the driving force for migration. The theory and practice of STAFLO-sedimentation of cells have recently been described in some detail (11). This treatment is an extension of previously reported STAFLO-electrophoresis (12) to the use of other force fields. The flow-cell employed (No. 7) has the rectangular migration-chamber dimensions of 30 cm long, 1.5 cm high, and 0.7 cm deep. The 12 inlet solutions, feeding the uniformly flowing horizontal streams, are numbered from top to bottom. They are isotonic in NaCl and have additional dextran (in wt/vol %) as follows: No. 1: 0%; No. 2: 0% (cell-sample solution); No. 3: 0.50%; No. 4: 0.65%; No. 5: 0.80%; No. 6: 0.88%; No. 7: 0.95%; No. 8: 1.03%; Nos. 9 and 10: 2.1%; Nos. 11 and 12: 3.1%. The flow rate for these experiments (identical for all solutions) was selected to give a steady-state sedimentation time of 32 min. Sample flow was 2.2×10^6 cells/min. After the steady state is established, generally 10 cc of each outlet fraction are collected. With the above experimental parameters, essentially all the cells collected are in fractions No. 2 through No. 8. The fractions are analyzed microscopically, either directly in suspension (e.g., in phase contrast, or after staining for viability) or after smears and stained slides have been prepared by ordinary techniques. Commonly, Jenner, Giemsa, and Ralph (for hemoglobin) stains are used.

RESULTS

Although differential counts are usually made from the stained slides, the purpose of this communication is to discuss behavior of only the two general

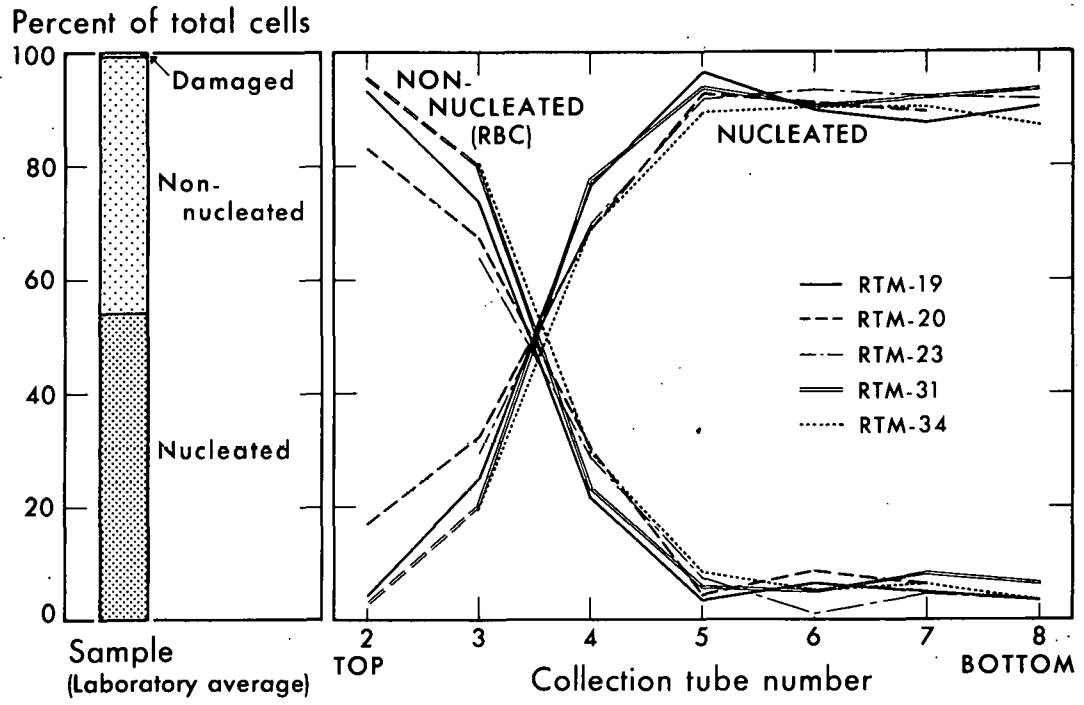

Figure 1. Relative composition of collected fractions after STAFLO sedimentation of rat bone marrow under 1 g. MU 30203

cell classes: nonnucleated (erythrocyte) and nucleated. In Fig. 1 are plotted the percentages of each type, in collection tubes No. 2 through 8, for five different runs typical of a large number performed over a 3-month interval. The small unaccounted-for balance consists of damaged, uncountable cells. Immediately obvious in the figure is the preponderance of (nonnucleated) erythrocytes in the top fractions. From values often exceeding 90% of the total in tube No. 2, their proportion drops sharply to about 5% by tube No. 5. The approximate constancy of this value below tube 5 does not signify that further segregation is not occurring, only that this particular kind of segregation is approximately complete by that time. The "background" of ~ 5% erythrocytes is undoubtedly due in part to the not-completely-ideal single-cell nature of the sedimentation process. (In one older experiment, erythrocyte values of 0% were found in tubes No. 5 and beneath, probably because of an RBC-impoverished starting sample.)

The most striking comparison occurs between tubes No. 3 and No. 4 which together contain the majority of the cells and have approximately equal cell concentrations. From about 75% mature reds and 25% nucleated cells in collection tube No. 3, the relationship changes to the inverse one in No. 4. With each flowing layer 1.25 mm in thickness, outlet No. 4 is, on the average, 1.25 mm below No. 3. Some biological variation is, of course, inherent in the

starting samples taken from different animals at different times. The range is indicated in these experiments by the erythrocyte values of 49.1% (RTM-31) and 42.7% (RTM-34). Our laboratory average is 45.4% as shown. There also is some measure of variability in the handling procedures. Nevertheless, the physical reproducibility of the sedimentation process indicated by Fig. 1 is encouraging. It provides a basis for discussing the apparently anomalous behavior of erythrocytes relative to that of nucleated red and white cells, namely the more rapid sedimentation of the latter nucleated components. This is also easily observed by the eye during the course of the experiment. By the time the outlets are reached, the top streams are quite reddish, those below whitish. The collection bottles reflect corresponding differences in appearance.

DISCUSSION

The sedimentation rate S, for perfect spherical particles of radius r and density ρ_p, in steady state sedimentation under 1 g, through a medium of viscosity η and density ρ_m (subject to the Stokes resistive factor), has the well known form:

$$S = \frac{2\ r^2}{9\ \eta}\ (\rho_p - \rho_m).$$

We may apply this equation in turn to mature erythrocytes and leukocytes. Specific data appear to be lacking for the densities of rat blood cells. However, we can judge from specific gravities of whole blood, from hematocrits, and from blood-cell morphology (13), that density values for human corpuscles should be sufficiently accurate analogues for the present purposes. Even for human cells (particularly for leukocytes), density data are sparse and often show poor agreement (7). Powell has recently measured a range of 1.079 to 1.089 for erythrocytes (7). Roberts, Watne, McGrath, McGrew and Cole report for leukocytes, $\rho > 1.065$ (14).

A greater density for the mature red cells clearly favors their more rapid sedimentation. We will use as probable extreme values in this conse: $\rho_{RBC} = 1.09$ and $\rho_{WBC} = 1.06$. For practical purposes in our experiments with the very small density gradients, $\rho_m = 1.00$, so the ratio of the (red/white) density factors in the sedimentation equation is $\frac{.09}{.06} = 1.5$. The radius enters as the square, however. Thus, if the ratio of the radii $\left(\frac{\text{white}}{\text{red}}\right)$ were greater than $\sqrt{1.5} = 1.22$, i.e., if the white (or other nucleated) cells were as much as 22% larger, according to the equation, the size factor would be more important than the density factor.

Even taking the disk-shaped erythrocyte's "size" to be its largest diameter (~ 7 μ), mature leukocytes in free solution are generally significantly more than 22% larger. Therefore, on this simple physical basis we should expect them to sediment faster than erythrocytes. This is precisely the result indicated in Fig. 1. Since younger nucleated white cells are often still larger, according to the sedimentation equation they should also sediment more rapidly

than the erythrocytes. Finally, the younger erythroid cells are either considerably larger, or with their relatively large nucleus they should be denser than the erythrocytes, again suggesting a higher S-rate than for the erythrocytes. Thus, the relative sedimentation difference shown in Fig. 1 is qualitatively consistent with the equation. The contrary result, i.e., the more rapid sedimentation of erythrocytes, commonly assumed to occur, should, perhaps, be more surprising and certainly more difficult to explain in this context.

What, then, is the likely explanation for the "usual" result of "more rapid sedimentation" of erythrocytes (5), or, perhaps more precisely, their sedimentation to a "lower" position? This result could arise either from rate or from equilibrium considerations. If the mature red cells were largely in the form of aggregates, the size as well as the density of the red-cell-sedimenting objects could easily exceed those for the other cell fractions. Thus, direct application of the equation to the aggregates would indicate their more rapid sedimentation, even for 1 g only. Such aggregation would certainly be favored by high cell concentrations. The protein composition of the medium has also been strongly implicated in blood-cell-sedimentation phenomena, particularly through its effect on intercellular interactions (5). In concentrated suspensions like blood, containing cells such as erythrocytes, which have known tendencies to associate or aggregate, the probability that they will be able to do so is very high (3,4,5).

In the presence of higher acceleration forces, such as those customarily employed when determining packed cell volumes or in preparing buffy coat, the same endpoint should eventually occur. Even when starting with dilute suspensions, the cells are usually concentrated or packed together either at the bottom of a tube or in bands in a density gradient. Therefore, by equilibrium and rate--or on equilibrium grounds alone--the red cells should go to the bottom. As a check on this point, our original dilute marrow samples were centrifuged for various times at differing speeds. After short times at low g's the sedimented pellet appears relatively white on the bottom, red on top. With 5 min at 600-g average, the red has partially moved to the bottom. In 10 min at 600 g, the reversal is complete--the red portion of the pellet is totally on the bottom, the whitish above.

A scheme that summarizes this discussion in the form of two possible extreme mechanisms for usual blood sedimentation is given in Table 1, lines 1 and 2. Of course, the sedimentation need not be by any single clear-cut mechanism, for, as commonly carried out, it is not a simple process. In addition to the influences of cell concentration and medium composition, the sedimentation may also be complicated by such things as direct effects of pressures from higher g forces on the size and density of the cells (8). To be contrasted with these situations is the present STAFLO-sedimentation indicated in Table 1, line 3.

Table 1. Comparison of some extreme mechanisms of differential cell sedimentation

Nature of procedure	Conditions	Forces	Cellular interactions important?	Type of sedimentation	Result
1. usual batch sedimentation	concentrated suspension (espec. with proteins)	1 g	yes	rate	RBC (objects) move faster, go to lower position
2. usual batch centrifugation	e.g., dilute, no proteins	usual g forces for packed cell volume measurement	no	equilibrium	RBC go to lower position
3. STAFLO-sedimentation (steady state)	dilute, no protein	1 g	no	rate	RBC move slower, go to higher position

REFERENCES AND NOTES

1. Ponder, E.; in Medical Physics, Vol. 1, edited by O. Glasser, Chicago, The Year Book Publishers, 1944, p. 1408.
2. de Duve, C.; Berthet, J., and Beaufay, H.; Progr. Biophys. Biophys. Chem. 9:326, 1959.
3. Easty, G. C., and Mercer, E. H.; Exp. Cell Res. 28:215, 1962.
4. Huggins, C. E.; Science 139:504, 1963.
5. Wintrobe, M. M.: Clinical Hematology, 5th Ed., Philadelphia, Lea and Febiger, 1961, p. 325.
6. Allfrey, V.; in The Cell, Vol. 1, edited by J. Brachet and A. Mirsky, New York, Academic Press, 1959, p. 193.
7. Powell, M. E. A.; Nature 193:1047, 1962.
8. Agranoff, B. W.; Vallee, B. L., and Waugh, D. F.; Blood 9:804, 1954.
9. McGrew, E. A., and Nanos, S.; Trans. Fifth Ann. Meeting Intersociety Cytology Council, 139, Nov. 14-6, 1957.
10. Schrek, R.; Am. J. Cancer 28:389, 1936.
11. Mel, H. C.: "Stable-Flow Free Boundary Migration and Fractionation of Cell Mixtures, I, II, III," J. Theoret. Biol., in press.
12. Mel, H. C.; J. Chem. Phys. 31:559, 1959; Science 132:1255, 1960.
13. Altman, P. L.; in Blood and Other Body Fluids, edited by D. S. Ditman, Fed. Am. Soc. Exp. Biol., Washington, D. C. 1961.
14. Roberts, S.; Watne, A.; McGrath, R.; McGrew, E., and Cole, W. H.; Arch. Surg. 76:334, 1958.
15. Mel, H. C.; Mitchell, L. M., and Thorell, B.; in preparation.

This paper will be published in a forthcoming issue of Nature.

Diffusion-Gravity Controlled Enzyme-Substrate Reaction

Howard C. Mel

Physico-chemical processes and reactions in solution are not generally influenced by the force of normal gravity. Exceptions involve certain phase changes, particulate sedimentation and convection from gross density instability. The phenomenon of induced microconvectional instability or "droplet sedimentation" is in this same class though not so widely known. First described by Brakke (1), it has been discussed in some detail by Svensson et al. (2), and observed in flowing systems by Mel (3). This paper describes the phenomenon in a continuous flowing system and reports experiments using it to control a steady-state model enzyme-substrate reaction. In effect, under conditions defined by the diffusion coefficients of inert constituents, the force of gravity induces mass transfer of lysozyme into its physically separated substrate, giving rise to the stated reaction.

The mass transfer process results from the outcome of a "molecular race" occurring on the way to diffusional equilibrium, starting from an initially stably layered density gradient system. If adjacent "top" and "bottom" solutions, separated by a fresh boundary, contain the same density-building solute of low molecular weight, e.g. NaCl, diffusion will gradually smooth out the initial discontinuity in a "well-behaved" fashion. If, on the other hand, the top solution owes its density to a macromolecular species, the initial downward diffusion of the macromolecule is so slow that the rapid upward diffusion of NaCl can quickly lead to small regions of the top solution (the "droplets") having higher density than that of the lower solution. The droplets, seen experimentally in the flow system as fine "streamers," move downward, bringing with them corresponding portions of whatever other substances are present in the top solution. Depending on the circumstances, they may (i) continue down through additional density boundaries, if present, (ii) be quickly dissipated, or (iii) be abruptly stopped by a "density shelf."

To help visualize this process, a simple analogue may be useful. Instead of a solution, consider a delicate cylindrical open-network structure. In the top half are 100 g of snails, in the bottom half 200 g of ants, each initially constrained to its half and uniformly distributed in it. The barrier is now withdrawn, permitting both species to fill the whole space. The ants move upward so much more quickly than the snails downward that, particularly near the

boundary, the structure around some of the snails cannot support the additional weight of the ants, so bits of the structure collapse downward.

The present experiments were carried out using the stable-flow free-boundary (STAFLO) method (3, 4). Twelve aqueous streams, pumped into the open-channel flow-cell at the right, proceed horizontally by a special kind of stable laminar flow through the 30-cm chamber and exit at the left into separate collection containers. Streams are numbered 1-12 from top to bottom, as indicated schematically in Fig. 1A. (The electrophoretic aspects of the apparatus are not involved in the present study.)

The compositions and densities of the entering solutions are given in Table 1. Solution No. 2 represents a dilution of 6% Injection Dextran in Normal Saline (Cutter). This dextran is an albumin substitute, with average molecular weight ~ 70,000. (The small amount of NaCl remaining after dilution is unimportant to the idea of the experiment.) Solution No. 2C was made up by adding NaCl until the solution density was exactly the same as that for No. 2 (to ± 0.0001 g/cc). Densities were determined at 23 ± 1°C, using a high precision Ostwald-Sprengel type glass pycnometer calibrated with distilled water, the values then corrected to 23.0°. Densities were checked periodically both by reweighing and with a Bausch and Lomb Precision Abbé refractometer. Sucrose was added to solutions No. 4 and below for its contribution to the flow stability, though equivalent NaCl might as well have been used. The abrupt increase in solute concentration from solution No. 4 to No. 5 serves to put a "density shelf" under solution No. 4. For simplicity, experiments with no dextran in solution No. 2 will be called "controls," those with dextran will be called "dextran" experiments. Except for solutions Nos. 2 and 2C, all other inlet solutions are identical for both the control and the "dextran" experiments. Solutions Nos. 2, 2C, 3, and 4 are the important ones to be accurately known and controlled. However, the particular compositions that can be chosen are arbitrary within wide limits.

As indicated by Table 1, the enzyme in streams Nos. 2 and 2C is initially separated from the substrate in No. 4 by the 2.5-mm-high buffered saline stream No. 3. Free boundary throughput times were 24.5 min or less. (A "throughput" time is the steady state transit time through the 30-cm free-boundary portion of the flow-cell, at any given flow rate.) Extensive experience with the STAFLO method has shown that no mixing ordinarily occurs between such separated streams: convection is ruled out by the method itself and appreciable diffusion over a 2.5-mm distance requires longer time. Thus, in the simplest case we should expect the substrate in collection container No. 4 to be unaltered by enzyme. Only if some other "unusual" transport mechanism were operative (e.g., "droplet sedimentation") should we find appreciable enzyme degradation of substrate in No. 4. Ordinarily, most of the enzyme should exit via outlet No. 2 but, because some diffusion-broadening of the strata must occur, some

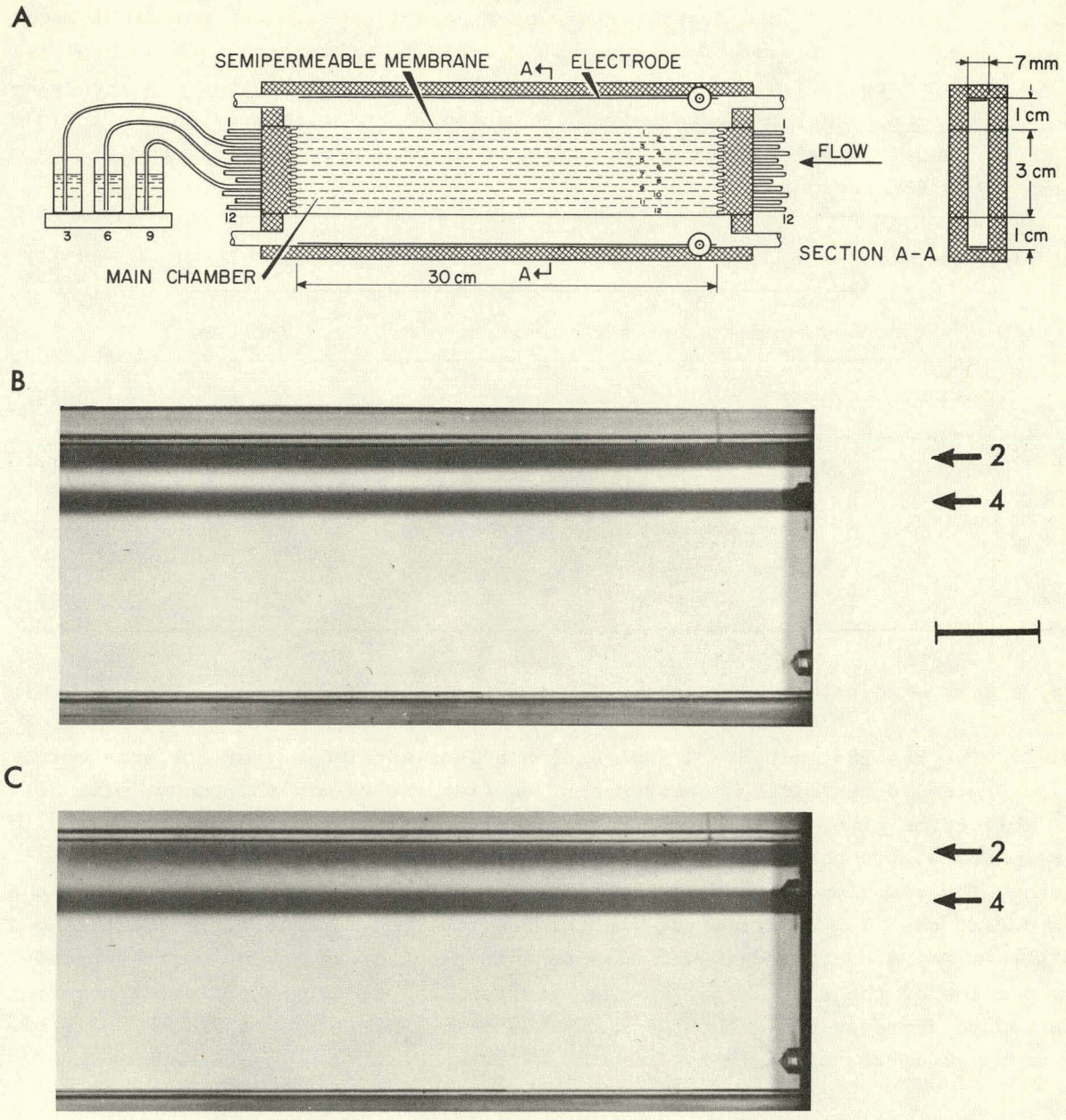

Figure 1A. STAFLO apparatus indicating separate strata. B. Portion of inlet during steady-state flow with 24.5-min throughput time. Streams Nos. 2 and 4 contain dye added for visibility. Control: NaCl in No. 2. Scale marker represents 1 cm. C. "Dextran": same conditions and densities but with dextran replacing NaCl in No. 2, showing instability at lower border of No. 2.

Table 1. Compositions and densities of entering solutions. Controls indicated by "C." All solutions are also 0.00653 M in Sorensen's phosphate buffer, pH 7.0. The lysozyme and its substrate, Micrococcus lysodeikticus, are from Worthington. Solution 1C and 1 is straight buffer; 5C and 5 is 3.92% sucrose; 6C and 6 is 4.90% sucrose; 7C-12C and 7-12 are 5.88% sucrose.

Solution No.	Composition (wt/vol %)					Density (g/ml at 23.0° C)
	Lysozyme	Substrate	Dextran	NaCl	Sucrose	
2C	0.0392	0	0	0.421	0	1.0013
2	0.0392	0	0.588	0.0882	0	1.0013
3C & 3	0	0	0	0.882	0	1.0046
4C & 4	0	0.0098	0	0.882	0.98	1.0082

enzyme must exit through adjacent outlets No. 1 and No. 3.

The results in Table 2 indicate an all-or-nothing effect for substrate, as determined by turbidity measurements. During the 24-min throughput plus 30-min collection time, there was no enzyme action on the control substrate in stream No. 4. On the "dextran" experimental substrate, enzyme action was complete. The reaction or lack of reaction was qualitatively easily visible to the eye during the flow experiments. In the control, the intense light scattering in stream No. 4 continued essentially undiminished across the 30-cm free-boundary portion of the flow cell. In the "dextran" experiment, the light scattering started to decrease after about 2.5 cm travel (~ 2 min) and was almost invisible by about 22 cm travel (~ 18 min).

Material balance for substrate recovery through outlet No. 4 was also measured for two control experiments at different flow rates. With a 24.5-min throughput time, 90% of the inlet substrate was recovered in collection fraction No. 4. With faster flow, in a 12.3-min throughput time experiment, 96% was similarly recovered. (Substrate diffusing up into stream No. 3 is degraded by action of the enzyme diffusing down from stream No. 2.)

The results of the lysozyme assay are given in Table 3 in activity units (slightly modified method of Shugar (5)). For high precision determinations of the exact mg lysozyme/ml, these figures should be corrected according to separate calibration curves for all the different solutions since presence of the

Table 2. Comparison of substrate entering by inlet No. 4 and exiting via outlet No. 4. Substrate determined by O.D. measurements at 450 mμ in a 1- by 1-cm cuvette with a Beckman DK-1 recording spectrophotometer. Initial substrate O.D. = 0.74. Residual O.D. blank, when excess enzyme completely reacts with solution No. 4, = 0.04. The O.D.'s were read immediately after collection. If a highly turbid solution showed no detectable O.D. decrease during at least 3 min of observation, it was classified as not having been degraded by enzyme during the given experiment. (24.5 min throughput time + 30 min collection time.)

Enzyme-induced reduction of substrate exiting through outlet No. 4 (%)	
Control experiment	0
"Dextran" experiment	100

Table 3. Enzyme activity in collected outlet solutions; 24.5 min steady-state throughput + 30 min collection times. Units of activity are 100 x decrease per min of the O.D. at 450 mμ, when 0.01 ml solution is added to 3 ml standard substrate in 0.00653 M phosphate buffer at pH 7.0. Inlet activity in solutions Nos. 2 and 2C was 10.2.

Solution No.	Control	"Dextran"
1	1.1	1.0
2	8.8	4.8
3	1.2	2.8
4	0 (see text)	0.4
5	0	0

other solutes affects the standard calibration curve somewhat. This calibration shift is the likely reason that overall material balance holds only to about ± 10%.

The figures in Table 3 are consistent with those in Table 2 and with the previous discussion. They emphasize the fact that major direct changes in solution composition can rapidly be effected by this transport phenomenon. In the control, most of the incoming activity exits through outlet No. 2, with smaller and approximately equal amounts through Nos. 1 and 3. As we would expect,

diffusional spreading of enzyme is greater than for the larger particle weight substrate. No decrease in O.D. for outlet solution No. 4C (containing the substrate) was noticed when observed for several minutes. From re-examination after 21 hr, an upper limit for enzyme activity in this solution is 0.0004. By contrast, in the "dextran" case, the enzyme exiting through No. 2 is considerably reduced. A similar amount appears in No. 1 as in No. 1C (e.g., by upward diffusion), but the "droplet sedimentation" phenomenon has greatly increased the enzyme that would otherwise exit through No. 3 and has also brought significant amounts down to stream No. 4, (which resulted in the elimination of the substrate inside the flow-cell). Nearly three times as much activity has been brought into streams No. 3 and No. 4 (starting within 1.5 min after formation of the fresh boundary) as was transported by diffusion in the control experiment.

The exact diffusion coefficients of the dextran and NaCl in the present solutions are not known. As a first approximation, we can use nominal standard values of 6×10^{-7} cm^2/sec for human serum albumin and 1.5×10^{-5} cm^2/sec for NaCl. With this 25-fold rate advantage for the NaCl, it alone is essentially responsible for the density changes occurring at the 2-3 free boundary during these short times.

A more direct demonstration of the "droplet sedimentation" is given in Figs. 1B and 1C. In place of lysozyme and its substrate, in No. 2 and No. 4, 0.005% bromphenol blue has been added for better visualization of the flow pattern. In the control experiment, Fig. 1B, with NaCl in solution No. 2, the lower boundary of stream No. 2 remains intact. Replacing the NaCl by dextran, Fig. 1C, a pronounced "fuzziness" develops in the lower boundary of stream No. 2, starting after about 1.5 cm (~ 1.2 min) of free boundary and increasing progressively downstream. Some of the short vertical "streamers" can be seen crossing stream No. 3. This behavior continues for about 5-10 cm (~ 4 to 8 min) after which the border between streams No. 2 and No. 3 appears to have become stabilized. The further downstream portion of the pattern just assumes a generally diffuse appearance. This is in marked contrast to the separate and distinct appearance of the individual streams seen in previously published STAFLO photographs (3, 4).

A number of interesting points about the detailed mechanism of "droplet" formation and sedimentation remain unsettled; some have apparently not even been discussed in the literature. How do the individual "droplets" or "streamers" actually form? What sizes can they have (e.g., can they be smaller than an average living cell)? What local excesses of density are required? To what extent does their formation depend on the velocity distributions of the molecules in the initiating competitive diffusion processes--i.e., could "droplets" represent local regions of higher NaCl concentration arising from those NaCl

molecules diffusing faster than the average?

Setting aside the above uncertainties about details of the mechanism of the transport process, its physico-chemical significance is clear and bears restating: At constant initial density in a steady-state layered flowing system, with solutes (that may be chemically and biologically inert) having "proper" diffusion coefficients, 1 g is a sufficient driving force to cause a reaction to be brought to completion. In the absence of gravity, i.e., the "weightless" condition, the reaction would not take place at all. That is, gravity, and the diffusion coefficients of inert components, are "controlling" a continuous steady-state chemical reaction.

The possible biological significance of this mechanism is much more obscure. Numerous instances of flow and streaming exist in biological systems (both intracellularly and on a larger dimensional scale) continuously forming fresh fluid interfaces. Platt (6) has recently suggested that the curious "bioconvection patterns" in cultures of free-swimming ciliates and flagellates might be useful for fertilization. To his list of five possible factors contributing to these "dynamic instabilities" should perhaps be added a sixth: "streaming droplet sedimentation" or a first cousin of it. Certainly, if this mechanism does play a controlling role in any biological function (e.g., in transporting material quickly over relatively large distances), then in the "weightless" state this function would be altered or removed.

SUMMARY

"Competitive diffusion" and normal gravity interact to transport lysozyme rapidly into its separated substrate in an initially stably layered, flow-system. A continuous steady-state enzyme reaction is thus controlled by gravity and the diffusion coefficients of inert components. Should this transport mechanism play a role in any biological function, then in "weightlessness" the function would be altered or removed.

ACKNOWLEDGEMENTS

I am indebted to Mrs. G. Hylton for her able assistance with the experiments. Part of my interest in this work was stimulated by previous association with the Space Biophysics project of Dr. C. A. Tobias. The support of the U. S. Atomic Energy Commission, Lawrence Radiation Laboratory, is also gratefully acknowledged.

REFERENCES

1. Brakke, M. K.; Arch. Biochem. Biophys. 55:175, 1955.
2. Svensson, H.; Hagdahl, L., and Lerner, K. D.; Science Tools 4:1, 1957.
3. Mel, H. C.: Stable-Flow Free-Boundary Migration and Fractionation of Cell Mixtures: I, II, III, J. Theoret. Biol., in press.
4. Mel, H. C.; Science 132:1255, 1960.
5. Shugar, D.; Biochim. et Biophys. Acta 8:302, 1952.
6. Platt, J. R.; Science 133:1766, 1961.

Convection in Low Gravitational Fields

Milton J. Polissar

The object of the present investigation is to examine the probable effects of weightlessness and of low gravitational fields upon living cells and upon larger living entities. The nature of the problem is illustrated in Fig. 1. In this figure the circle represents a cell, or a cavity filled with liquid. In one part of the system heat is produced at the rate dQ/dt. The local generation of heat tends to raise the temperature, thereby producing an increasing difference in the temperatures and densities of the system. However, steady state is maintained through the operation of the following fluxes: J_{TD}, the flow of heat by thermal diffusion; J_C, the circulation of the liquid by convection, caused by the inequalities of the densities within the system; J_{OW}, the osmotic flow of water across the boundary of the system, caused by the increased activity of water in the warmer part of the system.

Alternatively, the flows of different solutes across the boundary of the system may not be the same at different areas of the boundary. This may tend to create a local change in density. Under terrestrial conditions, convectional flow within the cell contributes toward the maintenance of a steady state. In low gravitational fields, or in weightlessness, the effect of convection is reduced or completely eliminated. The question arises, then, as to the possible effects of prolonged reduction or complete elimination of gravitational convection upon the behavior of the cell or of a larger system.

The flow of heat by thermal conductivity, the flow of substances by diffusion within a homogeneous system and the flow of substances across boundaries can in principle all be treated by mathematical analysis. On the other hand, not enough is known about the complexities of convectional flow. An experimental approach is called for.

EXPERIMENTAL PROCEDURES

INVESTIGATION OF MACROSCOPIC SYSTEMS. As a first step, it was decided to investigate convection, and effects of reduced gravity, in easily handled relatively large systems, e.g. a pipette filled with two solutions of different densities. The answers to the following types of questions were sought:

1. Given a cylinder containing a heavy solution in its lower half and a

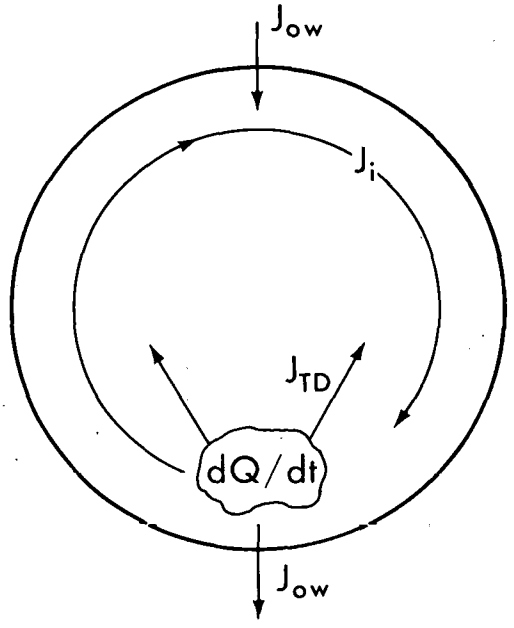

Figure 1. MU-31616

light solution in its upper half, what is the nature of the motion of the liquid when the cylinder is rotated through an angle of 90° about an axis perpendicular to its own axis? How is the motion affected by a decrease in the gravitational force?

2. Given two reservoirs containing solutions of densities ρ_1 and ρ_2, with $\rho_1 > \rho_2$, and with the denser solution situated above the lighter solution, what is the mechanism of exchange of solutions between the two reservoirs if they are connected by a tube of length H and radius R? How are the qualitative and the quantitative characteristics of the counterflow exchange affected by the values of H, R, and by the viscosity, η, of the fluid? What are the qualitative and quantitative effects on the volume exchange when the gravitational acceleration g (here considered as a variable) is progressively decreased to a very small fraction of the value of g at the surface of the earth?

SIMULATION OF LOW VALUES OF GRAVITY. Since convectional motion is powered by the joint effects of the difference in density, $\Delta\rho = \rho_1 - \rho_2$ and of the value of g, lower values of g can be simulated in a terrestrial laboratory by an appropriate decrease in the value of $\Delta\rho$.

USE OF INDICATORS. Convectional motion may be observed because of the differences in the refractive indices of the two solutions. This method of observation is not satisfactory, particularly when the two solutions are of nearly the same density, e.g. in an experiment in which a very low value of g is simulated.

Incorporation of a dye in one of the solutions facilitates greatly the observations of finer details of motion. However, as soon as some mixing takes place, the dye is also present in the originally colorless solution. Distinction between the two solutions becomes increasingly difficult, since the visual difference between the two solutions is quantitative, rather than qualitative, and the difficulty of distinguishing between the two solutions is aggravated by the distortion caused by the cylindrical vessels holding the solutions.

For these reasons, an acid-base indicator is incorporated in equal concentrations in each of the two solutions. A small amount of acid is added to one of the solutions, and a small amount of base is added to the other. With a judicious choice of indicator, each solution maintains its original color, even after a considerable amount of mixing has taken place. The large qualitative contrast in color makes it possible to observe the motion in various parts of the system in its finest details.

A relatively large number of acid-base indicators is available for use. There are two choices in the allocation of the acid and of the base, respectively, to the two solutions. There is some latitude in selecting the concentrations of acid, of base, and of indicator. All these degrees of freedom add to the effectiveness and versatility of this method of marking the two solutions. The choices to be made depend upon the objective sought in each experiment. Examples of the considerations governing the various choices for a particular experiment will be given in later parts of this report.

APPARATUS. The apparatus used for the study of convectional exchange through a cylindrical tube is shown in Fig. 2. The upper, denser solution is kept in a modified 100-cc pipette. The lower, lighter solution is kept in a white evaporating dish. The upper solution contains bromothymol blue (BTB), 0.01 M sodium hydroxide and a known concentration of sodium chloride. This solution is blue. The lower solution contains 100 cc of distilled water marked with BTB. To begin with, a known small volume of a known concentration of hydrochloric acid is added to the water. This acidified solution is yellow. At the beginning of the experiment, the yellow solution is quickly poured into the evaporating dish at zero time. Convectional exchange begins as soon as contact is made. The stirrer maintains a fairly uniform composition throughout the lower solution. When the blue end point is reached, the time is noted, and another, small volume of hydrochloric acid is added from a burette. So far, the following concentrations of hydrochloric acid were used, depending upon the speed of the up and down transport of the two solutions: 0.01M, 0.025M, and 0.10M. When the density difference is small, and 0.01M HCl is used, it is a simple matter to obtain 20 or more points on the curve relating the volume of sodium hydroxide transported downward and time. At the highest speeds, when 0.10M HCl is used, it is possible to obtain eight to 10 points.

The upper vessel is made from a commercial 100-cc pipette as follows: The upper stem is shortened and is provided with a short length of rubber tubing and with a screw cock. The lower stem is shortened and is left open. The diameter of the lower end is measured by attaching it to a 10-cc burette and measuring the volume of a column of water of known length.

Since it is desired to study the effects of the length, H, and of the radius, R, of the exchange tube, several pipettes have been modified by removing the lower stem completely and replacing it by a tube of desired length and diameter. Preliminary indications are that the rate of convectional exchange through a tube is very sensitive to the diameter of the tube. Commercial pipettes are not provided with stems of a precisely constant diameter. Different sticks of glass tubing with the same nominal outside diameter may have significantly different values of R. If the rate of exchange is proportional to the fourth power of the diameter, as is the case with laminar flow through a tube, then a 10% difference in diameters may cause a 46% difference in rates. To insure equal values of R, for the study of the effect of H (R constant) and for the concurrent observation of the rates determined by other variables, H and R constant, several pipettes were supplied with sections taken from the same stick of glass tubing. Even with these precautions, the diameters of sections taken from different parts of the glass stick may differ by as much as 2%. A record is kept of the pipette used in each experiment, and a suitable correction will be made after the effect of the diameter upon the rate of exchange is definitely known.

The pipette is mounted on a long and narrow carriage (a strip of plywood) by means of one or two spring clips. In turn, the carriage is mounted on a vertical pegboard by means of a single bolt. This arrangement permits easy and fast rotation of the pipette in a vertical plane. The lower end of the pipette is adjusted to be at the same level as the axis of rotation, so that rotation of the tube will cause a minimum of disturbance at the point of contact with the lower solution.

The angle between the axis of the tube and the vertical is measured by means of a protractor permanently attached to the wooden carriage. The protractor is provided with a plumb line consisting of a small brass weight attached by a thin thread to the center of the protractor.

When it is desired to make a quick change from $\theta = 0$ to some other value of θ, or in the opposite direction, two bolts are used as stops. They are inserted in appropriate holes of the pegboard.

The pegboard is backed by a plywood frame, 4 in. wide and perpendicular to the plane of the pegboard. The whole assembly is held firmly in position by

means of lead weights resting on the frame. The horizontal orientation of the table top is checked with a precision carpenter's level.

MODIFICATIONS OF THE ASSEMBLY. When it is desired to observe the behavior of an established surface of separation between the two solutions, following a change in the orientation of the pipette, the carriage is attached to the pegboard by a single bolt located at the midpoint level of the main body of the pipette. Both ends of the pipette are provided with rubber tubing and screw cocks. The pipette is first filled with the lighter solution, from below, by suction; the overflow is allowed to escape into another pipette. The heavier solution is then introduced, again from below, until the surface of separation is approximately at the middle of the pipette. The two exits are closed, the filling tubes are disconnected, and the assembly is ready for rotation about the midpoint of the pipette.

When it is desired to observe concurrently the behavior of several pairs of solutions, several pipettes are mounted on a larger pegboard and are supplied with the desired solutions. The whole pegboard is then rotated about one of its lower corners.

It may be worth while to call attention to the versatility of the assembly consisting of the pegboard, having numerous holes arranged in a geometrically precise grid, and the carriage. The versatility of the apparatus is enhanced by two long slots in the carriage and several holes, all located along the long axis of the carriage. A cabinet maker working in a well equipped carpenter shop can build pegboard, frame, and several carriages in less than an hour.

CHOICE OF METHOD OF MARKING THE TWO SOLUTIONS. As mentioned earlier, one solution is marked by the combination (acid + indicator) and the second solution is marked by the combination (base + indicator). For quantitative work it is desirable to select an indicator that changes color over a short range of pH , centering about pH 7. In addition, it is desirable to select an indicator that shows a marked contrast in colors. Bromothymol blue meets both of these specifications because it changes from yellow to blue over the pH range 6.0 to 7.6. The stock solution of this indicator is prepared by dissolving 0.40 g in 60 cc of 0.01$\underline{M}$ sodium hydroxide. This solution is diluted to one liter. Thus, this stock solution contains $6 \times 10^{-4}\underline{M}$ sodium hydroxide. When used in the ratio of 1 cc of stock solution per 100 cc of the experimental solution, the concentration of sodium hydroxide is further diluted to $6 \times 10^{-6}\underline{M}$. Thus, the presence of sodium hydroxide in the stock solution of indicator may be neglected.

The loading of the upper, denser solution is accomplished by addition of sodium chloride. For this reason there is a choice for the allocation of

the acid and the base, respectively; the base may be added either to the upper or the lower solution, provided the contributions of the two reagents to the specific gravities of the respective solutions are allowed for in the calculation of the initial difference in densities. In the method described in an earlier section the lower solution is exposed to air, with constant stirring. For this reason it is preferable to assign the sodium hydroxide to the upper solution, in order to minimize the absorption of carbon dioxide from the air.

When it is desired to watch the upward progress of the lower solution, after it enters the main body of the pipette, it is easier to watch the progress of a thin blue streak through a yellow solution than it is to watch the behavior of a thin yellow streak in a blue solution. For this type of experiment it is preferable to allocate the base to the lower solution and the acid to the upper solution.

With the upper solution containing initially some concentration, C_1M NaOH, and the lower solution containing a concentration of hydrochloric acid which varies between end points and takes a sudden upward jump upon addition of the next aliquot, after every end point, the difference in densities between the two solutions would be most erratic in the course of a single run, unless the concentrations of base above and acid below are kept small, as compared with the concentration of sodium chloride. On the other hand, too low concentrations of acid and base yield vague time readings for the end points. Some compromise is needed, and it was found that a concentration of 0.01M sodium hydroxide in the upper solution yields satisfactory results.

In a series of experiments with a variable density difference, the upper solution may contain, in separate experiments, 0.01M sodium hydroxide on X M sodium chloride, with X changed from one experiment to another. In this series of experiments of decreasing density differences, there is a lower limit to the density difference, namely when X = 0. Actually, the series was stopped at X = 0.01M. In other words, in the last experiment of this series the concentrations in the upper solution were 0.01M NaOH + 0.01M NaCl.

The series was extended downward by using the following series of concentrations: Y x (0.01M NaOH + 0.01M NaCl). In both series the concentration of indicator in the two solutions was kept constant, namely by dilution of the stock indicator solution in the ratio 1:100.

From the description of the quantitative method it is clear that the solution moving upward through the exchange tube contains a concentration of acid which is much smaller than the concentration of base in the solution moving downward through the same tube. When the movement of the two solutions is turbulent, the acid is quickly overwhelmed by the base, and the color is blue

over the entire tube, except for a very short section near the bottom. Even in these circumstances it is possible to observe the violence of the motion, due to the difference in refractive indices. However, it was difficult to see the movement in great detail. The difficulty of making visual observations increased toward the end of the run, because of the decrease in the difference between the two refractive indices. To obviate this difficulty, some of the quantitative experiments were preceded or followed by a qualitative experiment, in which the initial acid concentration in the lower solution was made equal to the initial base concentration in the upper solution. If this change in concentration, from quantitative to qualitative experiment, is not to change materially the nature of the movement, it is necessary that the added sodium chloride should carry the major burden of loading the upper solution. This is another reason for keeping the acid and base concentrations small.

In those qualitative experiments in which a pipette containing the two solutions was rotated in a vertical plane, the use of bromothymol blue yielded only two colors, the blue of the basic solution and the yellow of the acid solution. For this indicator the color change takes place over the short pH range 6.0 to 7.6. The intermediate green color was not seen at the boundary between the two solutions. In order to produce visual evidence of the behavior of the system at the boundary, it is necessary to use an indicator that changes colors over a much larger range of pH values. For this purpose universal acid-base indicator was used.

Universal indicator changes colors from red, below pH 2, through orange, yellow, green, to dark blue at pH 10 or more. When this indicator was used, it was easy to observe a zone of orange to green between the red of the acid solution and the blue of the basic solution. The width of the zone depended on the nature of the experiment and thus yielded further information about the behavior of the system. Up to the time of writing the present report no effort was made to design the experiments in such a way as to use this information. However, it was thought worth while to mention the availability of this type of information.

The versatility of this method of marking the two solutions will be illustrated by another example. In one qualitative experiment the upper solution was labeled with 0.01M NaOH; the lower solution was labeled with 0.0001M HCl. Bromothymol blue was used as the indicator. In this experiment the density difference was small, and the movement was non-turbulent. A thin yellow streak was observed to issue from the top of the 9.5-cm-long exchange tube. The streak meandered through the blue solution in the main body of the pipette and petered out about two-thirds of the way. The base was 100 times more concentrated than the acid. The mixing of a given volume of the acid solution with 1% by volume of the basic solution would have changed its color from yellow to blue. This experiment showed that it was possible for the yellow solution to travel more

than 15 cm in intimate contact with the blue solution, without incorporating as little as 1% of the latter.

The disappearance of the yellow streak in the main body of the pipette is probably associated with the much larger diameter of the main body. Other experiments had indicated definitely that the speed of exchange is very sensitive to the diameter of the tube and that higher speeds tend to produce turbulence and mixing.

EFFECTS OF TEMPERATURE. A change in temperature in the course of an experiment may affect the course of the experiment in several ways. Similarly, a difference in temperature between two otherwise identical experiments may affect the comparability of the experiments.

An increase in temperature decreases both the density and the viscosity of a solution. Table 1 shows the density and the viscosity of water at 20° and at 30°, respectively:

Table 1.

Temperature:	20°	30°	Mean temperature coefficient
Absolute density (Density units; 1 D.U. = 1 g/cc)	0.998203	0.996646	-1.56×10^{-4} D.U./deg
Viscosity (centipoise)	1.0050	0.8007	-0.02 centipoises/deg

All physical data given in this report are quoted from Handbook of Chemistry and Physics, Chemical Rubber Publishing Co., 38th Ed., 1956-57.

For a proper sense of perspective it is desirable to consider the effects upon the specific gravity of adding solutes such as sodium chloride, sodium hydroxide, and hydrochloric acid. The effect is not quite proportional to the molar concentration. In a calculation of the driving force for a given pair of solutions actual handbook values are used. However, for dilute solutions the change in specific gravity is approximately proportional to the molar concentrations. The following are the coefficients of proportionality for dilute solutions:

NaCl: 413×10^{-4} D.U. per mole per liter
NaOH: 447 " " " "
HCl: 182 " " " "

By comparing the two coefficients, it is seen that the effect upon the

density of a solution of 1° rise in temperature is the same as the effect of subtracting approximately 1.56/413 = 0.0038 moles of sodium chloride per liter.

In the present, exploratory stage of the investigation no attempt is made to keep the temperature of the solutions constant. Before starting an experiment, the two solutions to be used are kept on the same table. Room temperature readings are taken at the start and during the course of the experiment. In those experiments in which one of the solutions is easily reached by a mercury thermometer, several readings of the temperature of that solution are also taken.

In the earlier experiments, when the laboratory was kept warm by heating, the temperature was fairly constant, at around $25^{\circ}C$. With the advent of summer the temperature was more variable, from morning to evening or from one day to another. The range was approximately 20 to $27^{\circ}C$. The difference between the temperature of the accessible solution and room temperature may be, at times, as high as $0.3^{\circ}C$.

To allow for the change of viscosity with temperature, the observed rates were normalized to the temperature at which the viscosity of water is 1 centipoise. Thus, if the observed rate is q cc/min, and the viscosity is η centipoises, the normalized rate is $q.\eta$. This adjustment is only tentative, pending an investigation of the effect of viscosity upon the rate of convectional exchange. It may turn out that the effect of viscosity upon turbulent exchange is different from the effect upon non-turbulent exchange.

Let us consider other effects of temperature and estimate their probable magnitudes. The difference in densities of the two exchanging solutions is estimated from handbook values of specific gravities of solutions. These are given for one temperature, $20^{\circ}C$. In principle, the temperature coefficients of density of different solutions differ from one another and from that of water. When the upper solution is dilute, and the lower solution is almost the same as distilled water, the discrepancy between the two temperature coefficients must be a small fraction of the coefficient of water, which, in turn, is small. Therefore, this effect may be neglected. If the upper solution contains concentrated, say 5 molar, electrolyte, the discrepancy between the two temperature coefficients may be of the same order as the temperature coefficient of water. It was shown in a previous part of this section that a rise in the temperature of water of $1^{\circ}C$ produces the same effect as the removal of 0.0038 moles of sodium chloride per liter. Obviously, the effect is small, when compared with the total driving force, and may be neglected. We conclude, then, that handbook values of specific gravities for one temperature may be used to calculate the driving force at another not too different temperature, provided the two solutions are at the same temperature.

Let us examine the case when, in the absence of rigid temperature control, the temperatures of the two exchanging solutions are different. For the sake of concreteness, we will assume that the upper solution is warmer by $0.3^{\circ}C$. The effect upon the difference between the two densities is the same as that of removing from the upper solution 0.3 x 0.0038 = 0.00114 mole of sodium chloride per liter.

In the series of experiments mentioned earlier, in which the driving force may be described as a sum of concentrations: 0.01M NaOH + XM NaCl, the lowest member of the set had an initial driving force of 0.01M NaOH + 0.01M NaCl, which is a little larger than that of 0.020M NaCl. A temperature difference of 0.3° changes the driving force by 0.00114M NaCl, or by approximately five percent. If the two temperatures are known, a correction may be applied, to calculate the initial driving force. As the experiment progresses, and the driving force approaches zero, the effect of a difference between the temperatures of the two solutions becomes progressively more important.

The main conclusions to be drawn from the analysis carried out in this section are these: If temperature is the same in the two solutions, it affects the course of convectional exchange chiefly by affecting the viscosities of the solutions. The driving force between a given pair of solutions is approximately independent of the temperature within the relatively small range of operating temperatures. A difference in temperatures between the two solutions affects the driving force by approximately 0.0004M NaCl (using concentration as a driving force) for a difference of $0.1^{\circ}C$ between the two solutions. Lack of control of the temperatures of the two solutions introduces a vague lower limit to the magnitude of the driving force which may be used with confidence. An uncertainty of $0.1^{\circ}C$ in the temperature difference between the two solutions introduces an uncertainty of 0.0004M NaCl in the driving force.

EFFECTS OF HEAT OF NEUTRALIZATION. The value of the heat of neutralization is given by the following equation:

$$H^{+} + OH^{-} = H_2O + 13{,}700 \text{ cal}$$

Let us examine the effect, upon the temperature of the lower solution, of following the rate of exchange by titrating the transported sodium hydroxide with hydrochloric acid. In one of the fastest exchanges measured so far 20 cc of the upper solution exchanged with 20 cc of the lower solution (water) in the first minute. The upper solution was marked with 0.01M sodium hydroxide.

No. of moles of base transported in one minute:	$0.020 \times 0.01 = 2 \times 10^{-4}$ moles
Heat evolved upon neutralization:	$(2 \times 10^{-4}) \times 13{,}700 = 2.74$ cal

The initial volume of the lower solution was 100 cc. The base was neutralized with 0.1M hydrochloric acid. Therefore, the volume, after neutralization, was 102 cc, and the heat capacity of the lower solution was approximately 100 cal/deg.

Rise in temperature: $2.74/100 = 0.027^{\circ}C$

The conclusion is reached that the temperature effect caused by the heat of neutralization may be neglected. However, it should be emphasized that acid or base should be used as marker only, in small concentrations, and not as loading substances. The load in this particular experiment was 5M sodium chloride. Let us estimate the rise in temperature per minute if sodium hydroxide were used both as marker and load. To achieve the same rate of exchange, approximately 5M sodium hydroxide would have to be used. The volume exchanged per minute would still have been approximately the same, but the amount of base transported would have been 500 times larger, and the rise in temperature upon neutralization would have been of the order of $13.5^{\circ}C$.

METHOD OF LOADING THE UPPER SOLUTION. In general, a relatively large number of solutes may be used. However, in anticipation of supplementing in the future the quantitative method of acid-base titration with the method of using electrical conductivity as a means of following the course of convectional exchange, it was decided to use an electrolyte as a load. Because of the decision to use sodium hydroxide as one of the markers, the use of many salts was eliminated, to avoid complicating chemical reactions with the hydroxyl ion. Sodium chloride was therefore left as an obvious choice.

The range of driving forces available through the use of sodium chloride is limited, at its upper end, by the solubility of sodium chloride in water. The maximum driving force thus available is approximately 0.20 grams per cc. In order to extend this range, potassium iodide was used in recent experiments. This measure extends the range of driving force to approximately 0.6 g/cc.

QUANTITATIVE ASPECTS OF CONVECTION THROUGH A CYLINDRICAL TUBE

The investigation is still in progress, and the following notes are in the nature of a progress report.

QUANTITATIVE DESCRIPTION OF THE EXPERIMENTAL PROCEDURE. The pipette shown in Fig. 2 held 97 cc of an aqueous solution, containing 0.01M sodium hydroxide as a marker, XM sodium chloride as load and bromothymol blue as indicator. The length of the lower tube was 9.5 cm, and its inside radius was 0.266 cm. The lower solution consisted of distilled water, and bromothymol blue as indicator. The transport of the upper solution downward (and the equal

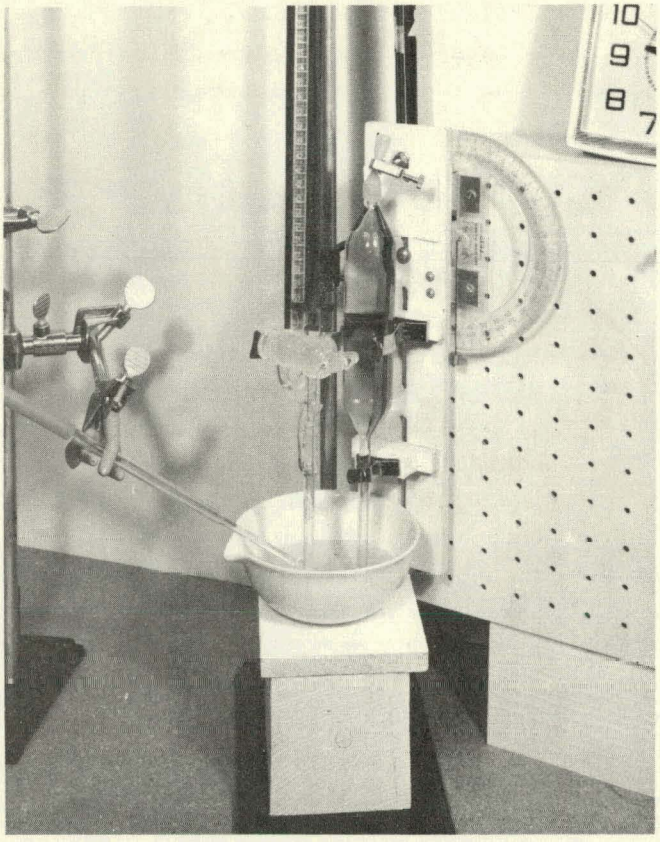

Figure 2. S.B.-58

transport of the lower solution upward) was measured by adding aliquot portions of an appropriate concentration of hydrochloric acid and by noting the time of appearance of each successive end point.

GRAPHICAL METHOD OF PRESENTING THE COURSE OF THE EXCHANGE. It is convenient to present, as a function of time, the number of cc of 0.01M sodium hydroxide transported into the lower solution. In this series of experiments the maximum value is 97 cc. The volume of base transported is not a direct measure of the actual volume of the two-way traffic in the same time. The sodium hydroxide is converted into sodium chloride by titration. On the other hand, a particle of water makes the down and up trip an infinite number of times before equilibrium is reached.

The method of calculating the actual volume of transport at a given time will not be taken up in this report. Suffice it to say that for relatively short initial intervals in which the transport of sodium hydroxide is not more than 10% of the original contents of the upper solution, the volume of 0.01M sodium transported is equal to the volume of water transported, to within approximately 1%.

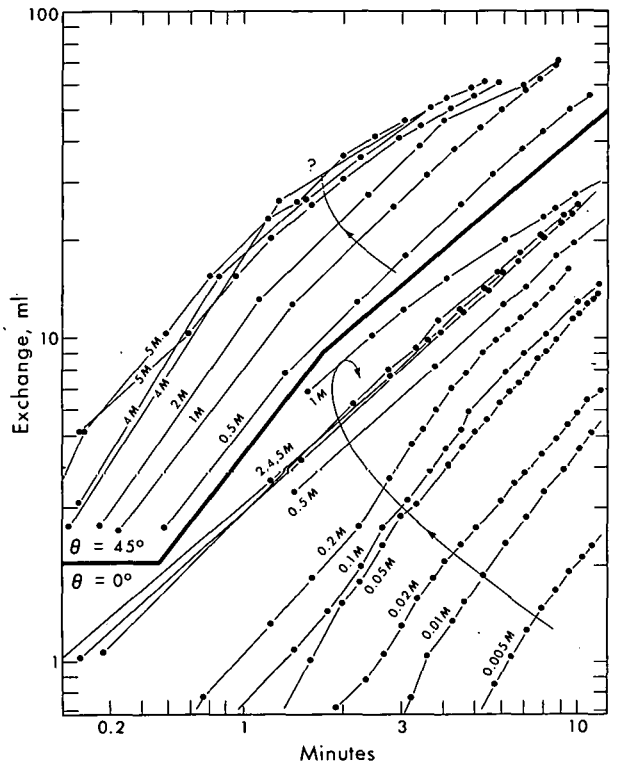

Figure 3. MU-31615

It is convenient to plot the volume of sodium hydroxide transported, against time, on a log-log field. This method of plotting spreads the curves, permits the representation of very fast and very slow rates with the same relative accuracy, and avoids the crowding of points near the origin. Furthermore, if the volume transported is initially approximately proportional to time, then the points fall approximately upon a line of slope 1.0.

Fig. 3 shows the results obtained in two series, in which the lower set shows the volume of transport when the exchange tube was vertical ($\theta = 0$); the upper set shows only the higher members of the same series of concentrations, with the tube inclined 45° to the vertical. In this figure each point is an observed experimental point.

Turning to the lower set ($\theta = 0$), and following the arrow, we observe that the rates increase with the load, from 0.005M to 1M sodium chloride. The rates are approximately equal when the load is 2, 4, 5M sodium chloride, and they are smaller than with a load of 1M sodium chloride.

Turning to the upper set of curves ($\theta = 45^{\circ}$) and comparing this set with the lower set of curves we find that, with the high loads shown, for equal loads, the rate is higher when the tube is in an inclined position. The lower members of this particular set of curves are not shown in this figure. However,

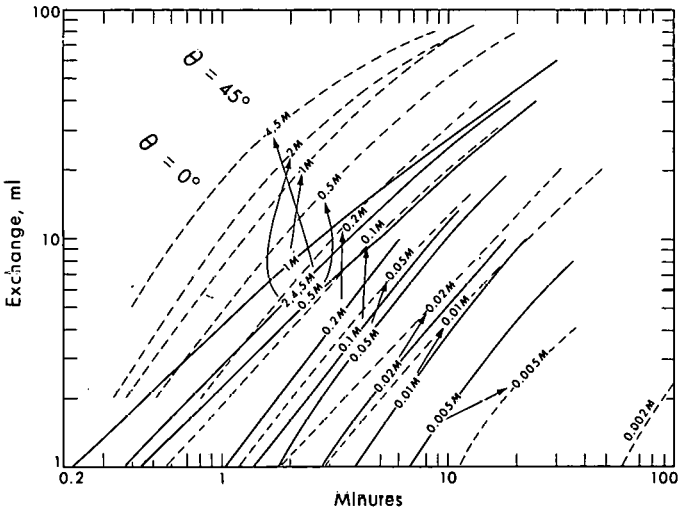

Figure 4. MU-31614

as will be seen in the next figure, the rate increases with the load, from 0.002M NaCl to 2M NaCl. For loads of 4M and 5M sodium chloride, each carried out in duplicate, the rates seem to be the same, within the accuracy of duplicating an experiment.

Fig. 4 shows the complete set of smoothed curves for both series, from the time when the volume of sodium hydroxide transported was 1.0 cc or more. The solid curves represent the series with $\theta = 0$; the dashed curves represent the series with $\theta = 45^{\circ}$. In this figure, the liberty was taken of representing the highest three loads by a single curve, in the set of solid curves, and of representing the highest two loads by a single curve in the set of dashed curves.

INITIAL RATES AS A FUNCTION OF THE LOAD AND THE ANGLE OF INCLINATION. As was mentioned earlier, the initial rate of transport of sodium hydroxide represents fairly accurately the initial rate of exchange. Unfortunately, the first experimental reading cannot be used, for the following reason: At time zero, the exchange tube contains the upper solution only. It takes a little time before steady state is achieved, and both solutions are present in the exchange tube. For this reason, two measures of the initial rate were obtained, whenever possible, in the following manner: The first measure was calculated from the difference between the time of transport of 1 cc and the time of transport of 5 cc. The difference in time, divided into the difference in volumes, yields the rate, in cc/min. The second measure was obtained from the difference of time of transport of 2 cc and of 10 cc. As a tentative effort to allow for differences in temperature, the calculated rates were normalized by multiplying the rate by the viscosity at the temperature of the experiment, expressed in centipoises.

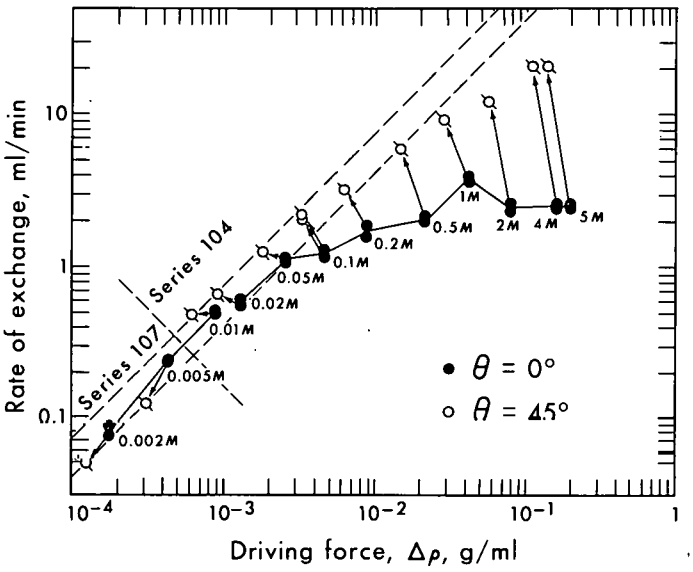

Figure 5. MU-31613

The results are shown in Fig. 5, in which the rates for the series with $\theta = 0$ are connected by line segments. Each of these rates is tied by an arrow to the corresponding rate at $\theta = 45^{\circ}$. The rates are plotted against the driving force in the respective experiments. The driving force in each case was calculated from the handbook values of specific gravities of sodium chloride solutions, with allowance for the presence in the same solution of 0.01M sodium hydroxide. The 45° points are shifted to the left, by a factor equal to $\cos \theta = 0.707$.

Turning our attention to the series at $\theta = 0$, we find that at small loads the initial rate is approximately proportional to the initial load, as may be seen from the fact that the points fall approximately upon a 45° line. Beyond a load of approximately 0.05M sodium chloride, or 2.5×10^{-3} g/cc, the rate increases slower than the load, reaches a maximum, then approaches a value that is independent of the load, up to the upper limit of the range of loads studied.

Comparing each of these rates with the corresponding rate at $\theta = 45^{\circ}$, we find that, at low loads, the effect of changing the orientation of the exchange tube is small and erratic. At the higher loads, there is a more systematic change. The larger the load, the larger is the difference between the rates at the two orientations of the exchange tube. At the highest loads studied, the rate in the inclined tube was 9.7 times larger than the rate in the vertical tube.

More insight into the nature of the convectional exchange was obtained from a few parallel, qualitative experiments.

QUALITATIVE OBSERVATIONS. As described in fuller detail in an earlier

part of this report, a qualitative parallel experiment is performed by marking the lower solution with 0.01M hydrochloric acid, in addition to the indicator.

When the load is large, there is violent, turbulent motion within the exchange tube. The yellow color of the lower, lighter solution does not survive its passage into the main body of the pipette, because of its turbulent mixing with an overwhelming basic solution. When the apparatus is inclined in the midst of a run, the turbulence disappears, the two opposing streams organize themselves into two layers, with the heavier, blue layer at the bottom. The yellow stream passes into the body of the pipette, and on to the top, forming a layer of yellow above the original blue solution. The blue solution issues downward, from the bottom of the pipette. If the lower solution is kept in a beaker, and in the absence of stirring, the blue solution collects at the bottom of the beaker. If, now, the apparatus is brought back to the vertical position, the motion becomes turbulent again. However, toward the end of the run, when the driving force approaches zero, and the rate of exchange is very much slower, the two colored streams begin to arrange themselves into parallel vertical layers.

When the initial driving force is small, the two streams arrange themselves into two parallel vertical layers, even in a vertical tube. Each stream survives passage into the main body of the other solution and collects as a separate layer. Inclination of the apparatus in the course of a run produces no striking changes in the nature of the convectional exchange.

Undoubtedly, the increase in rate of exchange when the tube is inclined is associated with the fact that the two streams organize themselves in such a way that neither interferes with the progress of the other. Further investigation of this phenomenon is intended.

ACKNOWLEDGEMENTS

This work was supported by the National Aeronautics and Space Administration.

Patterns of High- and Low-Density Lipoprotein Distributions in Man

Alex V. Nichols, Robert K. Tandy and Oliver F. deLalla

The significant differences in lipoprotein concentrations between healthy male and female populations have been well documented by many investigators (1, 2,3,4). These differences in concentrations appear in both segments of the total lipoprotein spectrum. Thus, in the low-density spectrum, males exhibit significantly greater mean concentrations of S_f^o 0-400 lipoproteins than females in the age range of 20-50 years. This differential accounts in great part for the observed serum triglyceride and cholesterol concentration differences between the sexes. Furthermore, this differential between the sexes in low-density-lipoprotein concentrations is maintained in spite of significant increases in their concentrations with age in both sexes up to the ages of 50-65 years.

In the high-density-lipoprotein (HDL) spectrum, the differential in lipoprotein concentrations is due in great part to the significantly higher mean HDL_2 concentrations encountered in females relative to males at all ages (5). The magnitude of this differential appears to be least in the early years (approximately 18-23 years) and then increases to a relatively constant value soon thereafter (6). After these early years, the absolute values of the mean HDL concentrations do not appreciably increase or decrease.

In abnormal subgroups of the population at large, specifically those comprised of individuals with diseases such as biliary obstruction, nephrosis, Tangier disease, xanthoma tendinosum, xanthoma tuberosum, and essential hyperlipemia, significantly lower HDL_2-lipoprotein concentrations are encountered relative to matched controls (7,8). In these subgroups, specific low-density-lipoprotein fractions are generally markedly elevated (9).

The inverse nature of the above distributions of low-density- and high-density-lipoprotein concentrations has given rise to considerations of possible metabolic associations between these lipoprotein species. Statistical tests of correlation between these species in healthy populations have yielded significant but low-order negative correlation coefficients (4). It was concluded from such low-order correlations that the metabolic factors regulating low-density- and high-density-lipoprotein concentrations are largely independent of each other. If, however, the population sampling did not adequately cover the complete range of possible lipoprotein-concentration values, then it is

possible that the actual correlations between the species may in fact be appreciably different than those determined above. Moreover, if the frequency distributions of the lipoproteins are appreciably skewed, then the criteria for computation of the Pearson coefficient of correlation may not be fully satisfied and the results may be misleading. It will be shown in this report that the distributions of certain lipoprotein species do exhibit appreciable skewness.

It is most interesting to note, however, that metabolic processes apparently do exist that, upon specific stimulation, produce reciprocal-type changes in serum-lipoprotein concentrations. Evidence for the existence of such processes has been gained through work on the influence of gonadal hormones on serum-lipoprotein concentrations (10,11,12,13). Thus, the administration of estrogens is generally associated with increasing HDL serum concentrations, while androgens have been associated with decreases in HDL concentrations. Concomitant reciprocal changes in low-density-lipoprotein concentrations frequently occur along with these HDL alterations, but they do not occur universally in all subjects receiving such hormones. This variability may be a question of dose and individual response in these subjects.

Since certain abnormal lipoprotein distributions associated with unfavorable risks from cardiovascular disease may be corrected by agents stimulating this reciprocal-type process (i.e., stimulating reductions in low-density lipoproteins and concurrently increasing high-density lipoproteins), clarification of this metabolic mechanism seems worthwhile. The suggestion could be made that some imbalance in the control of such processes may be responsible, in part, for the abnormalities occurring in human-lipoprotein distributions.

What these specific processes are is not yet clear. Recent observations indicate that glyceride metabolism may be implicated (14,15). These observations describe, (a) an increase in glyceride transport by high-density lipoproteins in association with increased concentrations of low-density lipoproteins during fat ingestion; and (b) an increased glyceride content of the high-density species as a function of the steady-state serum glyceride, or very low-density-lipoprotein concentrations. In the light of these observations and the considerations indicated above, we decided to investigate further, in greater detail than previously reported, the properties of the low- and high-density lipoprotein distributions in male and female population groups.

METHODS

The population group under investigation consisted of employees of the University of California Lawrence Radiation Laboratory at Livermore, California (4). Venous blood samples were collected from nonfasting subjects during routine periodic physical examinations. Excluded from the study were individuals with the following medical diagnoses: (a) acute infection; (b) poliomyelitis;

(c) surgery involving partial or complete organ removal; (d) medication involving steroids, thyroid extract, etc.; (e) cardiovascular disease; (f) cancer; (g) multiple sclerosis; (h) pregnancy; and also (i), persons with special dietary requirements. Ages of subjects ranged from 17 to 65 years. The group was comprised of 1,961 males and 326 females.

Lipoprotein determinations and analyses were performed according to methods previously described in detail elsewhere (5,16). Specifically, the lipoprotein groups measured were the low-density species S_f^0 100-400, S_f^0 20-100, S_f^0 12-20, S_f^0 0-12, and the high-density species HDL_1, HDL_2, and HDL_3. The accumulated lipoprotein data were first segregated by sex into the following age groups: males, 17-29, 30-39, 40-49, 50-65; and females, 16-29, and 30-49 years. Means and standard errors of the means were obtained for all lipoprotein species analyzed. From the means and the standard deviations of the distributions, we calculated for each lipoprotein group its values corresponding to $\pm$ one standard deviation, $\pm$ two standard deviations, etc. After selecting one lipoprotein group as reference, each individual's lipoprotein data were sorted according to his position on the standard deviation scale for the specific reference lipoprotein group in question. Following this sorting procedure, the means and standard errors of the means were calculated for each individual's lipoprotein data falling within the standard deviation scale described above. Thus, it was possible to determine the mean serum-concentration values of all species for individuals having values of the reference lipoprotein group a certain number of standard deviations below or above its mean for the population group. In this way, the lipoprotein distributions of specific subgroups in the population become apparent, and differences between them become calculable.

RESULTS AND DISCUSSION

The primary lipoprotein data for the population under investigation are presented in Table 1. Tables 2-15 show the resultant mean lipoprotein values obtained upon ordering the data by the standard deviation intervals of a particular lipoprotein species. Standard errors of the means and the numbers of individuals falling within each population subgroup by the above selection process are also reported, along with the mean lipoprotein-concentration values.

The following observations can be made on the data presented in the tables:

TABLE 1. These data define the population under investigation and show the influence of age and sex on lipoprotein levels as previously described in the literature. In addition, these data form the basis for calculation of the standard deviation intervals used in all subsequent tables. Reference will be made to this table in subsequent discussions.

Table 1. Mean lipoprotein concentrations in UCLRL[a] population (in mg/100 ml)

Age in years	Number of subjects	S_f^o 100-400	S_f^o 20-100	S_f^o 12-20	S_f^o 0-12	HDL_1	HDL_2	HDL_3
				MALES				
17-29	585	37(1.8)[b]	75(1.7)	40(0.9)	322(3.6)	23(0.3)	37(1.2)	217(1.7)
30-39	834	51(2.2)	91(1.9)	51(0.8)	355(2.9)	24(0.5)	36(1.0)	219(1.5)
40-49	399	66(4.6)	107(3.3)	57(1.2)	380(4.2)	25(0.8)	37(1.4)	226(2.5)
50-65	143	58(5.9)	103(4.9)	56(2.0)	383(6.3)	27(1.8)	42(2.7)	224(4.3)
				FEMALES				
17-29	190	9(1.0)	44(2.1)	30(1.2)	283(4.9)	21(0.5)	80(3.0)	228(2.8)
30-39	99	13(1.7)	51(3.6)	41(2.2)	324(8.7)	22(0.9)	81(4.5)	235(3.8)
40-49	37	18(4.0)	65(8.5)	42(3.5)	346(11.2)	23(0.8)	89(8.8)	241(7.2)

[a]University of California Lawrence Radiation Laboratory, Livermore, California.
[b]Standard error of the mean values are given in parentheses.

TABLE 2. In this table, the data are ordered on S_f^o 100-400 and several interesting points appear. Individuals with S_f^o 100-400 values below the mean for the age group have, on the average, significantly higher HDL_2 values than those with S_f^o 100-400 values above the mean. There is approximately a two-fold difference in magnitude between the mean HDL_2 values associated with the opposite extremes of the S_f^o 100-400 distribution. This difference is significant at the one-percent level of confidence for all ages. Another point of interest is the marked and significant depression of the mean S_f^o 0-12 lipoprotein level at the uppermost extreme of the S_f^o 100-400 distribution when it is compared with the mean S_f^o 0-12 value in the S_f^o 100-400 interval ("$+1\sigma$ to $+2\sigma$") adjacent to it in subjects 17-49 years of age. At this extreme position, we also observe, in all age intervals above 30 years, an almost twofold elevation in HDL_1 levels. This pattern of very high S_f^o 100-400, depressed S_f^o 0-12, and elevated HDL_1 values, has been previously reported as indicative of essential or idiopathic hyperlipemia (9). It is interesting to note that the S_f^o 0-12 depression is apparent prior to the HDL_1 elevation, while the HDL_1 elevation appears after much higher S_f^o 100-400 levels are attained than are present at 17-29 years of age. For the appreciable and significant increase in HDL_1 concentration associated with the transition from the 17-29- to the 30-39-year range, it would appear that a S_f^o 100-400 elevation of the magnitude of 100 mg/100 ml is required. The associated increases of S_f^o 20-100 with S_f^o 100-400 increases observed in this table are expected from the reported correlation between these two species. From these data and those for HDL_1 distributions, we estimate that the incidence of the complete lipoprotein abnormality associated with the diagnosis "essential hyperlipemia" is of the order of magnitude of two to three percent in males above 30 years.

Table 2. Mean lipoprotein levels in males associated with specific ranges[a] of levels of S_f^o 100-400 lipoproteins (in mg/100 ml)

Lipoprotein groups	Ranges of S_f^o 100-400					
	-2σ and less	-2σ to -1σ	-1σ to mean	mean to $+1\sigma$	$+1\sigma$ to $+2\sigma$	$+2\sigma$ and greater
Ages 17-29						
S_f^o 100-400		14(0.5)[b,c]		55(1.1)	98(1.7)	171(10.3)
S_f^o 20-100		56(1.4)		97(2.5)	122(5.6)	153(8.3)
S_f^o 12-20		35(0.9)		47(1.9)	55(3.6)	55(3.9)
S_f^o 0-12		309(4.1)		347(8.3)	361(12.7)	331(16.2)
HDL_1		22(0.4)		23(0.6)	23(1.1)	24(1.3)
HDL_2		41(1.5)		30(2.0)	26(2.7)	25(3.1)
HDL_3		219(2.0)		213(3.9)	217(4.5)	211(9.6)
N[e]		392		112	52	29
Ages 30-39						
S_f^o 100-400		20(0.6)[b]		74(1.3)	141(2.4)	281(19.4)
S_f^o 20-100		67(1.2)		117(2.3)	154(5.3)	248(13.7)
S_f^o 12-20		45(0.9)		60(1.7)	63(3.4)	64(4.1)
S_f^o 0-12		348(3.4)		380(6.1)	364(12.5)	311(16.9)
HDL_1		23(0.3)		23(0.5)	20(0.7)	51(10.8)
HDL_2		41(1.2)		26(1.6)	25(2.6)	22(3.0)
HDL_3		223(1.7)		211(3.0)	214(5.4)	212(9.9)
N		554		183	65	32
Ages 40-49						
S_f^o 100-400		30(3.9)[b]		99(2.4)	192(4.9)	376(35.8)
S_f^o 20-100		80(2.4)		139(3.7)	189(15.4)	302(35.6)
S_f^o 12-20		52(1.4)		67(2.2)	67(4.8)	68(7.4)
S_f^o 0-12		377(4.9)		396(9.3)	390(15.3)	305(21.0)
HDL_1		25(0.7)		24(1.2)	20(1.2)	46(16.8)
HDL_2		42(1.8)		27(2.4)	28(5.1)	17(3.2)
HDL_3		233(3.1)		214(4.6)	203(9.2)	204(11.2)
N		269		94	24	12
Ages 50-65						
S_f^o 100-400		25(1.7)[b]		87(2.9)	226(32.0)[d]	
S_f^o 20-100		78(3.5)		136(5.8)	208(23.5)	
S_f^o 12-20		50(2.2)		67(4.3)	71(5.9)	
S_f^o 0-12		377(7.9)		390(11.8)	411(20.6)	
HDL_1		26(1.1)		24(1.5)	42(18.5)	
HDL_2		48(3.6)		32(4.0)	24(4.0)	
HDL_3		226(5.3)		221(8.4)	220(14.4)	
N		97		33	13	

[a]Range of S_f^o levels is expressed in standard deviation units relative to mean level for S_f^o 100-400 group. This designation of range is followed in all subsequent tables.

[b]Values in this column are in range of S_f^o 100-400 values all below the mean. This broad range is used due to the fact that magnitude of standard deviation is greater than the value of the mean S_f^o 100-400 value.

[c]Standard error values are given in parentheses in this and subsequent tables.

[d]Values in this column are in range of S_f^o 100-400 values $+1\sigma$ and greater.

[e]N = number of subjects in each range interval; this symbol will be used in all subsequent tables.

The skewed character of this distribution, as evidenced by the unsymmetrical distribution of the population within the standard deviation intervals, should be noted.

TABLE 3. Here the data are ordered on S_f^o 20-100, and again we see the marked significant differences between the mean HDL_2 values associated with the extremes of the S_f^o 20-100 distributions. The mean HDL_2 values at the extremes vary by factors ranging from 2 to 2.5. In going from the low end of the S_f^o 20-100 distribution to the uppermost extreme, we find the HDL_2 values dropping to a relatively constant value upon reaching the values of S_f^o 20-100 in the interval defined by "Mean to $+1\sigma$." Further increases of S_f^o 20-100 or of S_f^o 100-400 are not associated with further decreases of any appreciable magnitude in mean HDL_2 concentrations. The distribution of S_f^o 12-20 is also found to be skewed for this population.

TABLE 4. When ordered on S_f^o 12-20, the data show appreciable changes in mean HDL_2 values. Significant lipoprotein trends are those expected in the S_f^o 0-12 and the S_f^o 20-100 arising from their statistical interrelation with the S_f^o 12-20 class. In addition, it should be noted that at the uppermost extremes of the S_f^o 12-20 distributions we find no evidence for any inversions in the trends of S_f^o 0-12 values as were noted for the distributions ordered on S_f^o 20-100 and S_f^o 100-400. The distribution of S_f^o 12-20 in this population group is unsymmetrical and skewed.

TABLE 5. In this table, the data are ordered on S_f^o 0-12 and the most striking lipoprotein interrelationships are those associated with the lowest S_f^o 0-12 values. At age intervals 30-39 and 40-49 years, we find very elevated mean S_f^o 20-100 and S_f^o 100-400 values associated with the very low means for S_f^o 0-12. Although these population groups are not large, these relationships are in complete agreement with those observed for the population groups having very high levels of S_f^o 20-100 and S_f^o 100-400. Excluding these two lowermost extremes of S_f^o 0-12 values at ages 30-39 and 40-49 years, we find the mean HDL_2 values decrease by approximately a factor of two in passing to the upper end of the S_f^o 0-12 distributions. The distribution of S_f^o 0-12 in this group is approximately normal.

TABLE 6. Data ordered on HDL_1 values are of greatest interest in the uppermost intervals of the distributions. At ages 30-39 and 40-49 years, very marked and significant elevations in S_f^o 20-100 and S_f^o 100-400 values are observed associated with high HDL_1 values. The mean S_f^o 0-12 value in the age interval 40-49 years is significantly lower than the mean S_f^o 0-12 value in the HDL_1 interval "$+1\sigma$ to $+2\sigma$" adjacent to it. The distribution of HDL_1 in the population appears nearly normal in males 17 to 29 years old but skewed in the older age brackets.

Table 3. Mean lipoprotein levels in males associated with specific ranges of levels of S_f^o 20-100 lipoproteins (in mg/100 ml)

Lipoprotein groups	Ranges of S_f^o 20-100					
	-2σ and less	-2σ to -1σ	-1σ to mean	mean to $+1\sigma$	$+1\sigma$ to $+2\sigma$	$+2\sigma$ and greater
Ages 17-29						
S_f^o 100-400	3(0.4)[a]	18(0.9)	50(2.8)	82(5.4)	150(16.6)	
S_f^o 20-100	21(1.3)	54(0.7)	92(0.9)	134(1.6)	195(7.2)	
S_f^o 12-20	22(1.3)	35(1.0)	45(1.4)	60(2.8)	73(4.8)	
S_f^o 0-12	281(9.6)	310(4.7)	342(6.5)	363(12.2)	326(24.2)	
HDL_1	21(0.7)	24(0.5)	22(0.5)	22(0.7)	23(2.4)	
HDL_2	53(4.0)	39(1.8)	34(1.8)	23(2.0)	25(4.3)	
HDL_3	221(5.0)	219(2.4)	218(2.9)	208(5.2)	204(10.5)	
N	71	255	182	56	21	
Ages 30-39						
S_f^o 100-400	4(0.4)[a]	24(0.9)	68(2.5)	116(7.6)	244(21.5)	
S_f^o 20-100	26(1.1)	65(0.7)	113(1.0)	168(2.0)	263(9.7)	
S_f^o 12-20	31(1.7)	44(0.9)	59(1.2)	72(3.5)	80(4.7)	
S_f^o 0-12	317(8.2)	351(3.8)	373(5.0)	375(14.0)	327(20.7)	
HDL_1	23(0.8)	24(0.4)	22(0.4)	21(0.9)	46(10.0)	
HDL_2	56(4.2)	38(1.3)	28(1.4)	28(3.3)	27(4.4)	
HDL_3	238(5.1)	221(1.9)	211(2.6)	221(6.7)	207(7.2)	
N	81	410	248	59	36	
Ages 40-49						
S_f^o 100-400	5(1.1)[a]	31(1.9)	87(4.4)	142(15.1)	377(64.4)	
S_f^o 20-100	30(1.9)	73(1.2)	135(1.7)	198(3.0)	338(27.6)	
S_f^o 12-20	36(3.7)	48(1.1)	70(2.0)	78(4.1)	77(8.3)	
S_f^o 0-12	345(15.6)	374(5.3)	408(7.7)	379(17.4)	314(24.9)	
HDL_1	24(1.7)	24(0.5)	22(0.6)	32(7.5)	35(10.5)	
HDL_2	65(7.7)	40(2.0)	29(2.0)	24(4.0)	26(6.6)	
HDL_3	257(11.7)	230(3.4)	220(3.9)	205(9.3)	201(15.2)	
N	25	213	117	30	14	
Ages 50-65						
S_f^o 100-400	6(1.7)[a]	32(2.7)	80(7.4)		174(39.6)[b]	
S_f^o 20-100	30(3.3)	76(1.9)	131(2.4)		230(19.1)	
S_f^o 12-20	33(3.4)	49(2.3)	64(2.8)		91(6.7)	
S_f^o 0-12	355(16.3)	370(9.3)	404(10.6)		411(19.2)	
HDL_1	31(4.2)	25(1.2)	24(0.9)		40(18.5)	
HDL_2	65(11.1)	48(3.9)	31(3.4)		24(4.8)	
HDL_3	233(15.3)	231(6.7)	215(6.0)		214(12.8)	
N	17	65	48		13	

[a]Values in this column are in range of S_f^o 20-100 values -1σ and less.

[b]Values in this column are in range of S_f^o 20-100 values $+1\sigma$ and greater.

Table 4. Mean lipoprotein levels in males associated with specific ranges of levels of S_f^o 12-20 lipoproteins (in mg/100 ml)

Lipoprotein groups	Ranges of S_f^o 12-20					
	-2σ and less	-2σ to -1σ	-1σ to mean	mean to $+1\sigma$	$+1\sigma$ to $+2\sigma$	$+2\sigma$ and greater
Ages 17-29						
S_f^o 100-400		17(2.4)[a]	30(2.1)	42(3.7)	66(7.0)	73(14.5)
S_f^o 20-100		44(2.9)	65(1.9)	83(2.9)	113(5.0)	132(13.7)
S_f^o 12-20		14(0.4)	30(0.4)	50(0.5)	71(0.7)	93(3.8)
S_f^o 0-12		237(6.5)	306(3.8)	341(5.9)	399(11.1)	464(17.7)
HDL_1		21(0.8)	23(0.5)	23(0.5)	23(0.8)	21(1.4)
HDL_2		52(3.6)	38(1.6)	33(2.2)	29(2.4)	27(3.8)
HDL_3		217(4.8)	216(2.3)	220(3.4)	217(5.1)	210(6.6)
N		85	259	152	67	22
Ages 30-39						
S_f^o 100-400		26(2.9)[a]	42(3.3)	64(4.3)	73(8.5)	85(11.8)
S_f^o 20-100		53(2.5)	76(2.1)	107(3.0)	133(7.4)	161(15.4)
S_f^o 12-20		21(0.5)	40(0.4)	61(0.4)	83(0.6)	114(3.3)
S_f^o 0-12		280(5.6)	335(3.3)	388(4.0)	404(10.3)	476(22.1)
HDL_1		23(0.6)	24(0.6)	23(0.9)	24(2.5)	27(5.8)
HDL_2		44(2.5)	38(1.6)	30(1.5)	33(2.8)	29(4.8)
HDL_3		218(3.7)	218(2.4)	218(2.7)	227(4.1)	221(5.6)
N		131	326	257	89	31
Ages 40-49						
S_f^o 100-400		27(4.1)[a]	63(8.9)	80(7.1)	92(12.2)	99(25.0)
S_f^o 20-100		61(3.5)	96(4.2)	122(5.5)	144(7.7)	221(37.5)
S_f^o 12-20		27(0.8)	47(0.5)	68(0.6)	90(1.2)	120(2.7)
S_f^o 0-12		333(9.0)	357(5.8)	410(6.5)	441(13.2)	446(30.4)
HDL_1		24(1.0)	26(1.7)	24(0.7)	24(1.1)	21(2.0)
HDL_2		49(3.6)	40(2.3)	30(2.4)	25(2.6)	31(6.9)
HDL_3		235(7.2)	222(3.5)	225(4.7)	225(7.6)	236(14.8)
N		67	160	115	42	15
Ages 50-65						
S_f^o 100-400		25(5.1)[a]	52(7.5)	78(15.5)	70(11.4)[b]	
S_f^o 20-100		58(6.6)	93(7.0)	119(9.0)	153(11.2)	
S_f^o 12-20		26(0.9)	45(0.8)	67(1.0)	100(3.3)	
S_f^o 0-12		319(12.7)	365(8.5)	416(10.1)	445(14.7)	
HDL_1		32(3.8)	24(0.8)	30(5.9)	22(1.5)	
HDL_2		58(9.1)	46(4.2)	30(3.1)	36(6.4)	
HDL_3		223(11.3)	226(7.3)	224(7.1)	222(11.2)	
N		24	57	42	20	

[a] Values in this column are in range of S_f^o 12-20 values -1σ and less.

[b] Values in this column are in range of S_f^o 12-20 values $+1\sigma$ and greater.

Table 5. Mean lipoprotein levels in males associated with specific ranges of levels of S_f^o 0-12 lipoproteins (in mg/100 ml)

Lipoprotein groups	Ranges of S_f^o 0-12					
	-2σ and less	-2σ to -1σ	-1σ to mean	mean to $+1\sigma$	$+1\sigma$ to $+2\sigma$	$+2\sigma$ and greater
Ages 17-29						
S_f^o 100-400		30(4.3)[a]	33(3.0)	38(3.0)	56(5.7)	46(9.2)
S_f^o 20-100		66(5.1)	68(2.4)	75(2.6)	102(5.6)	91(8.1)
S_f^o 12-20		26(1.7)	33(1.0)	42(1.1)	64(2.3)	84(5.1)
S_f^o 0-12		196(3.5)	283(1.7)	360(1.9)	445(2.8)	546(13.2)
HDL_1		21(0.9)	22(0.5)	23(0.4)	25(1.1)	24(1.5)
HDL_2		48(3.3)	40(1.9)	34(1.9)	24(1.8)	26(6.1)
HDL_3		222(4.3)	213(2.6)	219(2.9)	214(4.8)	225(12.5)
N		92	205	199	74	13
Ages 30-39						
S_f^o 100-400	83(31.4)	51(7.8)	49(3.9)	50(3.0)	53(4.7)	62(11.5)
S_f^o 20-100	144(27.7)	81(5.7)	85(3.0)	94(2.8)	101(4.4)	122(13.8)
S_f^o 12-20	49(8.8)	32(1.5)	43(1.0)	55(1.1)	72(2.0)	103(6.3)
S_f^o 0-12	145(7.0)	241(2.3)	318(1.4)	395(1.4)	468(2.3)	588(13.5)
HDL_1	14(1.8)	22(1.3)	25(1.2)	23(0.4)	25(0.7)	23(1.2)
HDL_2	43(6.5)	44(2.7)	37(1.7)	34(1.6)	26(1.7)	23(5.1)
HDL_3	212(11.5)	220(4.1)	221(2.4)	219(2.4)	217(4.1)	208(8.8)
N	17	108	306	285	99	19
Ages 40-49						
S_f^o 100-400	219(111.2)	69(13.5)	71(7.5)	52(4.2)	64(6.2)[b]	
S_f^o 20-100	153(38.0)	109(14.1)	108(6.1)	98(3.7)	118(6.0)	
S_f^o 12-20	45(5.8)	44(3.5)	51(1.6)	57(1.7)	81(2.8)	
S_f^o 0-12	178(8.7)	262(3.3)	341(2.2)	420(2.0)	503(5.7)	
HDL_1	47(15.8)	23(4.0)	22(0.8)	26(0.6)	26(0.8)	
HDL_2	42(9.6)	51(4.4)	40(2.4)	34(2.4)	23(2.2)	
HDL_3	246(19.9)	238(8.2)	222(4.0)	226(4.1)	219(6.2)	
N	10	51	131	147	60	
Ages 50-65						
S_f^o 100-400		31(5.1)[a]	67(12.2)	51(9.2)	73(13.2)[b]	
S_f^o 20-100		79(9.0)	100(8.4)	103(10.1)	127(9.0)	
S_f^o 12-20		37(3.4)	49(2.5)	60(3.3)	79(4.9)	
S_f^o 0-12		267(6.2)	350(2.9)	416(3.7)	493(4.6)	
HDL_1		26(3.8)	29(4.8)	25(1.0)	26(1.4)	
HDL_2		53(6.4)	44(4.9)	44(5.0)	25(4.1)	
HDL_3		234(10.6)	222(7.5)	220(8.3)	230(8.3)	
N		22	52	42	27	

[a] Values in this column are in range of S_f^o 0-12 values -1σ and less.

[b] Values in this column are in range of S_f^o 0-12 values $+1\sigma$ and greater.

Table 6. Mean lipoprotein levels in males associated with specific ranges of levels of HDL_1 lipoproteins (in mg/100 ml)

Lipoprotein groups	Ranges of HDL_1					
	-2σ and less	-2σ to -1σ	-1σ to mean	mean to $+1\sigma$	$+1\sigma$ to $+2\sigma$	$+2\sigma$ and greater
Ages 17-29						
S_f^0 100-400	39(17.0)	33(3.4)	37(3.0)	39(3.1)	38(7.7)	43(9.7)
S_f^0 20-100	69(13.1)	77(4.7)	75(2.7)	75(2.9)	67(5.0)	81(12.7)
S_f^0 12-20	33(5.8)	40(2.4)	40(1.3)	41(1.5)	38(2.6)	34(4.9)
S_f^0 0-12	216(25.8)	296(8.7)	319(5.6)	338(5.9)	353(12.2)	318(22.4)
HDL_1	8(0.5)	14(0.1)	20(0.1)	26(0.2)	34(0.2)	46(2.7)
HDL_2	50(6.0)	42(3.2)	40(2.0)	34(1.9)	28(2.7)	26(4.3)
HDL_3	213(13.8)	217(3.8)	219(2.6)	216(3.0)	216(6.6)	212(8.7)
N	12	94	220	199	44	16
Ages 30-39						
S_f^0 100-400	61(10.9)[a]		51(2.4)	45(3.8)	142(40.9)[b]	
S_f^0 20-100	131(15.9)		92(2.2)	84(3.0)	149(26.8)	
S_f^0 12-20	61(7.8)		51(1.0)	49(1.5)	51(5.4)	
S_f^0 0-12	252(21.3)		351(3.5)	373(5.4)	347(18.1)	
HDL_1	8(0.4)		19(0.2)	30(0.2)	87(14.2)	
HDL_2	49(9.5)		37(1.2)	30(1.2)	37(10.4)	
HDL_3	221(9.0)		219(1.8)	219(2.6)	227(13.9)	
N	18		554	243	19	
Ages 40-49						
S_f^0 100-400	66(4.5)[c]			50(4.1)	229(83.8)[b]	
S_f^0 20-100	110(4.4)			96(3.7)	154(31.2)	
S_f^0 12-20	57(1.5)			57(1.9)	46(5.1)	
S_f^0 0-12	368(5.4)			411(5.9)	329(27.9)	
HDL_1	19(0.2)			31(0.3)	73(14.4)	
HDL_2	37(1.7)			35(2.5)	42(11.3)	
HDL_3	224(3.1)			227(4.1)	245(21.6)	
N	256			129	14	
Ages 50-65						
S_f^0 100-400	54(5.3)[c]				69(16.4)[d]	
S_f^0 20-100	104(5.4)				100(10.5)	
S_f^0 12-20	58(2.4)				52(3.6)	
S_f^0 0-12	375(7.3)				405(12.1)	
HDL_1	21(0.4)				42(6.2)	
HDL_2	44(3.3)				35(4.1)	
HDL_3	222(5.1)				232(7.9)	
N	104				39	

[a] Values in this column are in range of HDL_1 values -1σ and less.

[b] Values in this column are in range of HDL_1 values $+1\sigma$ and greater.

[c] Values in this column are in range of HDL_1 values less than the mean HDL_1 value.

[d] Values in this column are in range of HDL_1 values greater than the mean HDL_1 value.

TABLE 7. The lipoprotein data, when ordered according to HDL_2 values, show very large (two- to fivefold) and significant differences in S_f^o 20-100 and S_f^o 100-400 values between the extremes of the mean HDL_2 distributions at all ages. In like manner, S_f^o 0-12 values are markedly different at the extremes. The HDL_3 values by virtue of their intercorrelation with HDL_2 levels increase regularly with the HDL_2 values throughout the HDL_2 distributions. The distribution of HDL_2 values in this male population appears quite skewed.

TABLE 8. When data are ordered on HDL_3 values, inverse trends in lipoprotein concentrations of any magnitude appear only in the S_f^o 20-100 and S_f^o 100-400 values in the 40-49 age bracket. Interestingly enough, in all other age ranges, the low-density levels are very comparable from one end of the HDL_3 distribution to the other. At the lowest end of the HDL_3 distribution for the 30-39 age bracket, the S_f^o 20-100 and S_f^o 100-400 values are apparently elevated but these elevations cannot be shown to be significant relative to values in the adjacent HDL_3 distribution interval. The distribution of HDL_3 values in the males is approximately normal.

The data on females suffer from the low numbers of subjects available in the population under study. Nevertheless, several features of the female data warrant their inclusion in this report. Because of the low numbers involved, no further comment will be made regarding the shapes of the distribution except that they do tend to resemble the male distributions for the same lipoprotein species.

TABLE 9. When ordered on S_f^o 100-400 values, the data show very appreciable and significant differences in HDL_2 values between the extremes of the distributions at all age intervals studied. However, the small absolute magnitude of the S_f^o 100-400 values encountered in the female distributions should be noted. No mean lipoprotein-value profiles even approximating the essential hyperlipemic pattern appear in the female sample studied.

TABLE 10. With S_f^o 20-100 values as control, large and significant differences in HDL_2 values are found between the extremes of the distributions studied. In the 16-29 year range, an appreciable and significant difference in S_f^o 0-12 exists between the extremes of the S_f^o 20-100 distribution. This is also observed in the young males (17-29 years) if the abnormal pattern at the uppermost end of the S_f^o 20-100 distribution (where the mean S_f^o 0-12 value is depressed) is excluded.

TABLE 11. When ordering data on S_f^o 12-20 distributions in the female sample, no marked trends appear in the dispersion of high-density-lipoprotein values.

Table 7. Mean lipoprotein levels in males associated with specific ranges of levels of HDL_2 lipoproteins (in mg/100 ml)

Lipoprotein groups	Ranges of HDL_2					
	-2σ and less	-2σ to -1σ	-1σ to mean	mean to $+1\sigma$	$+1\sigma$ to $+2\sigma$	$+2\sigma$ and greater
Ages 17-29						
S_f 100-400	55(8.5)[a]	43(2.5)	29(3.3)	23(4.0)	15(3.7)	
S_f 20-100	103(8.2)	81(2.3)	65(2.9)	57(4.3)	49(6.0)	
S_f 12-20	49(3.6)	43(1.1)	36(1.6)	33(2.6)	30(3.7)	
S_f 0-12	363(16.1)	336(4.6)	304(6.7)	283(11.4)	280(17.9)	
HDL_1	25(1.5)	24(0.4)	21(0.6)	21(0.8)	21(1.0)	
HDL_2	5(0.4)	22(0.4)	49(0.6)	78(1.0)	132(5.8)	
HDL_3	189(5.1)	212(2.1)	224(3.0)	234(6.2)	236(8.7)	
N	31	322	158	54	20	
Ages 30-39						
S_f 100-400	103(13.4)[a]	56(2.8)	36(3.4)	39(12.7)	21(5.1)	
S_f 20-100	128(7.9)	98(2.5)	79(3.3)	65(5.5)	69(7.9)	
S_f 12-20	58(3.1)	53(1.0)	47(1.7)	44(2.5)	45(3.8)	
S_f 0-12	383(14.2)	365(3.8)	337(5.8)	336(11.1)	314(9.4)	
HDL_1	28(3.8)	24(0.7)	22(0.5)	23(1.7)	20(1.3)	
HDL_2	5(0.3)	22(0.4)	49(0.6)	76(1.0)	120(4.5)	
HDL_3	191(6.2)	212(1.7)	229(2.9)	248(6.5)	254(7.5)	
N	45	500	196	52	41	
Ages 40-49						
S_f 100-400	111(20.6)[a]	72(5.4)	54(11.9)	46(8.0)	27(6.3)	
S_f 20-100	144(10.6)	113(4.6)	94(6.0)	89(11.7)	71(10.5)	
S_f 12-20	61(3.6)	62(1.6)	50(2.1)	48(3.6)	46(6.1)	
S_f 0-12	395(16.1)	398(5.7)	363(7.5)	336(12.9)	338(17.6)	
HDL_1	28(3.0)	25(1.1)	25(1.7)	21(1.2)	24(2.1)	
HDL_2	5(0.3)	22(0.6)	49(0.9)	76(1.4)	118(5.9)	
HDL_3	191(6.4)	217(3.0)	230(4.3)	269(9.4)	271(14.2)	
N	36	208	96	40	19	
Ages 50-65						
S_f 100-400	93(28.6)[a]	62(6.7)	53(10.9)	20(5.3)[b]		
S_f 20-100	133(17.2)	109(5.3)	97(11.6)	64(8.0)		
S_f 12-20	62(5.7)	59(2.8)	55(3.9)	43(6.0)		
S_f 0-12	404(15.6)	394(9.9)	368(10.2)	353(17.5)		
HDL_1	40(12.7)	25(1.0)	25(2.3)	24(1.3)		
HDL_2	9(0.5)	25(1.0)	57(1.5)	105(7.0)		
HDL_3	189(8.9)	214(5.5)	242(8.8)	263(9.4)		
N	19	68	37	19		

[a] Values in this column are in range of HDL_2 values -1σ and less.

[b] Values in this column are in range of HDL_2 values $+1\sigma$ and greater.

Table 8. Mean lipoprotein levels in males associated with specific ranges of levels of HDL_3 lipoproteins
(in mg/100 ml)

Lipoprotein groups	Ranges of HDL_3					
	-2σ and less	-2σ to -1σ	-1σ to mean	Mean to $+1\sigma$	$+1\sigma$ to $+2\sigma$	$+2\sigma$ and greater
Ages 17-29						
S_f^0 100-400		43(6.0)[a]	39(2.9)	34(2.7)	33(4.3)	41(12.4)
S_f^0 20-100		80(4.6)	78(2.9)	71(2.8)	70(4.2)	68(9.5)
S_f^0 12-20		38(2.0)	41(1.5)	40(1.5)	40(1.9)	42(5.4)
S_f^0 0-12		323(9.3)	319(5.5)	322(6.4)	325(9.8)	330(27.6)
HDL_1		23(0.7)	22(0.5)	23(0.6)	22(0.9)	21(1.1)
HDL_2		28(2.4)	32(1.6)	41(1.9)	49(4.1)	56(6.4)
HDL_3		159(1.3)	199(0.8)	235(0.8)	272(1.3)	314(3.7)
N		95	203	195	75	17
Ages 30-39						
S_f^0 100-400	140(59.9)	55(4.2)	57(4.1)	44(3.2)	44(5.4)	47(16.0)
S_f^0 20-100	124(24.0)	97(4.6)	97(3.1)	87(3.2)	82(4.8)	83(19.1)
S_f^0 12-20	37(3.8)	48(2.0)	52(1.4)	52(1.4)	49(2.1)	53(4.1)
S_f^0 0-12	321(24.5)	361(8.0)	360(5.1)	353(4.8)	344(7.0)	358(17.4)
HDL_1	28(6.7)	22(0.6)	25(1.2)	24(0.7)	22(0.6)	25(2.6)
HDL_2	30(6.2)	24(1.8)	30(1.5)	37(1.3)	56(3.8)	67(10.9)
HDL_3	124(3.0)	164(1.0)	199(0.7)	238(0.7)	280(1.2)	337(4.6)
N	12	126	274	308	94	20
Ages 40-49						
S_f^0 100-400		89(12.1)[a]	71(7.7)	66(8.9)	38(4.8)	26(5.4)
S_f^0 20-100		131(9.0)	106(4.2)	110(8.0)	89(7.1)	62(7.7)
S_f^0 12-20		58(3.1)	57(1.6)	57(2.2)	59(4.3)	47(6.2)
S_f^0 0-12		375(10.5)	393(6.3)	371(7.8)	375(14.0)	343(25.6)
HDL_1		25(2.3)	25(1.5)	24(0.8)	23(1.2)	25(2.5)
HDL_2		23(3.0)	31(1.7)	42(3.0)	51(4.1)	71(10.0)
HDL_3		159(2.6)	203(1.1)	247(1.4)	296(2.2)	363(7.6)
N		53	174	113	44	15
Ages 50-65						
S_f^0 100-400		49(11.4)[a]	68(11.0)	60(10.9)	38(8.4)[b]	
S_f^0 20-100		92(10.5)	119(7.4)	102(10.3)	77(9.4)	
S_f^0 12-20		49(5.5)	59(2.8)	56(4.1)	56(5.2)	
S_f^0 0-12		372(14.5)	393(9.8)	378(12.3)	378(16.1)	
HDL_1		23(1.6)	29(4.4)	26(1.3)	26(2.1)	
HDL_2		26(2.9)	32(4.4)	50(4.8)	63(5.5)	
HDL_3		152(4.3)	200(2.0)	245(2.4)	305(5.3)	
N		20	57	41	25	

[a] Values in this column are in range of HDL_3 values -1σ and less.
[b] Values in this column are in range of HDL_3 values $+1\sigma$ and greater.

Table 9. Mean lipoprotein levels in females associated with specific ranges of levels of S_f^o 100-400 lipoproteins (in mg/100 ml)

Lipoprotein groups	Ranges of S_f^o 100-400					
	-2σ and less	-2σ to -1σ	-1σ to mean	mean to $+1\sigma$	$+1\sigma$ to $+2\sigma$	$+2\sigma$ and greater
Ages 16-29						
S_f^o 100-400		3(3.0)[a]		15(0.6)	39(5.5)[b]	
S_f^o 20-100		30(1.6)		64(3.0)	90(7.1)	
S_f^o 12-20		26(1.3)		36(2.6)	42(3.9)	
S_f^o 0-12		279(5.6)		291(11.3)	293(19.2)	
HDL_1		21(0.6)		21(1.1)	22(1.8)	
HDL_2		85(3.5)		79(6.7)	51(7.7)	
HDL_3		224(3.2)		237(6.8)	231(8.5)	
N		126		45	19	
Ages 30-49						
S_f^o 100-400		5(0.5)[a]		22(1.1)	55(5.5)[b]	
S_f^o 20-100		37(2.3)		84(6.5)	115(14.0)	
S_f^o 12-20		36(1.9)		48(5.0)	60(5.9)	
S_f^o 0-12		317(8.0)		352(17.9)	375(19.2)	
HDL_1		21(0.8)		21(1.4)	28(2.6)	
HDL_2		92(5.1)		66(6.0)	54(8.6)	
HDL_3		233(3.8)		247(9.5)	243(11.6)	
N		96		23	17	

[a]Values in this column are in range of S_f^o 100-400 values all below the mean.

[b]Values in this column are in range of S_f^o 100-400 values $+1\sigma$ and greater.

Table 10. Mean lipoprotein levels in females associated with specific ranges of levels of S_f^o 20-100 lipoproteins (in mg/100 ml)

Lipoprotein groups	Ranges of S_f^o 20-100					
	-2σ and less	-2σ to -1σ	-1σ to mean	mean to $+1\sigma$	$+1\sigma$ to $+2\sigma$	$+2\sigma$ and greater
Ages 16-29						
S_f^o 100-400		0(0)[a]	4(0.4)	13(1.2)	27(4.5)[b]	
S_f^o 20-100		7(0.9)	31(0.9)	56(1.1)	94(4.0)	
S_f^o 12-20		21(2.4)	26(1.3)	31(1.9)	51(3.1)	
S_f^o 0-12		269(12.9)	280(6.6)	280(8.4)	312(17.5)	
HDL_1		20(1.2)	21(0.8)	20(0.8)	23(1.5)	
HDL_2		95(7.5)	85(4.3)	75(6.5)	62(6.3)	
HDL_3		229(8.6)	225(4.0)	231(4.9)	231(7.9)	
N		28	83	49	30	
Ages 30-49						
S_f^o 100-400		0(0)[a]	5(0.6)	22(2.7)	41(7.5)[b]	
S_f^o 20-100		5(1.2)	34(1.2)	72(1.7)	137(12.7)	
S_f^o 12-20		21(3.0)	32(1.8)	54(3.3)	62(5.6)	
S_f^o 0-12		278(15.8)	308(8.5)	357(13.4)	394(20.6)	
HDL_1		17(1.0)	21(0.9)	25(1.3)	24(2.7)	
HDL_2		103(12.5)	92(6.4)	71(6.1)	59(8.8)	
HDL_3		248(9.8)	232(4.7)	237(6.0)	245(13.8)	
N		15	63	42	16	

[a]Values in this column are in range of S_f^o 20-100 values -1σ and less.

[b]Values in this column are in range of S_f^o 20-100 values $+1\sigma$ and greater.

Table 11. Mean lipoprotein levels in females associated with specific ranges of levels of S_f^o 12-20 lipoproteins (in mg/100 ml)

Lipoprotein groups	Ranges of S_f^o 12-20					
	-2σ and less	-2σ to -1σ	-1σ to mean	mean to $+1\sigma$	$+1\sigma$ to $+2\sigma$	$+2\sigma$ and greater
Ages 16-29						
S_f^o 100-400		6(1.6)[a]	6(0.8)	11(1.8)	18(4.3)	25(10.6)
S_f^o 20-100		25(3.6)	35(2.2)	53(3.8)	61(8.2)	93(8.5)
S_f^o 12-20		10(0.5)	23(0.5)	37(0.7)	53(0.9)	70(3.0)
S_f^o 0-12		242(11.0)	270(5.2)	289(9.8)	356(16.6)	334(27.4)
HDL_1		21(1.2)	21(0.7)	21(1.2)	22(1.3)	21(2.6)
HDL_2		85(6.0)	78(4.4)	85(7.2)	80(9.0)	69(11.7)
HDL_3		229(7.7)	222(3.6)	225(5.6)	256(9.9)	231(10.2)
N		28	86	44	22	10
Ages 30-49						
S_f^o 100-400		3(1.0)[a]	10(1.5)	23(4.5)	19(4.8)[b]	
S_f^o 20-100		20(4.2)	41(3.3)	76(8.7)	81(8.9)	
S_f^o 12-20		13(1.2)	29(0.7)	52(1.2)	84(3.6)	
S_f^o 0-12		250(15.5)	307(7.9)	351(11.0)	427(21.0)	
HDL_1		20(1.4)	21(0.9)	25(1.4)	24(2.6)	
HDL_2		106(15.3)	88(6.1)	65(6.2)	86(9.6)	
HDL_3		237(10.4)	241(5.1)	223(6.4)	251(9.9)	
N		16	63	37	17	

[a]Values in this column are in range of S_f^o 12-20 values -1σ and less.
[b]Values in this column are in range of S_f^o 12-20 values $+1\sigma$ and greater.

Table 12. Mean lipoprotein levels in females associated with specific ranges of levels of S_f^o 0-12 lipoproteins (in mg/100 ml)

Lipoprotein groups	Ranges of S_f^o 0-12					
	-2σ and less	-2σ to -1σ	-1σ to mean	mean to $+1\sigma$	$+1\sigma$ to $+2\sigma$	$+2\sigma$ and greater
Ages 16-29						
S_f^o 100-400		9(3.3)[a]	7(1.0)	10(1.5)	14(4.0)[b]	
S_f^o 20-100		37(6.9)	40(3.0)	44(3.2)	56(6.2)	
S_f^o 12-20		22(2.7)	24(1.3)	32(1.8)	47(3.4)	
S_f^o 0-12		184(6.4)	249(2.3)	316(2.3)	388(5.3)	
HDL_1		18(1.3)	20(0.7)	23(0.8)	24(1.2)	
HDL_2		92(8.6)	85(5.4)	72(4.8)	76(5.6)	
HDL_3		230(5.9)	224(4.7)	223(4.3)	246(8.3)	
N		28	70	61	31	
Ages 30-49						
S_f^o 100-400		5(1.9)[a]	11(2.1)	19(3.5)	20(4.9)[b]	
S_f^o 20-100		29(5.2)	47(4.7)	64(6.6)	84(11.7)	
S_f^o 12-20		21(2.1)	35(2.2)	48(3.2)	64(4.9)	
S_f^o 0-12		216(5.7)	295(3.1)	368(3.5)	474(13.1)	
HDL_1		18(1.1)	22(1.0)	24(1.1)	26(3.1)	
HDL_2		100(11.2)	86(7.5)	72(5.3)	83(12.2)	
HDL_3		244(8.7)	229(5.4)	239(5.6)	241(11.6)	
N		24	46	49	17	

[a]Values in this column are in range of S_f^o 0-12 values -1σ and less.
[b]Values in this column are in range of S_f^o 0-12 values $+1\sigma$ and greater.

TABLE 12. Using S_f^o 0-12 as the controlling variable, significant inverse differences in mean HDL_2 values appear between females (16-49 years) with S_f^o 0-12 values above the mean S_f^o 0-12 and those with values below the mean.

TABLE 13. Ordering the data on HDL_1 does not reveal any significant differences in low-density values except for the mean S_f^o 0-12 values at the extremes of the distribution of HDL_1 for 16-29-year-old females.

TABLE 14. Using HDL_2 as control, we find considerable and significant differences in the means of the S_f^o 20-100 and S_f^o 100-400 values at the extremes of the distributions at all ages studied.

TABLE 15. No significant relationships in low-density lipoproteins appear when the data are ordered on HDL_3 values for this female population.

Two aspects of the distribution data warrant further discussion. Inasmuch as the average female lipoprotein distribution is generally considered a favorable one with respect to cardiovascular disease risk, it would be most interesting to determine the occurrence of this distribution pattern in the male population. One of the outstanding lipoprotein differences between males and females is the differential in mean HDL_2 levels. Therefore, we might expect that if we found a group of males with a mean HDL_2 value comparable to the mean female value for the same ages, then the rest of the lipoprotein values might also be similar. When this comparison is made with the present data, a close similarity is found in all lipoprotein groups except the S_f^o 20-100 and S_f^o 100-400. These two are appreciably and significantly higher in males than in females at ages 17-49 years. The absolute values, however, of the S_f^o 20-100 and S_f^o 100-400 for this subgroup of males are significantly lower than the average values for male population of the same age. Hence, these males have a more favorable risk outlook relative to their male cohorts; yet relative to the average female, their risk is somewhat elevated. It would appear then that other factors come into play than those strictly responsible for the control of HDL and S_f^o 0-20 levels in female serum, maintaining a certain elevation in male glyceride-containing lipoproteins. From the present HDL_2 distribution data, we find that roughly 12% of the males in the age brackets 17-29, 30-39, and 40-49 years, approximate the average female lipoprotein values for those ages. Comparable estimates may be made for the female population regarding the occurrence of male-type patterns but, unfortunately, the number of female subjects studied limits thorough evaluation.

The second point of interest is a consideration of the influence of aging on lipoprotein levels in individuals at various positions on the distribution scales. When the data for males are distributed on mean HDL_2 values,

Table 13. Mean lipoprotein levels in females associated with specific ranges of levels of HDL_1 lipoproteins (in mg/100 ml)

Lipoprotein groups	Ranges of HDL_1					
	-2σ and less	-2σ to -1σ	-1σ to mean	mean to $+1\sigma$	$+1\sigma$ to $+2\sigma$	$+2\sigma$ and greater
Ages 16-29						
S_f^o 100-400	6(1.7)[a]	9(1.5)	10(2.0)	12(3.3)[b]		
S_f^o 20-100	33(4.6)	46(3.1)	44(4.2)	46(5.7)		
S_f^o 12-20	27(2.9)	30(1.8)	31(2.1)	33(3.8)		
S_f^o 0-12	235(14.0)	275(6.4)	301(8.6)	324(15.0)		
HDL_1	11(0.3)	18(0.3)	25(0.2)	34(0.9)		
HDL_2	94(10.6)	85(4.4)	73(5.0)	64(6.6)		
HDL_3	222(7.6)	226(4.1)	229(5.5)	238(7.0)		
N	24	91	51	23		
Ages 30-49						
S_f^o 100-400	6(2.4)[a]	12(2.4)	16(2.6)	26(7.0)[b]		
S_f^o 20-100	45(13.2)	50(5.8)	60(5.0)	67(7.4)		
S_f^o 12-20	40(7.5)	38(2.6)	45(3.6)	45(4.1)		
S_f^o 0-12	312(28.0)	313(9.3)	345(11.2)	382(25.0)		
HDL_1	11(0.4)	18(0.3)	26(0.3)	40(2.1)		
HDL_2	97(14.1)	84(5.7)	80(7.4)	71(12.0)		
HDL_3	235(8.0)	234(5.1)	242(6.4)	235(10.0)		
N	14	65	44	13		

[a] Values in this column are in range of HDL_1 values -1σ and less.

[b] Values in this column are in range of HDL_1 values $+1\sigma$ and greater.

Table 14. Mean lipoprotein levels in females associated with specific ranges of levels of HDL_2 lipoproteins (in mg/100 ml)

Lipoprotein groups	Ranges of HDL_2					
	-2σ and less	-2σ to -1σ	-1σ to mean	mean to $+1\sigma$	$+1\sigma$ to $+2\sigma$	$+2\sigma$ and greater
Ages 16-29						
S_f^o 100-400	21(4.3)[a]	7(0.8)	8(1.9)	6(1.1)[b]		
S_f^o 20-100	65(6.6)	42(2.7)	39(4.0)	35(4.1)		
S_f^o 12-20	35(2.9)	28(1.8)	32(2.3)	28(2.9)		
S_f^o 0-12	284(13.3)	287(8.1)	287(9.2)	266(10.8)		
HDL_1	23(1.3)	22(0.8)	21(0.8)	18(1.3)		
HDL_2	28(1.3)	61(1.3)	99(1.4)	150(5.7)		
HDL_3	219(7.0)	221(3.7)	237(5.7)	237(7.6)		
N	30	75	56	29		
Ages 30-49						
S_f^o 100-400	22(4.9)[a]	17(3.0)	8(2.0)	6(2.2)[b]		
S_f^o 20-100	67(6.2)	64(7.3)	42(4.7)	38(6.8)		
S_f^o 12-20	43(4.2)	43(3.3)	42(3.5)	32(4.1)		
S_f^o 0-12	345(14.3)	333(11.6)	329(14.4)	303(15.4)		
HDL_1	25(2.1)	21(1.0)	23(1.3)	19(1.2)		
HDL_2	25(1.4)	61(1.9)	108(2.0)	169(7.8)		
HDL_3	209(8.1)	239(4.6)	248(6.5)	242(10.0)		
N	24	53	41	18		

[a] Values in this column are in range of HDL_2 values -1σ and less.

[b] Values in this column are in range of HDL_2 values $+2\sigma$ and greater.

Table 15. Mean lipoprotein levels in females associated with specific ranges of levels of HDL_3 lipoproteins (in mg/100 ml)

Lipoprotein groups	Ranges of HDL_3					
	-2σ and less	-2σ to -1σ	-1σ to mean	mean to $+1\sigma$	$+1\sigma$ to $+2\sigma$	$+2\sigma$ and greater
Ages 16-29						
S_f^0 100-400	6(1.5)[a]	10(1.7)	9(1.8)	13(2.9)[b]		
S_f^0 20-100	39(5.4)	45(3.3)	44(3.9)	44(5.2)		
S_f^0 12-20	28(3.2)	29(1.6)	31(2.2)	35(3.7)		
S_f^0 0-12	276(11.9)	279(7.2)	278(9.1)	316(14.7)		
HDL_1	19(1.0)	21(0.8)	21(0.9)	24(1.5)		
HDL_2	79(8.6)	67(4.2)	93(4.8)	93(9.3)		
HDL_3	172(3.2)	211(1.2)	244(1.5)	293(5.6)		
N	25	79	60	26		
Ages 30-49						
S_f^0 100-400	16(4.1)[a]	11(2.4)	12(1.9)	25(8.3)[b]		
S_f^0 20-100	61(7.0)	49(4.8)	50(5.6)	77(17.9)		
S_f^0 12-20	42(4.4)	40(2.9)	39(3.3)	49(6.6)		
S_f^0 0-12	331(15.9)	331(10.9)	326(13.0)	336(23.0)		
HDL_1	21(1.8)	23(1.1)	22(1.0)	23(2.6)		
HDL_2	66(10.4)	78(6.4)	91(6.7)	99(12.5)		
HDL_3	183(3.2)	221(1.6)	255(1.7)	311(7.3)		
N	23	50	47	16		

[a]Values in this column are in range of HDL_3 values -1σ and less.
[b]Values in this column are in range of HDL_3 values $+1\sigma$ and greater.

we find that increases in all low-density levels are associated with aging. The important point, however, is that the significant differences in low-density lipoproteins between the extremes of the HDL_2 distribution are maintained or even increased throughout the apparent life span. Thus, the group at the uppermost end of the HDL_2 values (i.e. highest HDL_2 values) maintains low-density-lipoprotein values significantly lower than the group on the opposite end of the distribution. This, of course, assumes that the individuals in a group maintain their position in the distribution as aging progresses. This appears reasonable as far as the HDL_2 fraction is concerned since its means and distributions do not appear to change much with age. Population data to prove or disprove this assumption are, unfortunately, not available at present. However, the consequence of these observations with this assumption would be that males with HDL_2 values significantly above the mean of their cohorts would, on the average, be exposed to a lower lipoprotein-associated risk from cardiovascular disease during their life span. In addition, the implication exists in these considerations that the presence of a highly elevated

HDL_2 level in a young male (17-29 years) is indicative, on the average, of a favorable prognosis with respect to his future serum lipoprotein status and its attendant risk.

SUMMARY

High- and low-density ultracentrifugal lipoprotein data for a healthy human population are evaluated in terms of their distribution properties. Appreciable and significant differences in the relative constellations of mean serum-lipoprotein concentrations appear at the extremes of the distributions determined for specific lipoprotein species. The implications of these distribution data for health and disease are discussed.

ACKNOWLEDGEMENTS

The authors gratefully acknowledge the assistance of Dr. John W. Gofman in this investigation.

REFERENCES

1. Russ, E. M.; Eder, H. A., and Barr, D. P.; Am. J. Med. 11:468, 1951.
2. Lewis, L. A.; Green, A. A., and Page, I. M.; Federation Proc. 10:84, 1951.
3. Glazier, F.; Tamplin, A. R.; Strisower, B.; deLalla, O. F.; Gofman, J. W.; Dawber, T., and Phillips, E.; J. Gerontol. 9:395, 1954.
4. deLalla, O. F.; Ph.D. Thesis; University of California, Berkeley, 1958.
5. deLalla, O. F.; Elliott, H. A., and Gofman, J. W.; Am. J. Physiol. 179:333, 1954.
6. Clark, D. A.; USAF School of Aerospace Medicine Report 62:142, 1963.
7. Gofman, J. W.; deLalla, O. F.; Glazier, F.; Freeman, N. K.; Lindgren, F. T.; Nichols, A. V.; Strisower, B., and Tamplin, A. R.; Plasma 2:413, 1954.
8. Fredrickson, D. S.; Altrocchi, P. H.; Avioli, L. V.; Goodman, D. S., and Goodman, H. C.; Ann. Internal Med. 55:1016, 1961.
9. Gofman, J. W.; Rubin, L.; McGinley, J. P., and Jones, H. B.; Am. J. Med. 17:514, 1954.
10. Eilert, M. L.; Metab., Clin. Exptl. 2:137, 1953.
11. Oliver, M. F., and Boyd, G. S.; Am. Heart J. 47:348, 1954.
12. Russ, E. M.; Eder, H. A.; Barr, D. P., and Raymunt, J.; Am. J. Med. 19:4, 1955.
13. Furman, R. H., and Howard, R. P.; Ann. Internal Med. 47:969, 1957.
14. Nichols, A. V.; Rehnborg, C. S.; Lindgren, F. T., and Wills, R. D.; J. Lipid Res. 3:320, 1962.
15. Lindgren, F. T.; Freeman, N. K., and Wills, R. D.; Some inter-relationships between serum lipids, serum lipoproteins, and lipoprotein composition; to be published in 1963.
16. deLalla, O. F., and Gofman, J. W.; in Methods of Biochemical Analysis, edited by D. Glick, Vol. 1, New York, Interscience, 1954, p. 459.

A Cytophotometric Method for Study of the Erythroid Development Sequence in Mammals

Lawrence R. Adams and Charles A. Sondhaus

A photographic cytophotometric system for measurements of hemoglobin and nucleic acid in single cells of the erythrocyte precursor series has been devised and evaluated. The measurements are intended to allow the erythroid sequence to be described with little recourse to morphological criteria. Descriptions of the development patterns that have been worked out elsewhere by means of spectrophotometry (1) and isotopic tracers (2) may thus be confirmed and extended.

Cytophotometric hemoglobin measurements of early cells in the erythroid sequence are quite rare (3), mainly because of problems in estimating total content of hemoglobin irregularly distributed through the cell, but also because of the complexity of equipment having sufficient sensitivity and stability to measure hemoglobin at the low concentrations in which it must appear in the early cells of the erythroid development sequence.

The system here described solves the problem of determining the total cellular quantities of absorbing materials in cells where such materials are irregularly distributed. Further, the system is sufficiently sensitive to measure with reasonable accuracy a total cellular hemoglobin amounting to less than 10% of the amount in a mature erythrocyte. Because a number (n) of mitoses are involved in the developmental sequence, cells that have completed the last division will outnumber the stem cells by a factor 2^n, and the jth stage by the factor $2^{(n - j)}$. Thus a large number of cells must be evaluated to find a statistically significant number in the early stages. The photographic method here described can easily record 100 usable cell images on an eight-inch strip of 35-mm film.

The film is exposed and developed in such a manner that the light transmission through the photographic cell image is a linear function of the amount of absorbing material in each sub area of the cell being analyzed. For this reason photometric integration to obtain the total absorbing mass is straightforward and may be accomplished on a large number of cells in a short time.

Because total cell hemoglobin in the stem cell must be zero and must increase discontinuously due to halving at each cell division up to the full

amount in the mature cell, the hemoglobin itself may be used in the manner of a tracer to fix the relative maturation stage of the precursor cell. An ambiguity is generated because a younger cell of stage j + 1 must have a total cellular hemoglobin of the order of that of an older cell of stage j. This ambiguity should be removed by determining the total DNA in each cell with Feulgen staining and use of the cytophotometric system described here. DNA doubles during a discrete interval in interphase and thus provides a method for specifying whether a cell of a given stage is older or younger, these terms being used as above. The relative number of cells in each stage should provide an indication of the duration of each stage--for instance, if there are $m(2^j)$ cells in stage j, then it may be concluded that the duration of stage j is m times that of stage one.

PHOTOMICROGRAPHIC APPARATUS

The photomicrographic arrangement for this study consists of a recently rebuilt Bausch and Lomb 250-mm monochromator with an achromatic quartz-fluorite condenser and Bausch and Lomb microscope components as follows: a research microscope stand fitted with a 61 X, N. A. 1.4 apochromatic objective, an N. A. 1.4 achromatic condenser, and a 10 X compensating ocular. The 35-mm film is carried in an Exakta camera mounted directly to the microscope barrel by means of an Ihagee microscope adaptor. Focusing is accomplished by means of an Ihagee Magnear viewfinder with bisected clear glass and a 10 X magnifier. Light is provided by either a tungsten band lamp or a 100-watt AH-4 mercury lamp. Because of severe nonuniformity of the light distribution in the grating image upon which the cell images are superimposed for photomicrography, sensitometric calibration is done by means of a separately mounted sector wheel sensitometer that accepts an image of the monochromator exit slit and forms a shadow image of the sector wheel upon the 35-mm film. The camera may be used interchangeably on the microscope or the sensitometer, hence each roll of film used in photomicrography may be separately calibrated. All rolls of film in a given experiment are obtained from the same one-hundred-foot roll.

Vibration of the photomicrographic apparatus is minimized as follows: The camera is mounted rigidly to the barrel of the microscope. The microscope is fixed to a shock-mounted and critically damped fifty-pound steel slab. Exposure is controlled by a solenoid-operated leaf shutter that is mounted near the exit aperture of the monochromator. The camera shutter is also operated by a solenoid control; it is opened several seconds before the exposure controlling shutter to allow vibrations in the microscope to settle down before exposure is made.

EVALUATION OF PHOTOMICROGRAPHIC PROCEDURE

Tests have shown lenticular flare in the microscope optics to be near minimum when the condenser is stopped down to a numerical aperture of 0.65. According to reasoning classical in the microspectrophotometric field (4), the

combination of high collecting aperture (1.4 in this case) and reasonably low condenser aperture should minimize error due to light being scattered out of the collecting aperture by diffracting particles and refractive index discontinuities in the specimen. However, because the illumination aperture is appreciable, though small relative to the collecting aperture, good resolution is achieved, and the sensitivity and accuracy of measurement is high.

A recent report (5) has stipulated that so-called "phase contrast effects" make apparent specimen absorbance a function of focus error, implying that such effects may be so serious as to make microphotometric quantitative assay impossible. Focus error effect has been evaluated in the system here described (see Fig. 1). The error is found to be negligible, amounting to about five percent in measured amount of hemoglobin over a focus range of 2 μ, where focus can actually be reproduced to within a quarter of a micron. The authors referenced above may have used faulty optics, or too low a numerical aperture.

The effect of refractive index mismatch has been evaluated, and conditions for optimum matching ascertained. When cells are not properly matched, scattering of light occurs at the abrupt changes of refractive index where particles of protoplasm are contacted by the immersing fluid (6). This leads to two effects: 1. All cells in the microscope field show an apparent absorbance--this effect produces background "noise," and makes the evaluation of truly absorbing cells difficult; 2. A spurious absorbance is added to the true absorbance of the cells of interest, so that the measured quantities will be too high. A series of immersants of sequentially differing refractive index was prepared and phase photomicrographs made of the same field of a methanol-fixed marrow smear, the immersant refractive index being changed .005 units between photographs. Non-hemoglobinized cells were matched best, that is, showed smallest phase contrast, at r. i. 1.545, while hemoglobinized cells were matched optimally, though not completely, at a slightly higher refractive index. Because relative rather than absolute quantities of hemoglobin are considered adequate for this study, it is planned to immerse in r. i. 1.545 and accept a small but constant fraction of spurious absorbance due to the slight mismatch of hemoglobin. If the hemoglobin were matched, one would measure a spurious absorbance in slightly hemoglobinized cells due to the nonhemoglobin protein which might be of the order of the true hemoglobin absorbance. The cleaning up of the background due to non-erythroid cells when smears are immersed in this medium is very notable. Studies have shown that the effect of 0.01 unit of refractive index mismatch is about a five-percent discrepancy in the measured absorbance at 405 mμ (see Fig. 2).

A further result of studies with refractive index fluids is that erythroid cells may be picked out of a population at a glance by reference to phase photomicrographs made from marrow-cell smears immersed in a fluid of proper

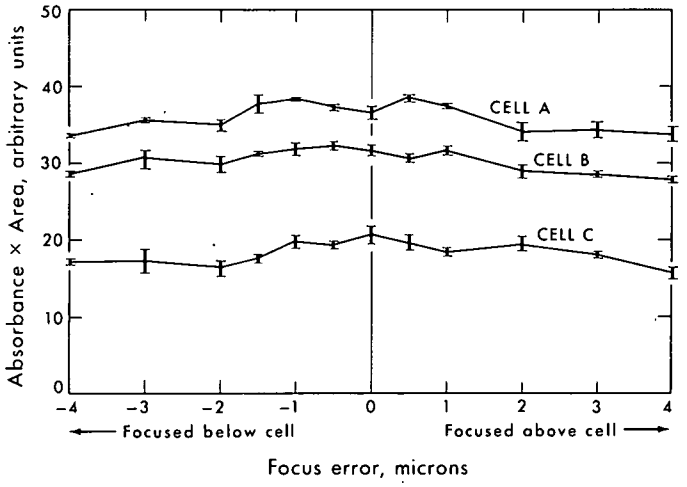

Figure 1. Variation of measured quantity with focus error: Photomicrographs were taken at wavelength 405 mμ. Each of the curves presented represents a series of photomicrographs at varying degree of out-of-focus of a single reticulocyte. Each point represents three readings on the same cell image. Photomicrographs were evaluated by the second method described in the text. Because of transient difficulty in reproducibly setting the photometer scale, the three curves for each cell were normalized to one another before the error limits $\left(\sqrt{\frac{\bar{\delta}^2}{n-1}}\right)$ were calculated.

MU-31617

refractive index. For the optics used (Tiyoda 20 X phase) the use of Cargille oil, Type A, r. i. 1.515, rendered the white blood cells and their precursors visible, showing the nuclei light in a cytoplasm slightly darker than background, and showed erythroid cells and one class of granulocyte definitely very dark. Comparison with quantitative measurements on photographs of the same fields, made at light wavelengths where hemoglobin absorbs strongly, shows that these phase micrographs reliably demonstrate hemoglobinized cells containing less than 10% of the mature amount of hemoglobin.

EVALUATION OF LIGHT SOURCE

Monochromatic light is desirable where measurements are made on the basis of the law of exponential absorption (the Beer-Lambert Law). Because monochromators necessarily admit a band of wavelengths, some error must be accepted when continuous spectrum light sources are used. Mercury lamps were tried, and, though they produce illumination of discrete wavelength, they were in general eliminated as a possibility for the following reasons: 1. The mercury line (405 mμ), although within the Soret hemoglobin band, is sufficiently far from the absorption maximum for oxyhemoglobin (412 mμ) so that optimal absorbance is not obtained; 2. There is an adjacent line at about 408 mμ that is too close to be eliminated with the monochromator; 3. It was found impossible to control the time variation of mercury-lamp intensity and thus to make accurate sequential photographic exposures; 4. Movement of the arc between the electrodes caused a time variation in the pattern of illumination both on the grating, the image of which appears in the specimen plane, and at the exit slit, the image of which is used for sensitometric exposures. Use of the tungsten band lamp, on the other hand, allows a fairly uniform illumination pattern to be obtained in the exit slit and a nonfluctuating pattern across the grating; furthermore, there is little time variation in intensity when the lamp is run from a voltage-regulating transformer.

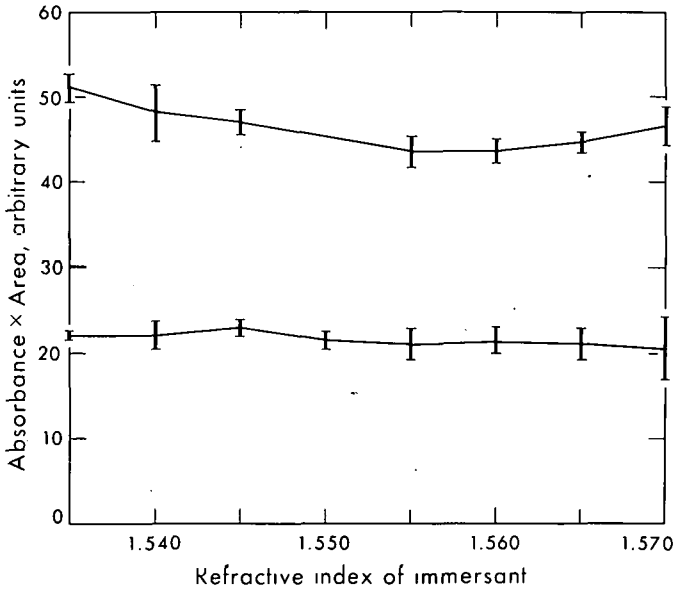

Figure 2. Variation of measured quantity with refractive index of immersant: Two reticulocytes of differing hemoglobin content are represented. Each point represents the average of measurements on six similar photographic images. Refractive index of the immersant was changed by increments of 0.005 as represented on the abscissa. Photographic images were evaluated by the first method as described in the text. Photographs were taken at 405 mμ.

MU-31618

In order to illuminate the condenser aperture of .65 N. A. with sufficient intensity for focusing at 412 mμ, it is necessary to operate the tungsten band lamp at about twice rated power and use a slit width corresponding to a bandpass of 13 mμ. The broadness of this bandpass makes it impossible to use an absorption coefficient taken from the literature or obtained at the small slit widths available with chemical spectrophotometry. An evaluation of the problem shows that, even over the wide range of wavelengths which should be considered for quantitative interpretation of the data obtained with the wide slit, an empirically determined "effective absorption coefficient" can describe attenuation; this follows an exponential law over the range of absorbance (0-0.5) encountered in erythroid cells.

Because green light at the Feulgen absorption peak is abundantly produced by the tungsten band lamp, there is little error from monochromator stray light at this wavelength. Such error as exists may be tolerated because only the mode, pre- or postreplicative, of DNA synthesis need be known. For hemoglobin measurements, on the other hand, there is much trouble from stray light. The wavelengths near the blue end of the spectrum are produced at low efficiency by the lamp, and the inside of the monochromator is flooded with light of longer wavelength. Inevitably a portion of this emerges with blue light for which the monochromator is set. Even if the extent of stray light is known, it is very difficult to correct the data for it, so it is held within tolerable limits by the use of filters.

THE PHOTOGRAPHIC CHARACTERISTIC

A number of films and developers have been evaluated with respect to resolution, graininess, and the property of showing a region of linearity

between transmittance and log exposure. As has been stated in a previous report (7), the aim of the present method is to obtain and integrate a quantity, namely film transmittance, which is linear with the specimen absorbance, such absorbance by the Beer-Lambert law being proportional to the area concentration (mass per unit area) in all incremental areas of the specimen. Log exposure and absorbance here measure the same quantity, and are related to one another by a constant and a multiplicative factor of minus one. Thus log exposure measures specimen absorbance or area concentration linearly and a substantial region of linearity between log exposure and the transmittance of the developed film is required. Experience indicates that high-contrast copy film can be made to show a linear region almost 0.5 absorbance units long when underdeveloped. Eastman's 35-mm High Contrast Copy film provides such a region when developed in Agfa's Rodinal at 1:100 for 10 min at 20°C. Development is carried out in a water bath according to a rigorous agitation schedule to achieve uniform development. The Eastman product, as are most copy films today, is panchromatic, hence may be used with green light for Feulgen studies as well as with far blue light for hemoglobin.

FEULGEN STAINING

Though the range of the photographic characteristic used is generally less than 0.5 units of absorbance, the absorbance of conventionally Feulgen-stained mammalian nuclei runs to well over 1.0 unit measured at the absorption peak of the Feulgen-DNA complex. Measurements on methanol-fixed rat-marrow cells stained according to a modified (attenuated) Feulgen procedure showed the absorption peak to be quite broad with a maximum between 550 and 560 mμ (see Fig. 3). The maximum absorbance of fully stained nuclei might be reduced so as to fall in the range 0-0.5 by using wavelengths off of the peak. However, with the broad bandpass described above, it seems more accurate to read the peak, hence it is necessary to attenuate the intensity of the stain. This can be done by hydrolyzing at reduced temperature, and the procedure is presently under investigation.

EVALUATING THE PHOTOMICROGRAPHS

Quantitative evaluation of the photomicrographs is made by either of two methods. The first uses a large portion of the slit height of the Jarrell-Ash microdensitometer and the second a photometer assembled from a Photovolt 514M photometer unit and a Beseler 2 1/4-inch by 3 1/4-inch photographic enlarger.

In the first method, the slit of the microdensitometer is set to accept the entire (vertical) height of the cell, and the drive actuated so that the cell is scanned. The recorder, which reads the output of the densitometer amplifier, traces the light intensity registered by the densitometer as the cell image moves across the slit. Later a baseline is inserted on the chart tracing, this baseline corresponding to the background of film transmittance which would hold

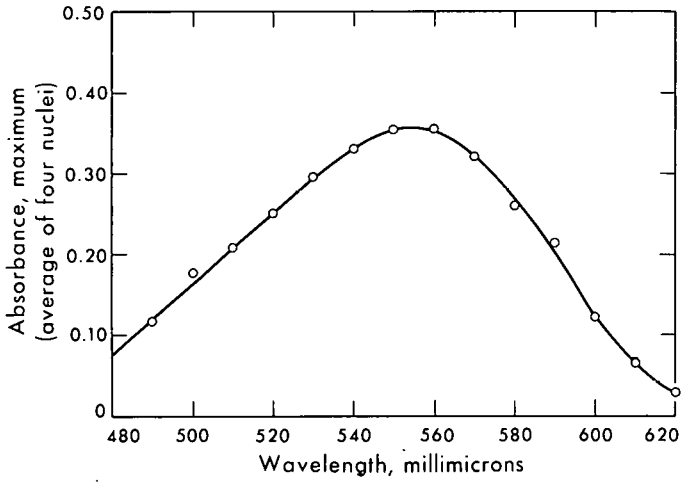

Figure 3. Feulgen absorption vs. wavelength: from a series of photomicrographs of four Feulgen-stained nuclei (hydrolysis time was four minutes at 50°C). Maximum transmittance was determined by microdensitometer and converted to absorbance by means of the photographic calibration curve, and the maximum absorbance average for the four cells was plotted. For photomicrography the monochromator bandpass was set to 15 mμ.

MU-31619

if the cell were absent. The area under the trace so defined is measured with a planimeter. This area should be directly proportional to the amount of absorbing material in the cell. It may be converted into a quantity with dimensions (absorbance x area) by a conversion factor that takes into account the slit width, the slope of the photographic characteristic, and the magnification and other dimensions of the system. When the absorption coefficient can be evaluated, its inverse is applied to the quantity (absorbance x area) to specify the absorbing mass.

In the second method, the film is positioned in a photographic enlarger so that the projected image falls just inside an aperture in the measuring unit. The measuring unit is located on the enlarger base. Just behind the aperture is a convex lens that focuses all the light passing through the aperture onto a small spot on an opal glass screen. This spot is read by the gas-filled photodiode of the Photovolt 514M photometer. The signal from this phototube is read by the galvanometer of the photometer unit. After noting the galvanometer reading, it is necessary to read an adjacent area of background. The difference between these readings is then directly proportional to the amount of absorbing material in the cell photographed. As in the above method, a constant dependent on the dimensions of the system and the slope of the photographic characteristic converts this difference into a quantity having the dimensions of absorbance times area, which can be interpreted as mass when the absorption coefficient is known.

THE METHOD IN PRACTICE

In practice, the method is as follows: A marrow smear is prepared and fixed in methanol. "Map" photographs are made with 20 X phase with the cells immersed in a fluid of r. i. 1.515. Sub-areas of the phase fields are systematically photographed using a band of light of wavelength around 412 mμ and an

immersant of r. i. 1.545. The slide is then Feulgen-stained according to the modified (attenuated) method. The same sub-fields of the original maps are photographed with the monochromator set to 555 mμ. Quantities of the respective absorbing materials are read in as many cells as contain hemoglobin. Hemoglobin content will be plotted against DNA content to yield groups of points lying in diagonal arrays. The number of arrays indicates the number of mitoses that intervene between the onset of hemoglobinization and the maturation of the cell. The number of points in each array should show the relative time spent in each intermitotic stage. Irregularities, such as early maturation of a reticulocyte from an early polychromatic erythroblast, should lead to a distinct irregularity in the corresponding array; further, the mechanism of nuclear loss, extrusion or necrosis, should be indicated.

APPLICABILITY

The basic study is designed to demonstrate the applicability of the described photographic-photometric system in a controversial problem, namely the sequence of erythroid development. A probable extension is testing the so-called "shunt" hypothesis, specifically that the enlarged reticulocytes which appear in hematopoietic stress (8, 9) result from the skipping of a mitosis, probably the last one (10). Other possible elaborations include studies of experimentally produced polycythemias and studies of the effects of radiations of various qualities on the erythroid development sequence.

REFERENCES

1. Thorell, B.: Studies on the Formation of Cellular Substances During Blood Cell Formation, London, Kimpton, 1947.
2. Cronkite, E. P.; Bond, V. P.; Fliedner, T. M., and Rubini, J. R.; Lab. Invest. 8:263, 1959.
3. Thorell, B.; Advan. Biol. Med. Phys. 6:95, 1958.
4. Caspersson, T.; Skand. Arkiv Physiol. 73 (Suppl. 8):1, 1936.
5. Latimer, P., and Robinson, T. K.; Effects of Defocusing in Microspectrophotometry; Abst. TE1, 7th Ann. Meeting, Biophysical Society, N. Y. C., Feb. 1963.
6. Gross, E., and Sondhaus, C. A.; Light Scattering by Refractile Particles and Its Effect on Cellular Microabsorption Measurements; in preparation.
7. Adams, L. R., and Sondhaus, C. A.; Lawrence Radiation Laboratory Report UCRL-9994, 1961.
8. Brecher, G., and Stohlman, F., Jr.; Proc. Soc. Exptl. Biol. Med. 107:887, 1961.
9. Ambs, E.; Schweiz. Med. Wochschr. 90:413, 1960.
10. Borsook, H.; Lingrel, J. B.; Scaro, J. L., and Millette, R. L.; Nature 196: 347, 1962.

Sensitivity of the Positron Scintillation Camera for Detecting Simulated Brain Tumors

Alexander Gottschalk and Hal O. Anger

More than 60 patients suspected of having brain lesions have now been examined with the positron scintillation camera. Ga^{68}-EDTA (ethylenediaminetetraacetic acid), a positron emitter with a half-life of 68 min, was used as the localizing agent (1, 2, 3). This paper describes the results of a phantom study with the positron scintillation camera and compares the findings with a similar study by Jacobson et al. (4) on the conventional positron scanner using As^{74}.

Sweet et al. (5) have shown that brain tumors accumulate As^{74} and Cu^{64}-EDTA in approximately the same concentrations. With EDTA chelates, the organic part of the molecule seems responsible for the pharmacologic behavior within the brain whereas the isotope merely serves as a tag. Consequently, it is reasonable to expect Ga^{68}-EDTA to accumulate in brain tumors in a fashion similar to that of Cu^{64}-EDTA. Although determination of Ga^{68}-EDTA concentration in human brain tumors is as yet lacking, the uptake of the isotope in tumors, as judged from the brain scintiphoto itself, is in agreement with the classification to be described.

Sweet and co-workers found that brain tumors accumulate the above agents in three broad categories. Meningiomas show the greatest accumulation with tumor to brain ratios frequently 15 to 1 or higher. Glioblastomas and metastases are examples of the middle group, with tumor to brain ratios about 7 to 1. The lowest ratios are found in the well differentiated gliomas which show an accumulation of approximately 3 to 1 or less.

MATERIALS AND METHODS

In order to simulate the human head, a phantom was constructed by placing 1,500 cc of water in a polyethylene jar eleven and a half cm in inner diameter and 15 cm high. Three μC of Ga^{68}-EDTA were added to the jar to simulate the low-level activity normally seen from a human head. This activity is largely due to isotope present in the skin and blood overlying the brain. The simulated tumors were made by filling thin walled containers (toy rubber balloons) with the desired quantity and concentration of isotopes relative to the rest of the phantom. The experimental setup is illustrated in Fig. 1.

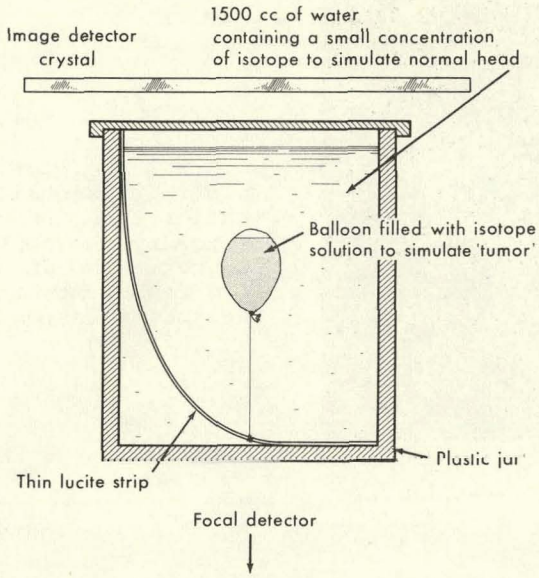

Figure 1. MU-31398

The phantom was counted until 3,500 dots were recorded on the picture. This gave a visual appearance comparable to that seen in the central area of a normal head during a Ga^{68}-EDTA brain examination with the usual exposure time of 10 min. The density of dots per square centimeter was the same in pictures of the phantom as in human scintiphotos. By keeping the total count per picture constant and by varying the exposure time, consideration of the physical decay of the short lived Ga^{68} was avoided. Correction for background was unnecessary as the background count rate of the positron scintillation camera is less than one count per minute; maximum exposure time was 20 min.

The plane of best focus of the scintillation camera was placed through the simulated lesion. Additional studies showed that the depth of field of the positron camera is quite broad. Using a 6-cc 15/1 phantom tumor, it was possible to move the plane of best focus two and a half inches below the "lesion" (toward the focal detector) and three and a half inches above the "lesion" (toward the image detector) before the image of the phantom tumor was no longer clearly visible.

Phantom tumors in each group described by Sweet were examined to determine the smallest size tumor detectable. At least four exposures were made with each "tumor" in order to eliminate statistical variations. A sample was considered borderline if it could be identified three out of four times.

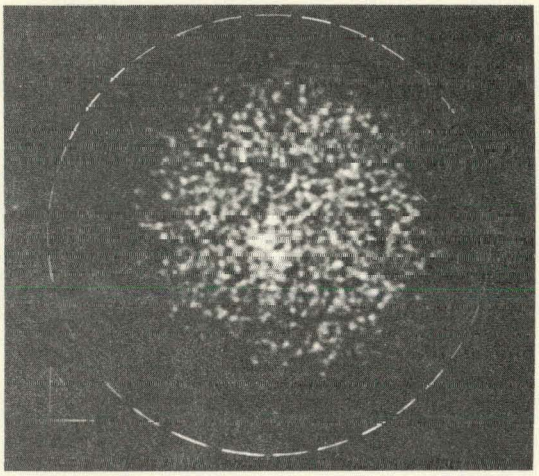

Figure 2. A representative scintiphoto showing a 6-cc phantom tumor with a 15/1 tumor to head concentration. It is easily seen although smaller than the minimum volume detected by the conventional positron scanner. The dashed circular outer line represents the field of view of the scintillation camera.

RESULTS

Table 1 compares the results of this study with those found by Jacobson and co-workers using the conventional positron scanning technique. It is apparent that the positron camera, with Ga^{68}-EDTA, will identify lesions with approximately 30% of the volume and 65% of the diameter necessary for detection by the conventional positron scanner.

DISCUSSION

Any comparison of results suffers from the obvious flaw that the studies were conducted by separate observers in separate laboratories using different phantoms. However, the basic design of the experiments is the same. Although they do not exactly duplicate the clinical conditions of brain scanning with the particular agent and apparatus used, they give some idea of the sensitivity of the two methods.

It is important to realize that the concentration ratios obtained by Sweet and co-workers only compare tumor tissue to brain tissue. Since the pictures of human patients include the isotope in skin, muscle and blood, as well as brain, a strict comparison of the phantom to actual patients is not valid. It is not known at the present time how much of the isotope goes to skin and other structures overlying the brain. Until the uptake in tumors relative to the uptake in a cross section of the head is known, a determination of the smallest tumor detectable in an actual subject cannot be made.

CONCLUSIONS

Phantom studies indicate that the positron scintillation camera is a more sensitive instrument for the detection of brain lesions than the conventional positron scanner. It detects lesions one-third to one-fifth as large in volume for each ratio of tumor to brain concentration studied.

Table 1.

Detector	Isotope	Ratio tumor/ brain	Minimum volume of smallest tumor detected	Approximate diameter of smallest tumor detected
Conventional positron scanner (4)	As^{74}	15/1	8 cc	2.0 cm
Positron scintillation camera	Ga^{68}	15/1	2 cc	1.3 cm
Conventional positron scanner	As^{74}	8.7/1	12 cc	2.8 cm
Positron scintillation camera	Ga^{68}	7.5/1	4 cc	2.1 cm
Conventional positron scanner	As^{74}	3.2/1	40-70 cc	not listed
Positron scintillation camera	Ga^{68}	3.25/1	12 cc	3.0 cm

ACKNOWLEDGEMENTS

The authors wish to thank Mr. Yukio Yano for technical assistance.

REFERENCES

1. Anger, H. O., and Gottschalk, A.; J. Nucl. Med. 4:326, 1963.
2. Anger, H. O., and Gottschalk, A.; Lawrence Radiation Laboratory Report UCRL-10697, 1963.
3. Greene, M. W., and Tucker, W. D.; Intern. J. of Appl. Radiation Isotopes. 12:62, 1961.
4. Jacobson, L. E.; Miller, W. N., and Hillsinger, W. R.; Am. J. Roentgenol. Radium Therapy Nucl. Med. 88:339, 1962.
5. Sweet, W. H.; Mealey, J.; Brownell, G. L., and Aronow, S.; in Medical Radioisotope Scanning, Vienna, Intern. Atomic Energy Agency, 1959, p. 163.

Use of a Whole-Body Counter in Turnover Studies with Ca^{47}

Thornton Sargent, John A. Linfoot, Henry Stauffer and John H. Lawrence

A number of investigations of calcium metabolism have been reported by workers using Ca^{45}, Ca^{47}, Sr^{85}, and stable strontium (1,2,3,4). Models have been proposed and mathematical treatments developed by Bauer et al. (5), Heaney and Whedon (6) and others to describe the dynamics of calcium. Aubert and Milhaud (7) have maintained that the simplified models of these workers were incomplete chiefly because they failed to take into account the component of serum-calcium disappearance, which does not appear until the seventh to the eighteenth day after injection. They demonstrated that this simplification can lead to errors of 35 to 76% in measurement of the size of the calcium pool, and 18 to 38% in the rate of disappearance from the pool.

In any system described by a sum of exponential functions, if one cannot measure the slowest rate constant of the system, an error will be introduced into the determination of all the others. The magnitude of the error will depend on the coefficient and on the rate constant of the unknown component. One cannot be certain that there is not still another component with a longer turnover time. In fact, Cohn et al. (8) have measured the turnover of Sr^{85} in a series of normal subjects for more than a year with a whole-body counter and found very long-lived components; the retention curve was best fitted by a power function. Considering the complex nature of recycling of bone mineral, discussed by Heaney and Whedon (6), it seems possible that a power function may best describe the behavior of calcium in compartments with such complex recycling; however, a power function yields little information about rates and compartment sizes. Exponentials may be more useful in describing turnover in the miscible-calcium pool and the initial incorporation into bone. Although a complete and satisfactory mathematical description has not yet been evolved, studies with calcium isotopes will continue to be valuable both in developing clinically useful measurements and in evolving a better model of calcium metabolism.

A whole-body counter can be used to advantage because it can measure the calcium deposited in bone without relying on calculation from serum measurements. The results of such measurements on a small group of patients will be presented here, and the advantages of the method discussed.

MATERIALS AND METHODS

All of the patients were ambulatory and generally were studied on an outpatient basis. Patients for whom blood, urine and stool collections were made were admitted to the Donner Pavilion for periods up to the first seven days of the study. Metabolic balance technique was not employed, but diets were controlled so that calcium intake was approximately 900 mg per day during the first week of study.

Ca^{47} from Oak Ridge, with Ca^{47}/Ca^{45} approximately 10/1, was given intravenously, buffered to pH 4 to 5, at doses between 2 and 25 μC. In some patients serial blood samples were drawn, and in some, complete urine and stool collections were made for periods up to two weeks.

The whole-body counter is of the Argonne type with 6-inch steel walls, a single NaI(Tl) crystal, 9 3/8 by 4 inches, and a 100-channel pulse-height analyzer. Patients were counted both in the one-meter-arc position and the tilting-chair position. In the one-meter arc, the patient lies on a couch with a radius of curvature of one meter with the crystal at the center of curvature. This geometry is usually considered to yield a count with minimum dependence upon localization of the isotope. In the tilting chair the sensitivity is five times that of the one-meter arc, but with Ca^{47} changes in the location of the isotope in the body yield a retention curve different from that of the one-meter arc until 12 to 18 days after injection. After 18 days the retention curves are parallel, so that the greater sensitivity of the chair position makes it possible to extend the retention curve beyond the time at which the 4.7 day Ca^{47} has decayed below detectable limits using the one-meter arc.

After the initial whole-body count, which is performed within five minutes after injection in order to establish a 100% point, the patient is counted again later during the first day, then daily for several days and finally at intervals of seven days. A patient with high calcium retention and an initial dose of 25 μC can be counted with sufficient accuracy 42 days after injection. Good gamma-ray resolution and a pulse-height analyzer are essential for accurate measurements late in the study, because all Ca^{47} so far used has contained a variable small amount of Zn^{65}, which often contributes counts in the range of the Ca^{47} photopeak to about the same degree as the patient's K^{40}. After all of the Ca^{47} has decayed, a final count must be made to obtain a background including the Zn^{65} which is subtracted from previous counts.

Blood samples were counted in a standard well counter with pulse-height discrimination against the Sc^{47} daughter of Ca^{47}, and against the I^{131} which some patients had received from iodine-uptake tests. One-liter samples of urine from each 24-hour collection, and the entire stool, were each counted on top of a 2-inch crystal, with a standard suitably diluted to correct for

self-absorption. Urine data were plotted as specific activity (counts per minute of Ca^{47}/mg Ca). Stool specimens were not assayed for calcium, so the data are plotted as counts per minute of Ca^{47}/g stool; since the diets were reasonably constant in calcium, this is equivalent to specific activity so far as the slope of the curves is concerned.

RESULTS AND DISCUSSION

In view of the current uncertainty as to the suitability of the various mathematical models which have been proposed for calcium metabolism, no complex mathematical treatment is attempted here. A simple graphical analysis is used, based on the assumption that retention can be expressed by a sum of exponentials. Interpretations are given here with the reservation that better models will undoubtedly be derived in the future.

All of the Ca^{47}-retention curves are plotted on semi-log coordinates, on which straight lines represent exponential functions. By extrapolation of a straight line fitted to the last segment of the curves, a "final" slope can be subtracted from the retention curve and the exponential components resolved consecutively in the usual way. When plotted on log-log coordinates the curves are convex upward demonstrating that the data are best fitted by exponential functions rather than by a power function. This is in agreement with the results of the first 30 days of Sr^{85} data of Cohn et al. (8), who found that after 30 days the data were best fitted by a power function to which an equivalent exponential could be fitted for purposes of resolving the exponentials of the earlier part of the curve.

NORMAL BONE METABOLISM. The first group of patients, whose Ca^{47}-retention curves are shown in Fig. 1, were chosen because their calcium metabolism was believed to be normal. Only one of these subjects, the 33-year-old male, was actually without any known disease. As can be seen, the three adult patients who had, respectively, diabetes, breast cancer (without demonstrable bone involvement), treated sprue, and the normal male do not exhibit retention curves markedly different from each other and probably represent the normal range of variation with initial half-times of 28 to 30 days. There is clearly another component appearing between the 24th and the 30th day; it has not yet been possible to measure its half-time accurately in normals.

MAMMARY CARCINOMA WITH OSSEOUS METASTASES. Calcium retention curves from four female patients with metastatic mammary carcinoma are shown in Fig. 2. All of the patients were premenopausal at the time their breast lesions were detected and had been oophorectomized prior to receiving pituitary ablation with 900-MeV alpha particles from the 184-inch cyclotron (9).

Patient I. S. was a 47-year-old housewife who had extensive cutaneous

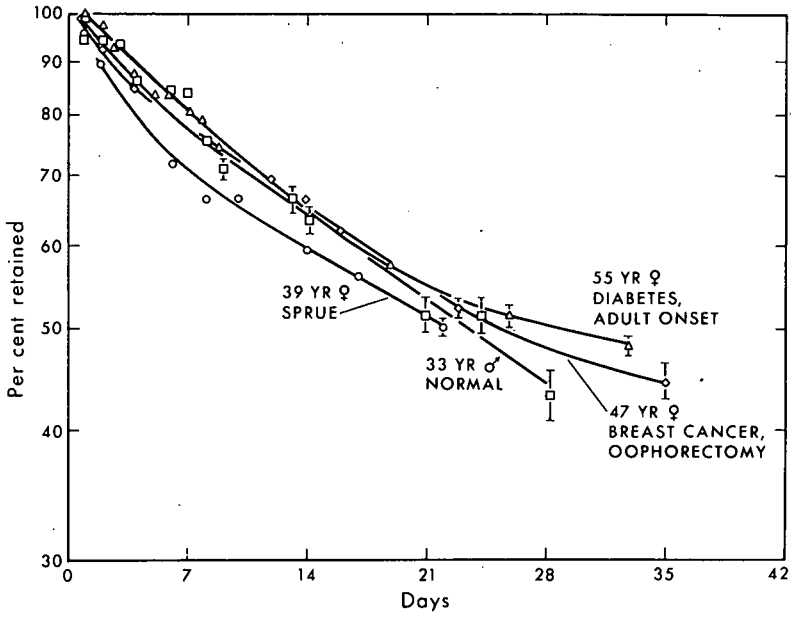

Figure 1. Retention of whole-body radiocalcium in patients with no demonstrable bone disease, and in one completely healthy subject.

MU-31667

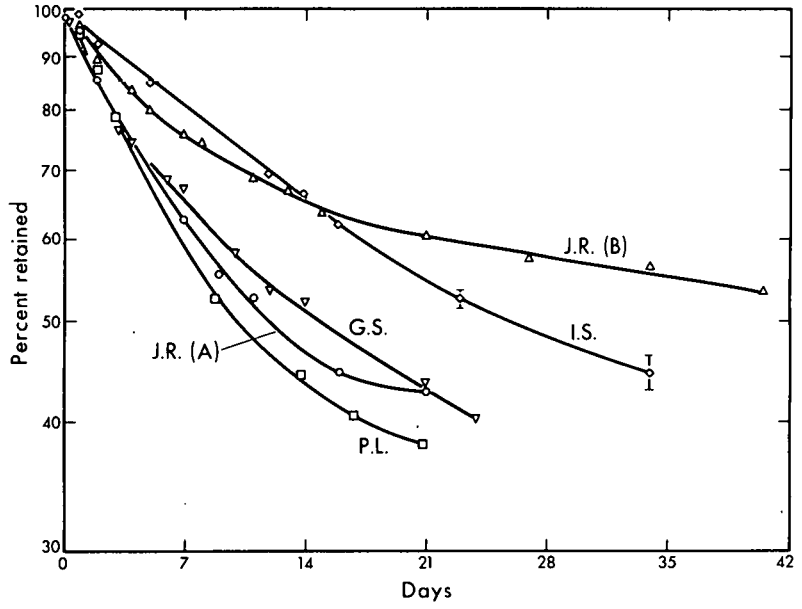

Figure 2. Radiocalcium retention in four women with metastatic mammary carcinoma. Three patients had osseous metastases of varying degrees. Patient J. R. was studied before treatment (A) and after treatment (B). No osseous metastases were demonstrable in patient I. S.

MU-31666

and pleural metastases. There were no obvious osseous metastases. The alkaline phosphatase, serum calcium, and 24-hour urinary-calcium excretion were normal. Her calcium-retention curve was considered to be normal and is shown in both Fig. 1 and 2.

Patient P. L. was a 48-year-old telephone operator who had extensive osseous and hepatic metastases. She had marked hypercalciuria and developed severe hypercalcemia (16.0 mg percent) while undergoing pituitary irradiation, and died shortly after treatment. Our study was terminated by her death. Her calcium curve showed an extremely rapid turnover.

Patient G. S. was a 49-year-old housewife with carcinoma en curasse, who also had metastatic involvement of the dorsal and lumbar spine. She had a normal alkaline phosphatase, mild hypercalcemia (13.0 mg percent), and hypercalciuria. Her calcium curve was slightly less steep than the former patient, but distinctly different from patient I. S.

Two retention curves are presented on patient J. R. who was a 56-year-old housewife in whom only osseous metastases were clinically detectable. The serum calcium and alkaline phosphatase were normal. The first curve (A) was obtained prior to treatment and resembles that of the preceding patients. The second curve (B) was obtained after she was in clinical remission following combined use of pituitary irradiation and chemotherapy. There is a striking difference between the two curves. The shapes of the curves are similar, but before treatment the turnover rate of calcium was much greater. The curve after treatment probably represents deposition of calcium into areas of the skeleton which were previously being destroyed by osteolytic lesions.

ACROMEGALY. The profound effects of growth hormone on cartilage and endochondrial bone formation are responsible for the skeletal changes which are characteristic of pituitary gigantism and acromegaly. Marked disturbance in calcium metabolism is not a clinically important feature of these disorders except in those relatively rare cases with multiple endocrine tumors and coexisting parathyroid adenomata (10). However, hypercalciuria and hyperphosphatemia are frequently seen in active acromegaly. Bauer and Aub (11), using the calcium-balance technique, found hypercalciuria and negative calcium balance in four acromegalics and concluded that the degree of negative calcium balance correlated with the clinical degree of severity, and improved with pituitary irradiation.

More recent studies (12) employing similar techniques showed that the hypercalciuria was associated with increased intestinal absorption of calcium, and calcium balance remained positive. Furthermore, the administration of primate growth hormone to human subjects produces hypercalciuria, but does not induce negative calcium balance (13,14). A study of total-body-calcium turnover should provide a clearer picture of calcium dynamics in acromegaly and also make it possible to determine whether abnormalities in calcium dynamics correlate with clinical findings.

Tracer studies of bone metabolism in acromegaly are not numerous.

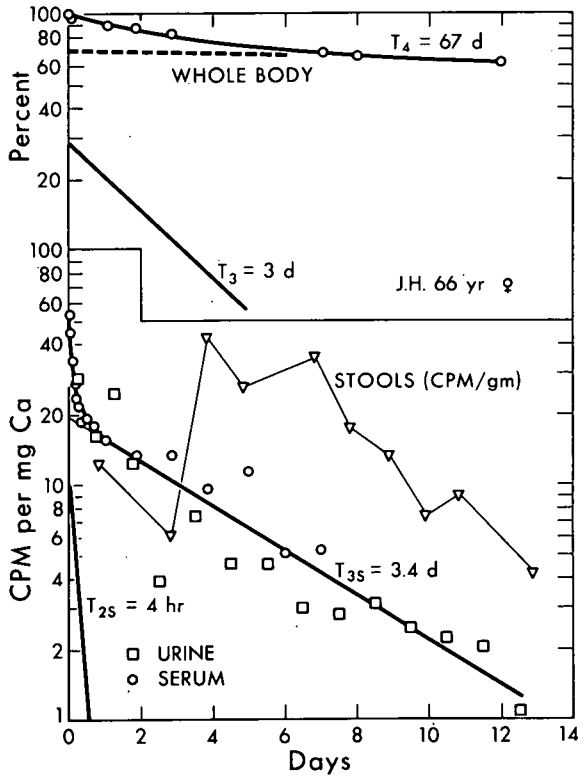

Figure 3. Retention of whole-body radiocalcium (above) and specific activity of urine, stools and blood (below) of patient J.H., a 66-year-old woman with acromegaly. These data are typical of those for the other patients with acromegaly, which are summarized in Table 1.
MU-31665

Stable strontium has been used to demonstrate an increase in the exchangeable calcium pools in acromegalics (15), but strontium is handled differently from calcium in the body and only short term studies can be carried out with non-radioactive tracers. In these studies the whole-body counter was used in conjunction with measurements of Ca^{47} in blood, urine, and stools on a group of six acromegalics who were considered to have varying clinical degrees of activity.

Typical data are shown in Fig. 3, in this case of patient J. H. In not all cases did the specific activity curves of the blood and urine coincide as here, but in all cases they were parallel, as was the fecal activity when calculated per gram of stool. The serum curves were resolved graphically into a sum of exponentials, and the half-times of each component are shown in Table 1. The half-times T_{s1}, T_{s2}, T_{s3} are calculated from serum data and correspond to the rate constants k_1, k_2, and k_3 of Bauer et al. (5) where $k = 0.693/T$. Analyses such as these are based on the assumption that the longest half-time, T_{s3}, is the final one which is not valid since serum activity cannot be measured for sufficiently long periods of time when tracer amounts of isotope are employed.

A similar analysis of whole-body-retention data revealed a half-time T_3, which had approximately the same value as T_{s3} in each patient, but in addition showed a longer half-time, T_4. The half-time T_{s1} and T_{s2} represent mixing with

Table 1.

Patient (age, sex)	Clinical findings: Enlargement of sella	Clinical findings: Serum phosphorus	Clinical findings: Degree of activity	Serum: T_{s1} Min.	Serum: T_{s2} Hours	Serum: T_{s3} Days	Serum: T_3 Days	Whole body: T_4 Days	Whole body: T_4 Intercept
J.M. 24 ♂	Large	5.8	Very active	102	8.5	2.7	1.7	102	82%
J.V. 17 ♂	Large	5.2	Active	45	7	5.5	5	265	73%
H.B. 33 ♂	Moderate	4.2	Moderately active	24	7	3.5	3.1	77	75%
C.L. 28 ♂	Normal	5.4	Moderately active					70	70%
J.H. 66 ♀	Slight	5.2	Moderate (also arthritis, osteoporosis)	16	2.8	3.4	3.0	85	67%
M.D. 48 ♀	Slight	3.5	Inactive (hysterectomy, arthritis)	28	3.8	3.2	4	57	49%

the various calcium pools in the body and not net loss, and hence do not appear in the whole-body-retention curve.

Table 1 also shows the patients' symptoms and the physician's total impression of the clinical degree of activity. The cases are arranged in order of their decreasing severity. While the half-times T_{s3} (serum) and T_3 (whole body) are in reasonable agreement in each patient, there is no apparent correlation with the clinical severity of the disease. Fig. 4 shows the retention curve for each of these patients. All the curves have very similar shapes and are strikingly different from the normals in Fig. 1. Since the smallest slope (longest half-time T_4) represents turnover of the tracer that has been deposited in bone, it can be seen by qualitative examination of the curves that the patients with acromegaly deposit far more calcium into this compartment than normals. Although, as mentioned previously, T_4 does not represent the final slope of the curve, extrapolation of its slope to injection time yields an intercept which is a fair representation of the amount of tracer that entered this compartment. The normals could not be followed long enough to see this longer half-time, but it is obvious from the curves that its intercept would be much lower than in acromegaly. In contrast to the shorter half-times shown in Table 1, the T_4 intercept appears to correlate with the severity of the disease, the higher intercepts occurring in the more severe cases.

Since the degree of activity in acromegaly is difficult to assess clinically, these preliminary studies indicate that the whole-body counter not only provides a highly satisfactory method of studying abnormal calcium metabolism in acromegaly, but may also be of value in determining the degree of ac-

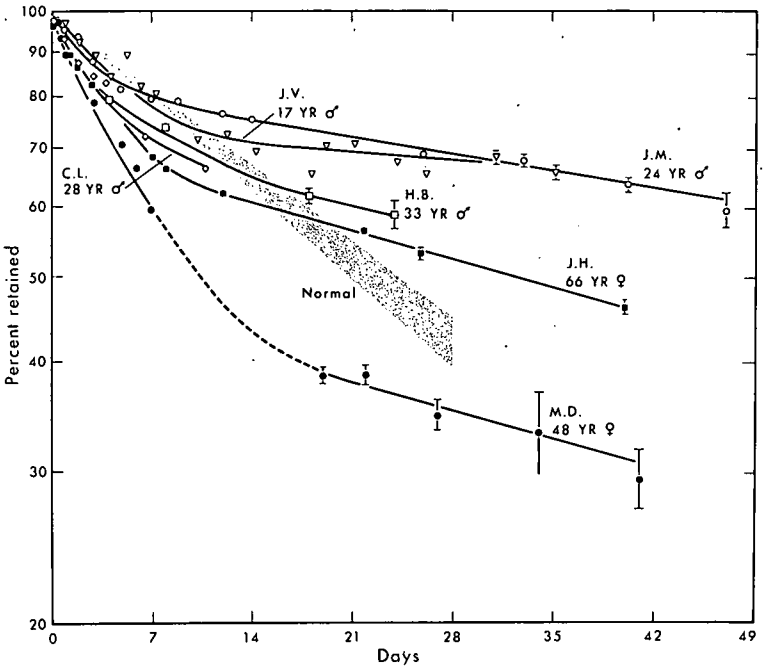

Figure 4. Radiocalcium retention in six patients with acromegly of varying degrees of severity.

MU-29975

tivity and the effectiveness of therapy. Follow-up studies of patients who have received treatment for their acromegaly should make such studies more complete.

It is highly desirable to extend the retention curves beyond the relatively short time possible with Ca^{47}, so that the curves may be analyzed accurately and completely for half-times and compartment sizes. The only feasible way to extend the retention curve is to administer Sr^{85} and Ca^{47} simultaneously to the same patients. It is known that strontium is not a perfect tracer for calcium and that the body discriminates against strontium in favor of calcium (2). By using both isotopes simultaneously, however, it should be possible to normalize and fit the data of Sr^{85} to obtain an equivalent long-term retention curve for calcium. This is planned for future studies.

SUMMARY

A whole-body counter has been used to study Ca^{47} turnover in normal subjects, in patients with metastatic breast cancer, and in patients with acromegaly. Patients with osseous metastases of breast cancer have greatly increased turnover rates. Patients with acromegaly have increased retention of calcium, presumably in bone, and the extent of increased retention seems to correlate with the severity of the disease.

REFERENCES

1. Krane, S. M., Brownwelt, G. L., Standbury, J. B., and Corrigan, H.; J.Clin. Invest. 35:874, 1956.
2. Spencer, H.; Li, M.; Samachson, J., and Laszlo, D.; Metabolism 9:916, 1960.
3. Corey, K. R.; Kenny, P.; Greenberg, E.; Payianos, A.; Pearson, O. H., and Laughlin, J. S.; Am. J. Roentgenol. 85:955, 1961.
4. Fraser, R.; Harrison, M., and Obbertson, K.; Quart. J. Med. 19:85, 1960.
5. Bauer, G. C. H.; Carlson, A., and Lindquist, B.; Acta Med. Scand. 158:143, 1957.
6. Heaney, R. P., and Whedon, G. D.; J. Clin. Endocrinol. 18:1246, 1958.
7. Aubert, J. P., and Milhaud, G.; Biochem. Biophys. Acta 39:122, 1960.
8. Cohn, S. H.; Spencer, H. S.; Samachson, J., and Robertson, J.; Radiation Res. 17:173, 1962.
9. Lawrence, J. H.; Tobias, C. A.; Born, J. L.; Wang, C. C., and Linfoot, J. A.; J. Neurosurg. 19:717, 1962.
10. Underdahl, L. C.; Woolner, L. B., and Black, B. M.; J. Clin. Endocrinol. 13:20, 1953.
11. Bauer, W., and Aub, J.; J. Clin. Invest. 20:295, 1941.
12. Jackson, W. P. U., and Dancaster, C.; J. Clin. Endocrinol. 19:658, 1959.
13. Bergenstoll, D. M., and Lipsett, M. B.; J. Clin. Endocrinol. 20:1427, 1960.
14. Beck, J. C.; McGarry, E. E.; Dyrenfurth, I.; Morgen, R. O.; Bird, E. D., and Venning, E. H.; Metabolism 9:699, 1960.
15. Eisenberg, E., and Gordon, G. S.; J. Clin. Invest. 40:1809, 1961.

Heavy-Particle Ionization (H, He, Li, B, C, N, O, F, Ne, Ar) and the Proliferative Capacity of Neoplastic Cells In Vivo

Karen Sillesen, John H. Lawrence and John T. Lyman

The biologic effects of the ionization produced in mammalian tissues by heavy particles, such as penetrating neutrons, are of special interest because of several characteristics having possible therapeutic advantage. First, as shown in our early studies (1,2), heavy particles have a greater biologic effect per unit dose than electromagnetic radiations (such as 200-kV X rays or gamma rays) per unit of ionization produced in normal tissue, and also in neoplasms in animals (3,4,5). Secondly, biologic effects of heavy particles are less dependent on the oxygen environment than in the case of electromagnetic radiation (6, 7). A third characteristic of heavy-particle tissue ionization is less tissue recovery than occurs after sub-lethal doses of electromagnetic radiation (8). A fourth characteristic is the so-called Bragg curve (9,10) which makes it possible with high-energy, charged particles to reverse the usual surface-to-depth dose relationship -- that is, a much greater relative total-tissue ionization is produced in the depths as compared to that produced by X rays or gamma rays, enabling us to produce localized destructive lesions (10,11,12,13,14,15,16).

The first characteristic cited above prompted us, in 1935, to consider using tissue ionization produced by relatively low-energy heavy particles in the treatment of advanced cancer patients (17). The results of these early attempts were not favorable due, we believe, to the great scatter and lack of penetration of these proton-producing neutrons (18). Later, the availability of heavier, charged particles of high energy (19,20,21) led us to reconsider their possible use in therapeutic investigation, because the energies now were such that the peak of the Bragg curve could be placed at great depths in tissue (10), and furthermore, the incoming beam traversing tissues had little scatter. These favorable characteristics of high-energy-proton or alpha-particle beams led to their use in the investigational therapy of certain neoplastic, metabolic and neurological diseases in animals and man (22,23,24,25,26,27,28), using the Bragg peak as early as 1948 (10) with considerable success. In more recent years, two other groups, in Boston and Uppsala, reported studies using these heavy particles in animal and human therapeutic investigations (29,30,31,32).

The characteristics of the ionization produced in tissue by various high-energy, heavy particles have prompted the present study. Using two neoplasms in

mice, the relative biologic effect of several heavy particles with various energies, nuclear mass and charge was studied in an attempt to aid in further understanding the mechanism of action of densely ionizing radiation. We had in mind also the questions: 1) In the case of mammalian tumor cells, at what LET (linear energy transfer) does the oxygen effect disappear? and 2) At what LET is the RBE (relative biologic effect) the greatest? We hoped the results would also aid in the selection of the most appropriate particle and energy for the treatment of neoplastic and other diseases.

In the absence of the basic knowledge required for the understanding, prevention, and/or treatment of certain neoplastic, metabolic and neurological diseases -- and, knowing that the treatment of neoplastic disease still rests mainly upon surgery and radiation therapy -- it seems extremely important to assess the relative importance of the unique qualities of heavy-particle beams with reference to the optimal combined conditions of little scatter, optimal depth-dose, and linear energy transfer (LET). These factors can then be related to optimal RBE and correlated with the relative absence of the oxygen effect, a factor which may be especially important in the treatment of neoplasms which on the whole are relatively anoxic.

MATERIALS AND METHODS

In the study and determination of the growth-inhibiting or lethal effects of various types of radiations on neoplastic cells, the ideal situation would seem to be the irradiation of the tumor cells in vivo in an animal which had no resistance to the growth of the cells irradiated, or even better, no ability to develop resistance to the innoculation of such cell or cells within its body (33). Such a situation is possible when a spontaneous tumor arises in a genetically uniform strain of mice which for some generations has been propagated by brother to sister mating. The ideal situation occurs when the tumor arises in, and is transplanted to, first cousins only; however, in a study requiring hundreds of animals this is not practical. We have therefore used all the descendents of brother to sister mating. In addition, we have found it necessary to use various, but genetically closely related, strains of mice such as A/Heston, LAF_1, A/JAX, and CAF_1, and the innoculation of two different tumors into them -- a lymphoma (diploid)* (34) and a mammary carcinoma (aneuploid)† (35), both of which "take" in the several lines of mice used after the administration of from 2 to 500 cells intraperitoneally or subcutaneously. Both of these transplantable tumors have characteristics similar to the transplantable lymphoma (36,37) and mammary carcinoma (3) we used in our first studies with heavy particles in 1935 (4,38). However, unlike the studies of Hewitt and Wilson (39), in which titration of cells in recipient animals is carried out after irradiation of the donor animal with various doses of radiation, we were forced to irradiate the cells in vitro

* Kindly sent to us by Dr. D. B. Amos of Buffalo.

† Kindly given to us by Dr. G. A. LePage.

in thin chambers or on millipore filters because of the limiting energies of several of the beam particles studied.

In the present studies lymphoma cells and mammary carcinoma cells were used in the previously mentioned strains of mice (34,40) supplied by the Bar Harbor Laboratories. The tumors were passed every six or seven days in ascites form by intraperitoneal or subcutaneous innoculation for lymphoma, and every 10 to 12 days for the slower-growing mammary carcinoma (TA_3 tumor). About one week after innoculation the lymphoma mice can be used as donor animals. Mammary carcinoma mice can be used after 12 days.

The cells, contained in ascitic fluid, were placed in thin chambers (see Fig. 1) and exposed to varying doses of irradiation using 910-MeV alpha particles from the 184-inch synchrocyclotron at a dose rate of 300 rads per minute. The LET of these particles in tissue is 1.6 keV/μ. In order to irradiate the cells with a higher LET we placed a 2.176-inch copper absorber in front of the irradiation chamber and were thus able to irradiate with the Bragg peak of the alpha-particle beam (see Fig. 2). In this situation the highest LET to which the cells are exposed could be in excess of 250 keV/μ; however, due to the initial energy-spread of the beam and the range-straggling of the particles as they pass through an absorbing medium, the cells are also exposed to particles of lower LET values (the lowest may be in the order of 10 keV/μ).

In order to irradiate the cells with a more precisely defined LET, further experiments were carried out with the Heavy-Ion Linear Accelerator (HILAC) (41). When the cells are spread out in a very thin layer, it is possible to irradiate them with the shank, or plateau, of the total path-length of the heavy ions, and thus avoid the Bragg peak and the corresponding spread in LET values. In order to insure a uniform irradiation of the cells, it is necessary to obtain a condition as close to a monolayer as possible, and therefore, we could not use the chambers employed in the cyclotron experiments. For the HILAC experiments we used a cell suspension made by washing the ascites cells three times in tissue culture medium TC-199 (42). (This was necessary because if the cells are left in ascites the whole suspension will dry on top of the millipore filter, whereas, if the cells are washed to remove the ascites and resuspended in TC-199, the fluid is absorbed through the filter onto the pad and the cells remain on top of the filter). We placed an aliquot of this cell suspension on a millipore filter that was glued to a pad kept wet with an osmotically normal solution, thus preventing the cells from drying out. The millipore filters were kept in either an oxygen or nitrogen atmosphere during exposures. The cells were bombarded with particles listed in Table 1, the dose rate being from 300 to 600 rads per minute.

Following exposures, either the cells were washed off of the filters with ice-cold tissue-culture medium (TC-199) in the case of the HILAC experiments, or

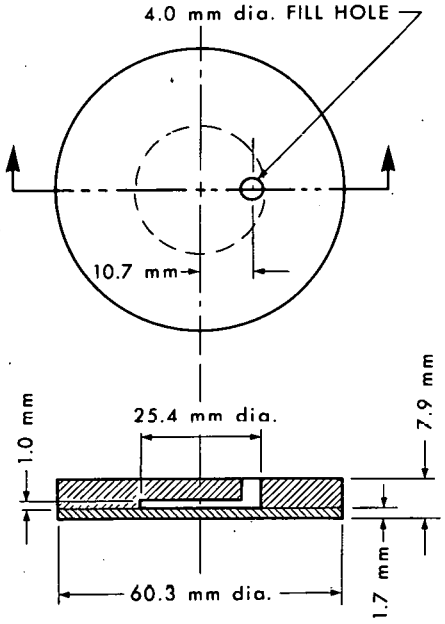

Figure 1. Diagram showing the thin chamber into which cells, contained in ascitic fluid, are placed for cyclotron irradiation experiments. MU-31718

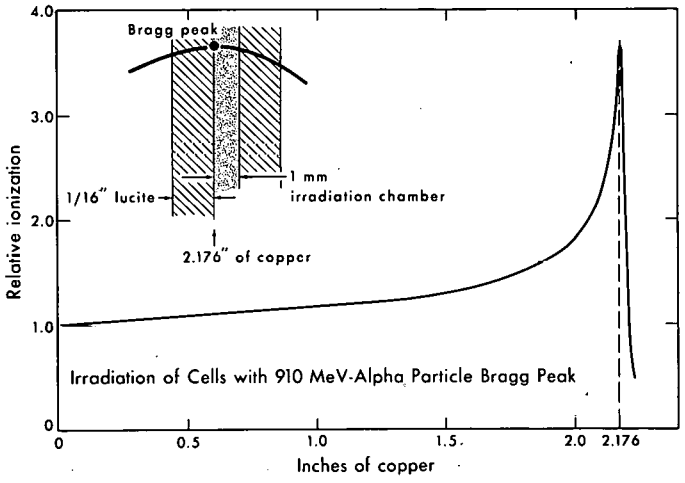

Figure 2. Bragg curve of 910-MeV alpha particles showing placement of cells for irradiation with the Bragg-peak portion of curve. Insert in upper left corner is enlargement of Bragg-peak portion. MU-31719

the cell suspensions from the "cyclotron chambers" were diluted 1:3 in the cyclotron experiments. Dilutions, made with ice-cold Tyrodes or TC-199 solution from these cell suspensions, were then injected intraperitoneally or subcutaneously into the mice, usually using five mice for each dose and titration level. The mice were then followed for lethality, the follow-up period lasting about eight weeks for the lymphoma and 12 weeks for the mammary carcinoma.

On the whole, each experiment was completed within a period of 3 to 4 hr, and examination of the cells by eosin dye revealed that only a few of the cells (less than 5%) were nonviable by this standard prior to injection in those

Table 1.

HILAC

HEAVY ION	LET in tissue (keV/μ)
H^2 (deuterons)	4.5
He^4 (alphas)	18.6
Li^7	43.2
B^{11}	124.
C^{14}	185.
N^{14}	260.
O^{16}	348.
F^{19}	449.
Ne^{20}	575.
Ar^{40}	1715.

experiments where millipore filters were not used. In the experiments using millipore filters, 20 to 30% of the cells were nonviable prior to injection, and corrections were made accordingly. As in our previous studies, we used 200-kV X rays as the baseline for the comparison of various LET's as related to RBE. Thus, the LD_{50} survival after X rays administered at the rate of 100 r per minute was compared to the LD_{50} of each of the various heavy-particle irradiations, and the RBE was determined by the ratio of the X-ray dose to the heavy-particle dose.

In some X-ray experiments the ascitic fluid was irradiated, undiluted, in test tubes. In other experiments, millipore filters were used in order to study the oxygen effect, and to use a technique as similar as possible to that used in the heavy-particle experiments. A special chamber was made for this purpose (see Fig. 3). It consisted of a box divided into three compartments, one for oxygen and one for nitrogen, and one in between the two for the Victoreen ionization chamber.

RESULTS

We will first summarize our results obtained with the 910-MeV alpha-particle beam from the 184-inch synchrocyclotron. Lymphoma and TA_3 tumor cells were irradiated with both the peak and plateau portions of the Bragg curve, as well as with 200-kV X rays, in order to study the RBE of the Bragg peak.

The three graphs in Fig. 4 summarize the results of 11 experiments, six using X rays and five using the plateau and the peak of the Bragg curve, which were carried out with the TA_3 tumor cells injected intraperitoneally into three strains of mice. The surviving fractions of cells are plotted as a function of irradiation dose. Surviving fractions were calculated by comparing the LD_{50} of the controls with that of the irradiated samples, using the method of Hewitt

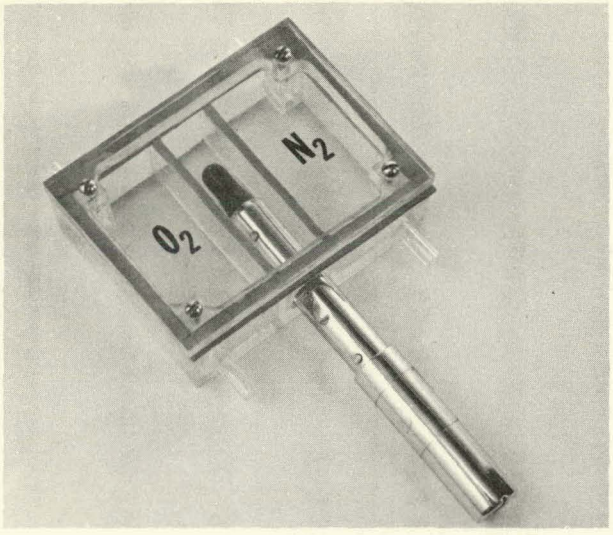

Figure 3. Photograph showing Victoreen ionization chamber located between a nitrogen and an oxygen chamber. JHL-3801

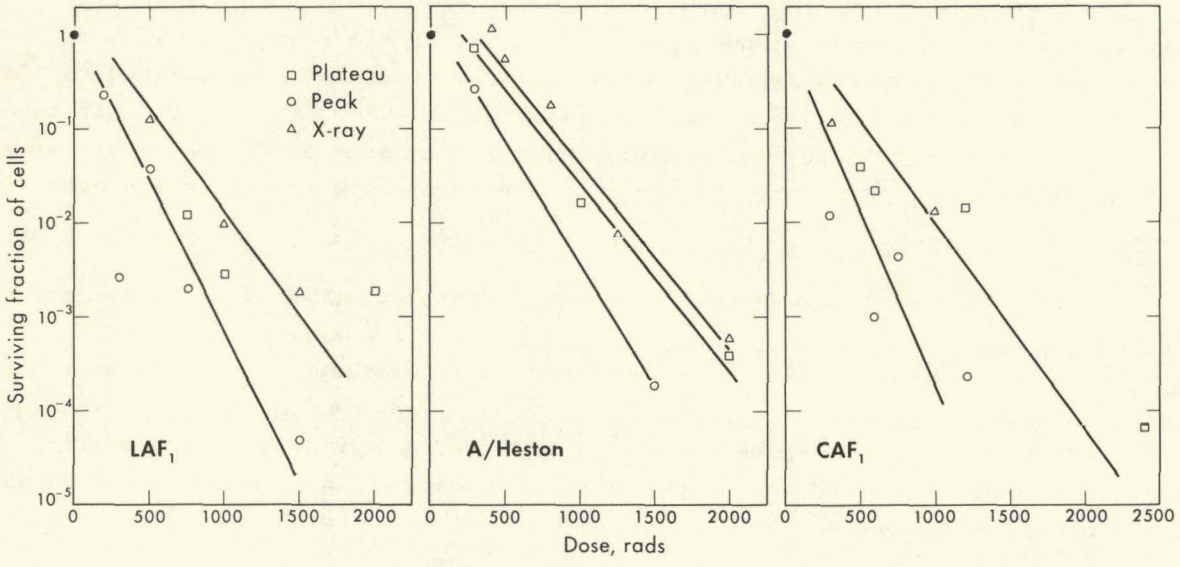

Figure 4. The surviving fraction of irradiated TA_3 tumor cells injected intraperitoneally into three strains of mice. Irradiation was given with 200-kV X rays, or with the plateau or Bragg peak portion of a 910-MeV alpha-particle cyclotron beam. MUB-2174

and Wilson (39,43). A clear difference is noted between the peak and the plateau for each strain of mice, and the plateau values are similar to those of X rays.

Figure 5 shows the results of seven X-ray and two alpha-particle experiments using lymphoma implanted intraperitoneally in two strains of mice, and Fig. 6 the results of seven X-ray and three alpha-particle experiments using lymphoma implanted subcutaneously in two strains of mice. Again, note the greater effect of the Bragg peak in all cases.

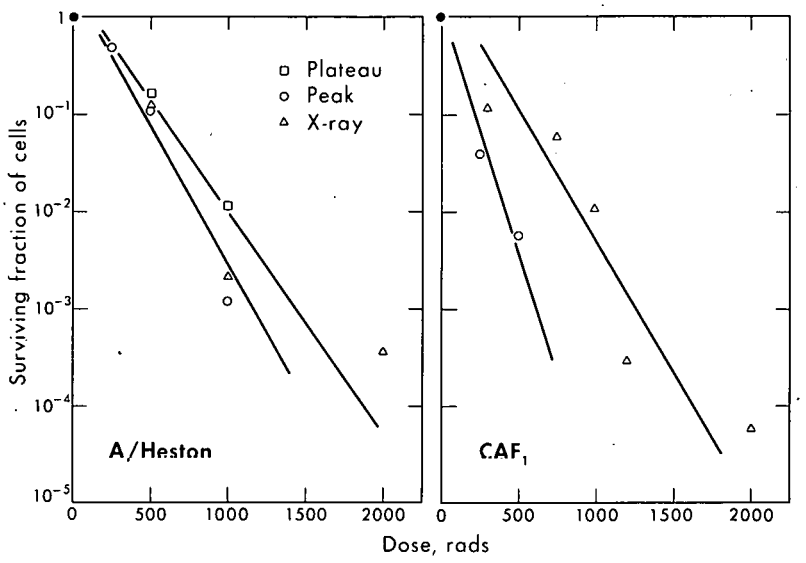

Figure 5. The surviving fraction of irradiated lymphoma cells injected intraperitoneally into two strains of mice. Irradiation was given with 200-kV X rays, or with the plateau or Bragg peak portion of a 910-MeV alpha-particle cyclotron beam. MU-32175

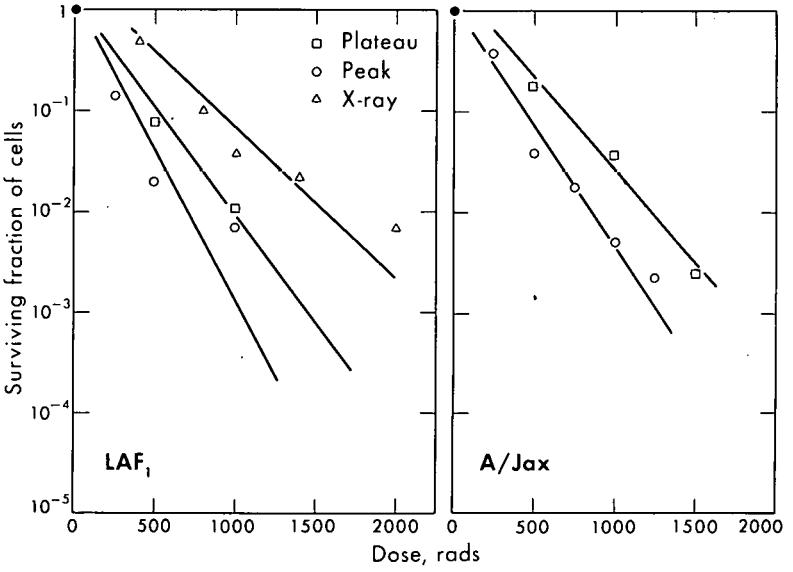

Figure 6. The surviving fraction of irradiated lymphoma cells injected subcutaneously into two strains of mice. Irradiation was given with 200-kV X rays, or with the plateau or Bragg peak portion of a 910-MeV alpha-particle cyclotron beam. MU-32174

The surviving fractions are based on the average LD_{50} for the controls of each experiment done with the particular tumor in each strain of mice. The LD_{50}'s vary from strain to strain (see Table 2), but by calculating the surviving fractions this is taken into account, and one can then combine the results of the different strains for each tumor. Thus, in Fig. 7 the data for Figs. 4, 5 and 6 have been combined so that Figure 7(a) shows the average of all strains for the intraperitoneally injected TA_3 tumor, Figure 7(b) those for the intraperitoneally injected lymphoma, and Figure 7(c) those for the subcutaneously injected lymph-

Table 2. Average number of cells for LD_{50} in control experiments

Strain	Tumor		
	Intraperitoneal TA_3	Intraperitoneal lymphoma	Subcutaneous lymphoma
CAF_1	42	3	*
A/Heston	188	21	*
LAF_1	62	6	591
A/JAX	119	10	177

* Not used because subcutaneously implanted tumors regress in these strains.

Table 3. RBE for Bragg peak of 910-MeV alpha-particle beam compared with 200-kV X rays

	RBE
TA_3 (intraperitoneal)	1.9
Lymphoma (intraperitoneal)	1.4
Lymphoma (subcutaneous)	1.8

oma. We can now calculate the RBE of the Bragg peak for each tumor, and these values are found to lie between 1.4 and 2.0 (see Table 3) when compared to X rays. The RBE's are the same when compared to the plateau, except in Figure 7(c), in which case the plateau curve lies between that of the Bragg peak and X rays, the RBE, comparing the peak to the plateau, being 1.4.

Thus, with the lymphoma and the TA_3 tumor, the Bragg peak was demonstrated to have a greater biologic effect than that of both X rays and the plateau portion of the alpha-particle beam. Studies with these tumors in oxygen and nitrogen environments are now under way comparing X rays, plateau and Bragg peak.

Further results are available on lymphoma cells irradiated with Li^7, B^{11}, or Ne^{20} particles accelerated in the HILAC (see Table 1). The irradiated cells were then injected intraperitoneally into LAF_1 mice. In these experiments we planned to study both the RBE and the oxygen effect, related to the LET of the different particles. However, we are still in the early stages of this work and the X-ray data and some of the other data are not yet available. Therefore this discussion will be limited to a preliminary report concerning whether or not an oxygen effect was observed for the three particles studied.

In all experiments, the irradiation in a nitrogen atmosphere was performed before that in the oxygen atmosphere. This means that the cells irradiated in the oxygen atmosphere were stored from 30 to 60 min longer under rather unphysiological conditions, which would tend to make the LD_{50} in controls

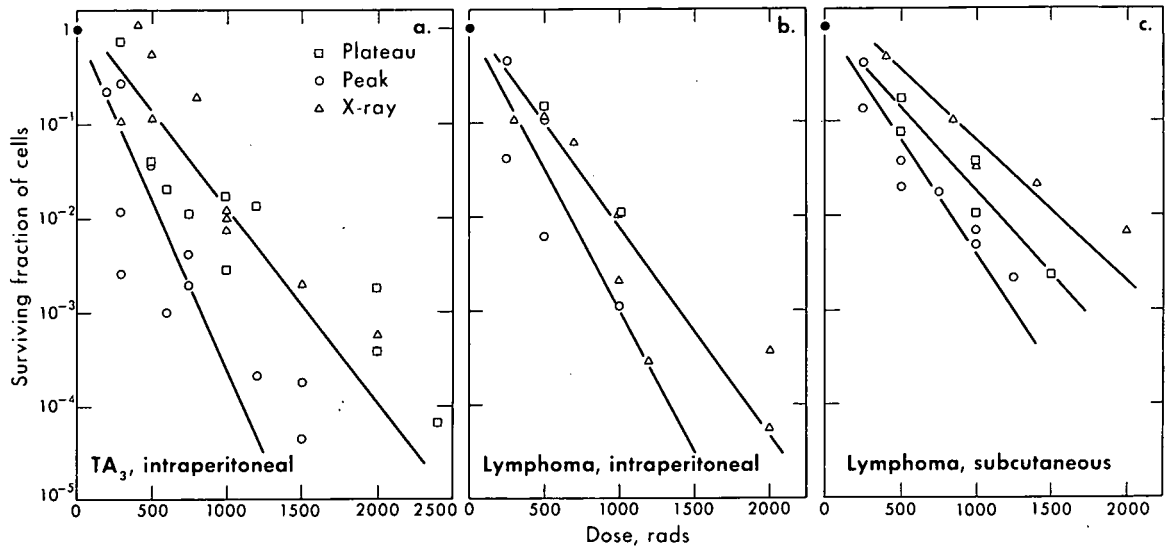

Figure 7. The data in Figures 4, 5 and 6 have been combined so that the average curves for all strains of mice used with each tumor are shown. The RBE's for (a), (b) and (c) are 1.9, 1.4 and 1.8, respectively, for Bragg peak compared to X rays.

MUB-2173

higher for the oxygen environment than for the nitrogen environment. However, in two of the three experiments we found that the LD_{50}'s for the oxygen controls were much higher than expected from the longer storing. Because of this complication, the surviving fractions are based on the "regular" control. Therefore, the HILAC data cannot, at this time, be considered quantitative, because the regular controls were made from ascitic fluid in the test tube and not on the millipore filters. However, the slope of the numerical curves, after the cells were exposed to radiation of various LET's in nitrogen or oxygen, can be compared. Fig. 8 shows the surviving fractions in oxygen and nitrogen atmospheres for the three particles studied. In the case of irradiation with Li^7 particles, which have a relatively low LET, we observed that surviving fractions of cells irradiated in an oxygen atmosphere were smaller than those for cells irradiated in a nitrogen atmosphere, or in other words, some oxygen effect was present. However, in the cases of both B^{11} and Ne^{20} particles we observed no clear differences between the surviving fractions of cells in oxygen and nitrogen atmospheres. Additional experiments have been performed and are being observed for end results, and others are currently under way, using all the particles listed in Table 1, with LET's ranging from 4.5 keV/μ up to 1717 keV/μ. It is hoped that further valuable data on the relationship of LET to RBE, and also to the oxygen effect, will result.

DISCUSSION

These results, although incomplete, nevertheless are of interest in relation to the question of RBE as related to LET and the oxygen effect (44,45).

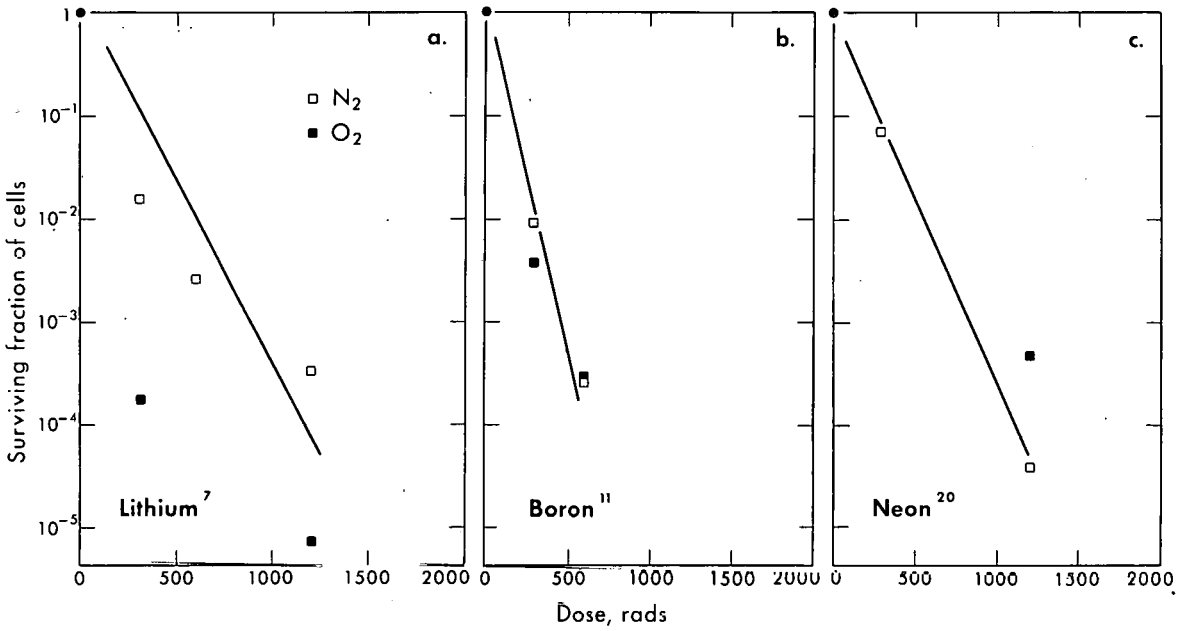

Figure 8. Surviving fractions of lymphoma cells irradiated with ions from the HILAC, using both nitrogen and oxygen atmospheres, and then injected intraperitoneally into LAF_1 mice. In the cases of neon and boron ions there are no differences between the surviving fractions in oxygen and nitrogen; with the relatively low LET lithium ions, however, an oxygen effect is noted. These preliminary data are of interest but small differences in survival between oxygen and nitrogen atmospheres would not be evident with the technique used.

MUB-2172

Many studies on the relationship of LET to RBE using various test objects have been carried out in recent years, especially by Tobias and associates in Berkeley and by the Yale group. In general, depending on how RBE is calculated and what test object is used, RBE increases with LET up to a point and then decreases (46,47,48,49,50,51). However, work with mammalian cells is relatively limited. For example, Hornsey and Silini at Hammersmith (52) showed that fast neutrons had less of an oxygen effect than X rays, but the oxygen effect was only partly abolished. Berry and Andrews (53) showed some decrease in the oxygen effect with 910-MeV Bragg-peak alpha particles.

Our preliminary results indicate that the oxygen effect may not disappear completely until a very high LET is attained -- considerably higher than the 20 keV/μ for fast neutrons indicated by Fowler and associates (54). If our present experiments hold, the secondaries from pi mesons also would have some oxygen effect (55), and we hope to have data on the effects of pi mesons on these neoplasms in the future.

Studies now under way with these two tumors, and other mammalian tissues in vivo, will be directed toward answering some of the interesting questions re-

lating to LET, RBE, the oxygen effect, recovery factors, etc., keeping in mind the better understanding of the biologic effect of various types of particulate radiations, and also of their implications in radiation therapy (56).

Finally, the authors are aware of some of the irregularities in these data. These are largely due, we believe, to the necessarily long and varying period of time the cells must be kept outside of the animal body during preparation for and exposure to radiation. Therefore, these data are not necessarily quantitative, and small effects might be missed. In other words, further work is necessary to define the degree of residual oxygen effect present, if any, with the LET's of boron or neon. However, these cells are grown within the living animal, unlike studies of cells in tissue culture, and for this and other reasons are of radiobiologic and therapeutic interest.

CONCLUSIONS

The following conclusions can be drawn from the present studies: 1. the Bragg-peak ionization produced by 910-MeV alpha particles has a greater RBE than the plateau region of ionization as measured by the proliferative capacity of neoplastic cells grown in the living animal after irradiation. This is of advantage in the use of these particles in therapy (56). 2. Preliminary results in the same system using various heavy particles producing various LET's indicate that disappearance of the oxygen effect requires a very high LET. 3. Further and more quantitative studies are necessary to define the Z number and energy of the particle with optimal characteristics based on width of the Bragg peak, absence of oxygen effect, and RBE.

ACKNOWLEDGEMENTS

Valuable technical assistance was provided by Miss Alice Beckman and Miss Penelope Atherton. During the latter part of the experiments Dr. Robert Tym and Mr. Lawrence Brennan gave us assistance with the tumor injections.

REFERENCES

1. Lawrence, J. H., and Lawrence, E. O.; Proc. Nat. Acad. Sci. U.S. 22:124, 1936.
2. Lawrence, J. H., and Tennant, R.; J. Exptl. Med. 66:667, 1937
3. Lawrence, J. H.; Horn, R., and Strong, L. C.; Yale J. Biol. Med. 10:145, 1938.
4. Axelrod, D.; Aebersold, P. C., and Lawrence, J. H.; Proc. Soc. Exptl. Biol. Med. 48:251, 1941.
5. Aebersold, P. C., and Lawrence, J. H.; Ann. Rev. Physiol. 4:25, 1942.
6. Thoday, J. M., and Read, John; Nature 163:133, 1949.
7. Gray, L. H.; Lectures Sci. Basis Med. 7:314, 1957-58.

8. Barendsen, G. W.; in Conference on Physical Factors Modifying Response to Radiation, New York Academy Science, Section on Biology & Medicine, Nov. 30, 1962; 1963, in press; personal communication.
9. Bragg, W. H., and Kleeman, R. D.; Phil. Mag. 8:726, 1904.
10. Tobias, C. A.; Anger, H. O., and Lawrence, J. H.; Am. J. Roentgenol. Radium Therapy Nucl. Med. 67:1, 1952.
11. Anderson, A.; Garcia, J.; Henry, J.; Riggs, C.; Roberts, J. E.; Thorell, B., and Tobias, C. A.; Radiation Res. 7:299, 1957 (abstract).
12. Anderson, A.; Roberts, J. E.; Thorell, B., and Tobias, C. A.; Radiation Res. 7:300, 1957 (abstract).
13. Malis, L. I.; Loevinger, R.; Kruger, L., and Rose, J. E.; Science 126:302, 1957.
14. Malis, L. I.; Rose, J. E.; Kruger, L., and Baker, C. P.; in Response of the Nervous System to Ionizing Radiation, edited by T. Haley and R. S. Snider, New York, Academic Press, 1962, p. 359.
15. Tobias, C. A.; in Response of the Nervous System to Ionizing Radiation, edited by T. Haley and R. S. Snider, New York, Academic Press, 1962, p. 325.
16. Van Dyke, D. C., and Janssen, P.; J. Neurosurg 20:289, 1963.
17. Stone, R. S.; Lawrence, J. H., and Aebersold, P. C.; Radiology 35:322, 1940.
18. Stone, R. S.; Am. J. Roentgenol. Radium Therapy 59:771, 1948.
19. Brobeck, W. M.; Lawrence, E. O.; MacKenzie, K. R.; McMillan, E. M.; Serber, R.; Sewell, D. C.; Simpson, K. M., and Thornton, R. L.; Phys. Rev. 71:449, 1947.
20. Hubbard, E. L.; Ann. Rev. Nucl. Sci. 11:419, 1961.
21. Gordon, H. S., and Behman, G. A.; Section 8i, in American Institute of Physics Handbook, 2nd Ed., New York, McGraw-Hill Book Co., 1963, in press.
22. Lawrence, J. H., and Tobias, C. A.; Cancer Res. 16:185, 1956.
23. Tobias, C. A.; Lawrence, J. H.; Born, J. L.; McCombs, R. K.; Roberts, J. E.; Anger, H. O.; Low-Beer, B. V. A., and Huggins, C.; Cancer Res. 18:121, 1958.
24. Lawrence, J. H.; Tobias, C. A.; Born, J. L.; Wang, C. C., and Linfoot, J. A.; J. Neurosurg. 19:717, 1962.
25. Lawrence, J. H.; Tobias, C. A.; Born, J. L.; Sangalli, F.; Carlson, R. A., and Linfoot, J. A.; Acta Radiol. 58:337, 1962.
26. Linfoot, J. A.; Lawrence, J. H.; Born, J. L., and Tobias, C. A.; New Eng. J. Med. 269:597, 1963; also this report, p. 29.
27. Lawrence, J. H.; Tobias, C. A.; Linfoot, J. A.; Born, J. L.; Gottschalk, A., and Kling, R. P.; Diabetes, 1963, in press.
28. Lawrence, J. H.; Tobias, C. A.; Born, J. L.; Gottschalk, A.; Linfoot, J. A., and Kling, R. P.; J. Am. Med. Assoc., 1963, in press.
29. Kjellberg, R. N.; Sweet, W. H.; Preston, W. M., and Koehler, A. M.; in Transactions of the American Neurological Association, 1962, p. 216.
30. Kjellberg, R. N.; Koehler, A. M.; Preston, W. M., and Sweet, W. H.; Second International Congress of Radiation Research, Harrogate, Yorkshire, England, August 11, 1962.

31. Falkmer, S.; Fors, B.; Larsson, B.; Lindell, A.; Naeslund, J., and Stenson, S. Acta Radiol. 58:33, 1962.
32. Larsson, B.; Leksell, L., and Rexed, B.; Acta Chir. Scand. 125:1, 1963.
33. Scott, O. C. A.; Radiation Res. 14:643, 1961.
34. Amos, D. B.; Ann. N. Y. Acad. Sci. 63:706, 1956.
35. LePage, G. A., and Jones, M.; Cancer Res. 21:642, 1961.
36. Lawrence, J. H., and Gardner, W. U.; Am. J. Cancer 33:112, 1938.
37. Graff, W. S.; Scott, K. G., and Lawrence, J. H.; Am. J. Roentgenol. Radium Therapy 55:44, 1946.
38. Lawrence, J. H.; Aebersold, P. C., and Lawrence, E. O.; Proc. Nat. Acad. Sci. U.S. 22:543, 1936.
39. Hewitt, H. B., and Wilson, C. W.; Brit. J. Cancer 13:69, 1959.
40. Handbook on Genetically Standardized JAX Mice. Roscoe B. Jackson Memorial Laboratory, Bar Harbor, Maine. The Bar Harbor Times Publishing Co., 1962.
41. Brustad, Tor; Ariotti, P., and Lyman, J.; Lawrence Radiation Laboratory Report UCRL-9454, 1960.
42. Morgan, J. F.; Morton, H. J., and Parker, R. C.; Proc. Soc. Exptl. Biol. Med. 73:1, 1950.
43. Reed, L. J., and Muench, H.; Am. J. Hyg. 27:493, 1938.
44. Zirkle, R. E.; Am. J. Cancer 23:558, 1935.
45. Zirkle, R. E.; in Radiation Biology, Vol. 1, edited by A. Hallaender, New York, McGraw-Hill Book Co., 1954, p. 315.
46. Storer, J. B.; Payne, S. H.; Furchner, J. E., and Langham, W. H.; Radiation Res. 6:188, 1957.
47. Deering, R. A.; Hutchinson, F., and Schambra, P. E.; Aerospace Med. 32:915, 1961.
48. Tobias, C. A.; Brustad, T., and Manney, T. R.; in International Symposium on Primary and Initial Effects of Ionizing Irradiations on Living Cells, Moscow, October 1960, edited by R. J. C. Harris, New York, London, Academic Press, 1961, p. 257.
49. Tobias, C. A.; International Congress Series #36, 2nd International Congress of Neurological Surgery, Washington, D. C., Oct. 14-20, 1961.
50. Powers, E. L.; Smaller, B.; Tobias, C. A.; Lyman, J., and Brustad, T.; in International Congress in Biophysics, Stockholm, 1961, p. 96 (abstract).
51. Brustad, T.; in Advances in Biological and Medical Physics, Vol. 8, edited by C. A. Tobias and J. H. Lawrence, New York, Academic Press, 1962, p. 161.
52. Hornsey, S., and Silini, G.; Inter. J. Radiation Biol. 4:135, 1961.
53. Berry, Roger J., and Andrews, J. R.; Brit. J. Radiol. 36:49, 1963.
54. Symposium, Annual Congress of British Institute of Radiology, April 27, 1962, Brit. J. Radiol. 36:77-121, 1963. (Fowler, J. F., and others).
55. Fowler, P. H., and Perkins, D. H.; Nature 189:524, 1961.
56. D'Angio, G. J., and Lawrence, J. H.; Nucleonics, 1963, in press.

STAFF PUBLICATIONS

Amer, Nabil: Modification of radiation injury with magnetic fields (abstract), Radiation Res. 19:215, 1963.

Dobson, E. L.; Kelly, L. S.; Finney, C. R., and Parker, H. G.: Further complications in interpretation of RE system blockade (abstract), Federation Proc. 22, No. 2, Pt. 1, 1963.

Fish, M. B.; Pollycove, M., and Feichtmeir, T. V.: Differentiation between vitamin B_{12}-deficient and folic acid-deficient megaloblastic anemias with C^{14}-histidine, Blood. 21:447, 1963.

Freeman, N. K.; Lindgren, F. T., and Nichols, A. V.: The chemistry of serum lipoproteins, in Progress in the Chemistry of Fats and Other Lipids, Vol. 6, London, Pergamon Press, 1963, p. 216.

Garcia, J. F., and Schooley, J. C.: Immunological neutralization of various erythropoietins, Proc. Soc. Exptl. Biol. Med. 112:712, 1963.

Gutnisky, A., and Van Dyke, D.: Normal response to erythropoietin or hypoxia in rats made anemic with turpentine abscess, Proc. Soc. Exptl. Biol. Med. 112:75, 1963.

Hawthorne, D. C., and Mortimer, R. K.: Super-suppressors in yeast, Genetics. 48:617, 1963.

Hildreth, P. E., and Lucchesi, J. C.: Fertilization in Drosophila 1. Evidence for the regular occurrence of monospermy, Develop. Biol. 6:262, 1963.

Kalbhen, D. A., and Sargent, T. W.: Preliminary studies of the distribution and fate of ^{82}Br-labeled 2-brom-D-lysergic acid diethylamide (BOL) in the human body, Med. Exp. 8:200, 1963.

Lawrence, J.H.: Isotopes and nuclear radiations in medicine, in Conference on the Uses of Radioisotopes in Animal Biology and the Medical Sciences, Mexico, 1961. Use of radioisotopes in animal biology and the medical sciences; proceedings. New York and London, Academic Press, pub. for the International Atomic Energy Agency, 1962, 1:1.

Lawrence, J. H., and Parker, H. G.: Use of radioisotopes in hematology, J. Am. Med. Ass. 184:136, 1963.

McDonald, L. W.: Carcinomatous change in cysts of skin, A. M. A. Arch. Derm. Syph. 87:208, 1963.

McDonald, L. W.: Transplantation of antibody producing cells or their precursors by parabiosis, Life Sciences. 2:36, 1963.

Manney, T. R.; Brustad, T., and Tobias, C. A.: Effects of glycerol and of anoxia on the radiosensitivity of haploid yeasts to densely ionizing particles, Radiation Res. 18:374, 1963.

Mortimer, R. K., and Hawthorne, D. C.: Chromosome maps of saccharomyces, Microbial Genet. Bull. Suppl. to no 19, pp. 3 and 14, 1963.

Naets, J. P. (Introduced by J. H. Lawrence): Relation between erythropoietin plasma level and oxygen requirements, Proc. Soc. Exptl. Biol, Med. 112:832, 1963.

Nelson, G. J.: An apparatus for production of concave gradients and its application to chromatography of lipids, Anal. Biochem. 5:116, 1963.

Parker, H. G.; Sargent, T. W., III; Pollycove, M.; Carpe, L. M.; Linfoot, J. A.; Saito, H., and Lawrence, J. H.: Biomedical tracer studies with the whole-body counter, in 4th Inter-American Symposium on the Peaceful Application of Nuclear Energy, (Mexico City, 1962) Washington, D.C., Pan American Union, Vol. 2, 1962, p. 101.

Rescigno, Aldo: Flow diagrams of multicompartment systems, Ann. N.Y. Acad. Sci. 108:204, 1963.

Rosenberg, L. L.; Dimick, M. K., and LaRoche, G.: Thyroid function in chickens and rats: Effect of iodine content of the diet and hypophysectomy on iodine metabolism in White Leghorn cockerels and Long-Evans rats, Endocrinology. 72:749, 1963.

Rosenberg, L. L.; LaRoche, G., and Dimick, M. K.: Thyroid function in chickens and rats: Equilibration of injected iodide with existing thyroidal iodine in White Leghorn cockerels, Endocrinology. 72:759, 1963.

Slater, J. V.; Tobias, C. A., and Amer, N. M.: Modification of radiation response during embryonic development by the use of elevated temperatures, in 2nd International Congress of Radiation Research, Harrogate, England, 1962. Radiation effects in physics, chemistry and biology, Amsterdam, North Holland, 1963.

Slater, J. V.; Rescigno, A.; Amer, N. M., and Tobias, C. A.: Temperature dependence of wing abnormality in Tribolium confusum, Science. 140:408, 1963.

Steinkamp, R. C.; Lawrence, J. H., and Born, J. L.; Long term experiences with the use of P^{32} in the treatment of lymphocytic leukemia, J. Nucl. Med. 4:92, 1963.

Van Dyke, D., and Janssen, P.: Removal of cerebral cortical tissue with negligible scar formation using a beam of high-energy particles, J. Neurosurg. 20:289, 1963.

Winchell, H. S.; Pollycove, M.; Richards, V., and Lawrence, J. H.: Selective irradiation of lymphatic tissues in preparation for tissue homografting, Am. J. Surg. 105:177, 1963.